STRUCTURE OF THE TRANSLATING NEUROSPORA RIBOSOME ARRESTED BY CYCLOHEXIMIDE

A Dissertation

by

LUNDA SHEN

Submitted to the Graduate and Professional School of
Texas A&M University
in partial fulfillment of the requirements for the degree of

DOCTOR OF PHILOSOPHY

Chair of Committee,	Matthew S. Sachs
Committee Members,	Deborah Bell-Pedersen
	L. Rene Garcia
	Junjie Zhang
Head of Department,	Alex Keene

December 2021

Major Subject: Biology

ABSTRACT

Ribosomes translate RNA into proteins. The protein synthesis inhibitor cycloheximide (CHX) is widely used to inhibit eukaryotic ribosomes engaged in translation elongation. However, the lack of structural data for actively translating polyribosomes stalled by CHX leaves unanswered the question of which elongation step is inhibited. We elucidated CHX's mechanism of action based on the cryo-electron microscopic structure of actively translating *Neurospora crassa* ribosomes bound with CHX at 2.7 Å resolution. The ribosome structure from this filamentous fungus contains clearly resolved ribosomal protein eL28, like higher eukaryotes but unlike budding yeast, which lacks eL28. Despite some differences in overall structures, the ribosomes from *Neurospora*, yeast, and humans all contain a highly conserved CHX-binding site. We also sequenced classic *Neurospora* CHX-resistant alleles. These mutations, including one at a residue not previously observed to affect CHX-resistance in eukaryotes, were in large subunit proteins uL15 and eL42 that are part of the CHX binding pocket. In addition to A-site tRNA, P-site tRNA, mRNA, and CHX that are associated with the translating *N. crassa* ribosome, spermidine (SPD) is also present near the CHX-binding site close to the E site on the large subunit. The tRNAs in the peptidyl transferase center are in the A/A site and P/P site. The nascent peptide is attached to the A-site tRNA and not the P-site tRNA. The structural and functional data obtained show that CHX arrests the ribosome in the classical PRE state and does not interfere with A-site reactivity.

ACKNOWLEDGEMENTS

This project would not have been possible without the support of many people.

I would first like to express my sincere gratitude to my advisor, Dr. Matthew S. Sachs. I am so blessed to have your invaluable supervision, insightful feedback, and constant support during the course of my PhD degree.

I'm deeply grateful to my committee members, Drs. Deborah Bell-Pedersen, L. Rene Garcia, and Junjie Zhang. I want to thank you for your guidance and support throughout the course of this research and for revising this dissertation.

I would like to thank my collaborators, Drs. Zhaoming Su, Kailu Yang, Cheng Wu, and Thomas Becker, for their contribution to this project. Thanks also go to Dr. Wah Chiu for cryo-EM support.

I would also like to thank the staff in the Microscopy & Imaging Center, especially Drs. Anindito Sen, Hansoo Kim, and Michael Pendleton, for the training and support.

I would also like to thank the faculty and staff in the Department of Biology for making my time at Texas A&M University a great experience. I especially want to thank Jennifer Bradford, Dr. Chris Lee, and Dr. Andy Tag for their support during the course of my PhD degree.

Thanks also go to my lab mates and friends, Ananya Dasgupta, Matthew Breuer, Dr. Michael Werry, David Silva, Dr. Mengqiu Jiang, Dr. Jeng-Yih Chang, Dr. Ran Meng, Dr. Zhicheng Cui, Dr. Yue Xing, Yi Sun, Dr. Yinghong Lan, and Yan Luo, for their support and encouragement all through my studies.

Finally, thanks to my husband, parents, parents-in-law, and children, for their endless support, patience, and love.

CONTRIBUTORS

This work was supervised by a dissertation committee consisting of Professors Matthew S. Sachs, Deborah Bell-Pedersen, and L. Rene Garcia of the Department of Biology, and Professor Junjie Zhang of the Department of Biochemistry and Biophysics.

The *N. crassa* strains were obtained from the Fungal Genetic Stock Center. The cryo-EM data to solve the *N. crassa* ribosome structure at 2.7 Å resolution were collected by Dr. Zhaoming Su on the Titan Krios microscope in the SLAC National Accelerator Laboratory. Dr. Kailu Yang participated in the data collection on the F20 microscope at Texas A&M University. Dr. Cheng Wu conducted the toeprinting assay and participated in the *in vitro* translation. All of them, together with Drs. Thomas Becker, Deborah Bell-Pedersen, Junjie Zhang, and Matthew S. Sachs, participated in the interpretation of results.

All other work conducted for the dissertation was completed by the student independently.

FUNDING SOURCES

The work was supported by National Institute of Health Grants [S10OD021600, U24GM1167, R21 AI138158, R35 GM126966], and Welch Foundation Grant [A1863].

NOMENCLATURE

CFTS	Cell-free translation system
CHX	Cycloheximide
cryo-EM	Cryogenic electron microscopy
CTF	Contrast transfer function
CYH	Cycloheximide
DNA	Deoxyribonucleic acid
eEF	Eukaryotic elongation factor
eIF	Eukaryotic initiation factor
EMDB	Electron Microscopy Databank
eRF	Eukaryotic release factor
GDP	Guanosine diphosphate
GTP	Guanosine triphosphate
KO	Knockout
LSU	Large subunit
mRNA	Messenger RNA
nt	Nucleotide
PCSK9	Proprotein convertase subtilisin/kexin type 9
PDB	Protein Data Bank
PET	Polypeptide exit tunnel
PRE	Pre-translocation
PTC	Peptidyl transferase center

RNA	Ribonucleic acid
rRNA	Ribosomal RNA
SPD	Spermidine
SSU	Small subunit
tRNA	Transfer RNA
UTR	Untranslated region

TABLE OF CONTENTS

Page

LIST OF FIGURES

Page

LIST OF TABLES

Page

CHAPTER I

INTRODUCTION AND LITERATURE REVIEW

1.1 *Neurospora crassa*

Neurospora crassa is a filamentous fungus in the phylum Ascomycota [1]. Its spores resemble axons, so it was given the genus name *Neurospora* which means “nerve spores” in Greek. In Chinese, it is called 粗糙脉孢菌 because the surface of its ascospores looks like leaf veins or 粉色面包霉菌/红面包霉菌 which means pink/red bread mold.

Since the mid 20th century, *N. crassa* has been used as a model organism for genetics [2], biochemistry [3], and molecular biology [4]. In the 1940s, George Beadle and Edward Tatum exposed *N. crassa* to X-ray radiation and caused mutations in genes [2]. They found that some of the resulting *N. crassa* mutants lost the ability to grow in minimal medium unless supplemented with important metabolites. They hypothesized that this was because the mutations in the genes caused the loss of the normal enzymes that produced these compounds, and proposed the “one-gene-one-enzyme” hypothesis, for which they shared, with Joshua Lederberg, the 1958 Nobel Prize in Physiology or Medicine [5]. In 2003, a high-quality draft sequence of the *N. crassa* genome was reported, revealing that the genome of *N. crassa* is about 40-megabase in size, and encodes about 10,000 protein-coding genes [6]. Analysis of the genome shows that *N.*

crassa possesses a wide array of genome-level defense mechanisms, including repeat-induced point mutation (RIP), a process unique to fungi, that can detect and mutate both copies of a sequence duplication [6]. So far, numerous studies using *N. crassa* have been published, to elucidate the mechanisms for events such as circadian rhythms [7], gene silencing [8], cell cycle [9], cell fusion [10], and cell translation regulation [11]. Recently, *N. crassa* has also been established as a model organism for translational control in circadian rhythms [12] and for fungal virology [13].

In this study, we are using N. crassa for the following reasons. First, although *N. crassa* has been used in many studies to explore the events related to translation, the structure of its mitochondrial ribosome has not been solved until recently [14], while prior to the work described here, the structure of its cytosolic ribosome had not been solved. This leaves potential gaps in understanding the mechanisms of the translational events. Second, our lab has developed a cell-free translation system (CFTS) from *N. crassa* [15]. The whole-cell extracts are generally prepared from germinating *N. crassa* conidia, and the CFTS has been used to examine translational regulation at the initiation [11, 15-17], elongation [18], and termination [19], to perform real-time analyses of translation kinetics [20, 18], and to analyze the peptidyl transferase center reactivity to puromycin [21]. Combining the structural study of the *N. crassa* ribosome and the functional study using the *N. crassa* CFTS may provide more insights into the mechanism of interest. Moreover, *N. crassa* has advantages over the most widely used fungal model organism, the yeast *Saccharomyces cerevisiae*, in that *N. crassa* is multicellular, has more complex

events such as circadian rhythms [22], and in some respects is more similar to higher eukaryotes. At the same time, *N. crassa* also has advantages over mammalian model organisms in that it is easier to maintain, to grow, and to get materials from, and to use for forward genetics studies. Finally, as a well-studied model organism, many *N. crassa* strains, wild-type or mutants, including a full set of gene-deletions, can be obtained from the Fungal Genetics Stock Center [23].

1.2 Ribosomes

Ribosomes are the heart of translation. They translate the sequence information encoded in messenger RNA (mRNA) molecules to sequences of amino acids [24]. They exist in prokaryotes [25], eukaryotic cytoplasm [26], mitochondria [27], and chloroplasts [28], and can have various sizes because of the different numbers and lengths of ribosomal RNAs (rRNAs) and ribosomal proteins. Based on the sedimentation rates that are related to the particles' sizes, prokaryotic ribosomes are often referred to as 70S ribosomes (S, the Svedberg unit, is a measure of sedimentation rate) [25], eukaryotic cytosolic ribosomes are 80S [26], chloroplast ribosomes are 70S [29], and mammalian mitochondrial ribosomes are 55S [30, 31].

The ribosome in the eukaryotic cytoplasm usually contains more or longer rRNA molecules compared to those in prokaryotes or organelles [26]. For example, the ribosome in the bacterium *Escherichia coli* contains 3 rRNA molecules, including the

23S (2904 nt), 5S (120 nt), and 16S (1542 nt) rRNAs [32]; the chloroplast ribosome in *Spinacia oleracea* contains 4 rRNA molecules, including the 23S (2810 nt), 5S (121 nt), 4.5S (106 nt), and 16S (1491 nt) rRNAs [33]; the ribosome in the *N. crassa* mitochondria contains 2 rRNA molecules, including the 23S (3464 nt) and 16S (1864 nt) rRNAs [14]; the ribosome in *N. crassa* cytoplasm contains 4 rRNA molecules, including the 26S (3338 nt), 5S (120 nt), 5.8S (158 nt), and 18S (1796 nt) rRNAs [34-36]. Ribosomes from different sources can have different numbers of ribosomal proteins. For example, the *E. coli* ribosome contains 49 ribosomal proteins [32], the spinach chloroplast ribosome contains 54 ribosomal proteins [33], the *N. crassa* mitochondrial ribosome contains 78 ribosomal proteins [14], and the *N. crassa* cytosolic ribosome contains 74 ribosomal proteins.

In 2009, Venkatraman Ramakrishnan, Thomas A. Steitz, and Ada E. Yonath received the Nobel Prize in Chemistry for their contributions to the studies of the structures and functions of ribosomes [37]. Ramakrishnan and colleagues solved the first structure of the 30S small ribosomal subunit [38]. Steitz and his colleague Peter Moore determined the first structure of the 50S large ribosomal subunit [39]. Yonath and colleagues introduced a new approach called cryo bio-crystallography, which exposes ribosome crystals to cryo-temperature during X-ray measurement, and first solved the complete structure of both subunits of a ribosome [40]. These structures were all determined by X-ray crystallography, and all were solved between 1999 and 2001. Since then, with the improvement of sample preparation and the development of new techniques such as

NMR [41] and cryo-electron microscopy [42], thousands of structures of different ribosomes or ribosome-related proteins have been solved. Recently, the cryo-EM structure of *E. coli* 70S ribosome reached a global resolution of 2.0 Å [32], revealing the unambiguous positioning of each residue of the rRNAs and ribosomal proteins as well as the chemical modifications.

After determination of the atomic structures of ribosomes from prokaryotes, eukaryotic cytoplasm, mitochondria, and chloroplasts, it was shown that some of the ribosomal proteins, although from different sources, are structurally homologous [43-45]. To eliminate the previous naming discrepancies that were often confusing and misleading, a new naming system for ribosomal proteins was proposed in 2014 [46]. In the new nomenclature, the names of eukaryotic cytosolic ribosomal proteins either start with an e or u, meaning eukaryote-specific or universal (*i.e.* found in both prokaryotes and eukaryotes), respectively. Here we follow the new nomenclature instead of the traditional names. For example, one of the ribosomal proteins that we will discuss later, CYH2, which was also called L27A, L28, or L29 [47-49] in previous literature, is called uL15 in the new nomenclature and in this thesis.

An actively translating ribosome consists of a large subunit (LSU, 50S in prokaryotic and 60S in eukaryotic cytosolic ribosomes), a small subunit (SSU, 30S in prokaryotic and 40S in eukaryotic cytosolic ribosomes), tRNAs, mRNA, nascent peptide, and has translation factors transiently associated with it [26]. The LSU contains the peptidyl

transferase center (PTC), which is the catalytic center of the ribosome and is responsible for peptide bond formation and peptide release [21]. Also within the LSU, spanning from the PTC to the surface of the ribosome, is the polypeptide exit tunnel, which can accommodate up to around 40 amino acids and is involved in translation regulation and co-translational protein folding [50]. The SSU contains the decoding center, which is responsible for the fidelity of the codon-anticodon interactions and also important for mRNA quality control pathways [51]. The tRNAs are associated with both LSU and SSU, and they bridge the intersubunit space. There are three distinct tRNA binding sites in the ribosome: the aminoacyl site (A site) that accepts and decodes the incoming tRNA, the peptidyl site (P site) that holds the tRNA with the growing polypeptide, and the exit site (E site) where the deacylated tRNA binds before dissociating from the ribosome [52].

1.3 Cryo-electron microscopy

The major techniques for ribosome structure determination include X-ray crystallography [53] and cryo-electron microscopy (cryo-EM) [42]. In this study, we used cryo-EM, because cryo-EM allows us to study ribosomes using near-native conditions [42].

In 2017, Jacques Dubochet, Joachim Frank, and Richard Henderson were awarded the Nobel Prize in Chemistry “for developing cryo-electron microscopy for the high-

resolution structure determination of biomolecules in solution" [54]. Dubochet and colleagues developed the method to vitrify aqueous samples by rapidly plunging them in liquid ethane. This vitrification method does not damage biomolecules as crystallization can, and also results in a decreased level of background noise because the vitrified water interferes with electrons more uniformly [55]. Frank and colleagues established the concept of single-particle reconstruction, establishing the structure determination of particles that do not have any symmetry [56, 57]. Henderson and his colleagues overcame the difficulty that electron beams destroy biological structures by blasting a weaker electron beam through the sample and taking pictures from many different angles under the electron microscope, and solved the structure of bacteriorhodopsin, a light-driven proton pump and membrane protein from *Halobacterium halobium*, at atomic resolution in 1990 [58].

The cryo-EM techniques have been evolving rapidly. The electron source has been switched from tungsten or lanthanum hexaboride filaments to the field emission gun, which has a better coherence and thus results in a better phase contrast generated by defocusing [59]. The vacuum system and the stability of the specimen stage have been improved. The camera technology has evolved from photographic film to charge-coupled devices and then to direct electron detectors [60], which have lower noise levels as well as record electrons faster, leading to an easier and better correction of the specimen's drift during imaging. The advancement of software is also revolutionizing cryo-EM. To determine the orientations of the particles in the 2D images and to

determine the 3D structure based on the 2D images, the maximum-likelihood algorithm was first introduced to EM by Frederick Sigworth in 1998 [61], and was further implemented in the software RELION by Sjors Scheres in 2012 [62]. In 2017, stochastic gradient descent, branch-and-bound maximum likelihood optimization algorithms, and Bayesian marginalization were combined in the program cryoSPARC, which speeds up the cryo-EM structure determination significantly [63]. In 2018, a new convolutional neural network particle picker was developed and added to the software EMAN2 [64]. This new method can dramatically improve the accuracy of particle picking, especially for difficult data sets such as those with low contrast, with contaminants, or those from partially denatured samples or partially assembled complexes. Also in 2018, the third major release of RELION was published [65], with both CPU-based vector acceleration and GPU support, and with new functions that can provide higher resolution reconstructions, such as per-particle refinement of CTF parameters, correction of estimated beam tile, and Bayesian polishing.

The current single-particle cryo-EM method can be summarized as follows. First, the aqueous sample containing the complex of interest is vitrified on the cryo-EM grids, and the cryo-grid is loaded into a transmission electron microscope (TEM) equipped with a vacuum system to maintain the liquid nitrogen temperature. Second, in the TEM, images are formed by directing a high-energy electron beam at the sample. Each image would contain many particles of the complex of interest, and the particles may be in the same or different orientations. The imaged particles are then boxed, extracted, and clustered. The

images in each cluster are then averaged to improve the signal-to-noise ratio. Finally, the 3D orientation of each of these average images is found, and the images are back-projected to produce a 3D Coulomb potential map [66].

The *N. crassa* ribosome-specific workflow we used can be summarized as follows. Based on the 3D Coulomb potential map of the ribosome and the sequences of the rRNA, ribosomal proteins, tRNA, and ligands, and with the help of web servers for databases and alignments such as SILVA ACT [67], web servers that predict secondary structures such as RNAfold [68], and computational modeling software such as PHENIX [69] and Rosetta [70], we generated the atomic model of the *N. crassa* ribosome, to show how it interacts with the translation inhibitor cycloheximide and at which translation step inhibition occurs.

1.4 Translation

Translation is the process of synthesizing proteins from an mRNA template. Translation uses the mRNA template, the ribosome, the tRNAs which transfer the appropriate amino acids to the corresponding codons, and translation factors. In the eukaryotic cytoplasm, translation occurs in repeated cycles with four stages, including initiation, elongation, termination, and recycling [71-73]. These four translation stages are summarized as follows.

For standard initiation (Fig. I1) [71], the eIF2–GTP–Met-tRNA^{Met}i ternary complex is formed, and then the 40S ribosomal subunit associated with eukaryotic initiation factors (eIFs) eIF1, eIF1A, and eIF3 binds to the ternary complex and eIF5 to form a ribosomal 43S preinitiation complex [74]. Separately, the eIF4F cap-binding complex, consisting of the cap-binding protein eIF4E [75], the RNA helicase and DEAD-Box protein eIF4A [76], and eIF4G which connects eIF4E and eIF4A [77], cooperates with eIF4B or eIF4H [78] to unwind the 5’ cap-proximal region of the mRNA, preparing it for 43S preinitiation complex attachment. After the mRNA is activated by the binding of the eIF4F complex at the 5' 7-methylguanosine cap and the binding of poly(A) binding protein at the 3' poly(A) tail, the 43S preinitiation complex attaches to the mRNA and scans the 5’ untranslated region (UTR) of the mRNA in a 5′ to 3′ direction until it recognizes the initiation codon [74]. The initiation Met-tRNA^{Met}i binds to the initiation codon through codon-anticodon base pairing, forming the 48S initiation complex [79]. With the eIF5-mediated hydrolysis of eIF2-bound GTP and Pi release, the initiation complex switches from an open conformation to a closed conformation and is locked onto the mRNA, followed by the joining of it with the LSU and the displacement of initiation factors including eIF2–GDP, eIF1, eIF3, eIF4B, eIF4F, and eIF5 [79]. Finally, eIF5B-bound GTP is hydrolyzed and eIF5B and eIF1A are released, leaving an assembled 80S ribosome that has an initiator tRNA in the P site and is ready for elongation [80].

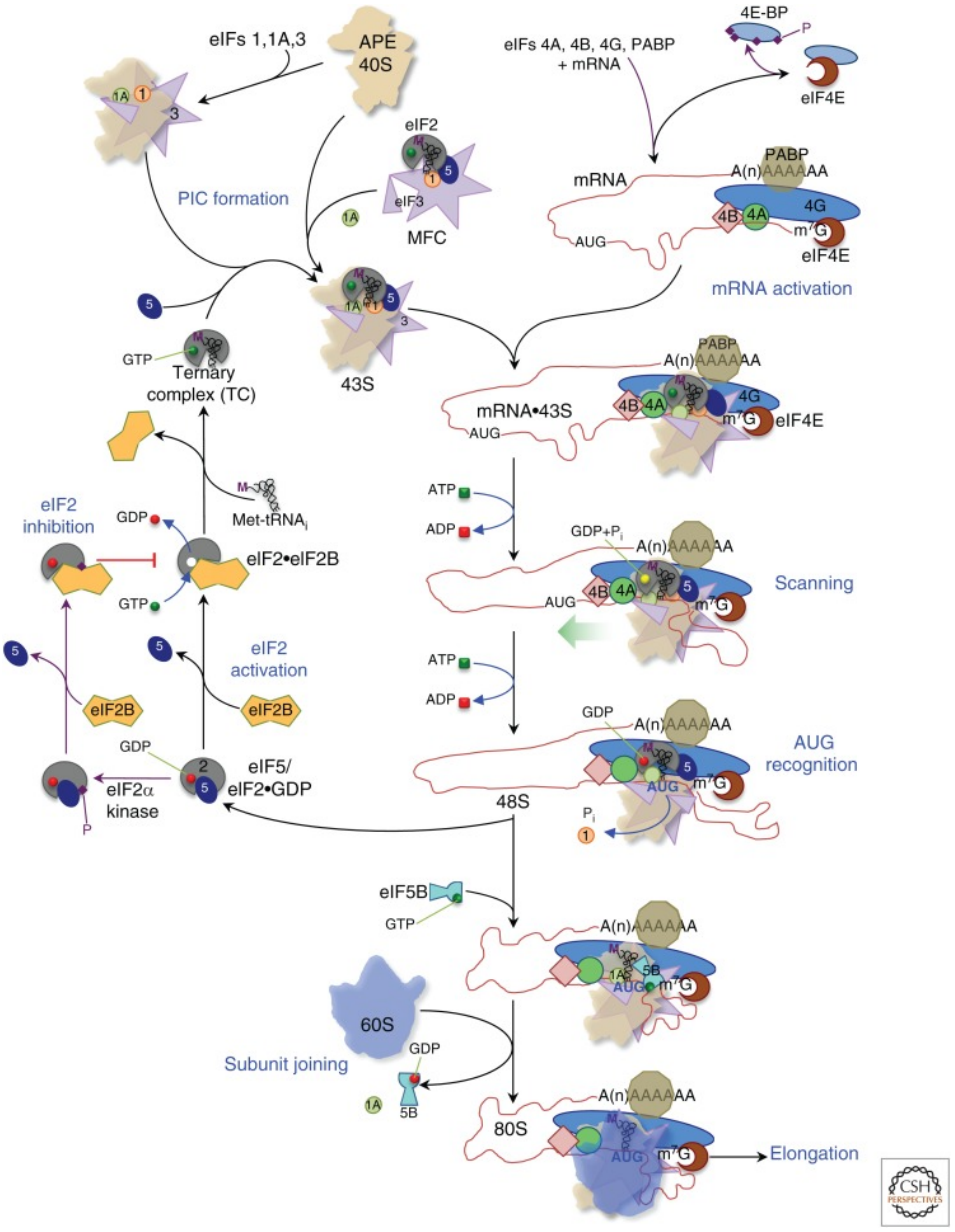

Fig. I1. Model of the general eukaryotic translation initiation pathway (Reprinted with permission from Cold Spring Harbor Laboratory Press [71]). The black arrows indicate the order of the major steps; the blue arrows indicate the nucleotide hydrolysis/inorganic phosphate release reactions; the broad green arrow shows the direction of scanning in a 5′ to 3′ direction.

At the elongation stage (Fig. I2) [72], the ribosome continues to translate each sense codon in turn on the mRNA. It involves repeated elongation cycles as amino acids are successively added to the growing polypeptide chain. In each elongation cycle, the aminoacyl-tRNA enters the empty A site, followed by nascent peptide transfer from the P-site tRNA to the A-site tRNA. Then the ribosome SSU rotates and rolls relative to the LSU, the deacylated tRNA leaves the E site (if it is present at that site), and the tRNA molecules translocate from A/A and P/P sites to the A/P and P/E sites [72]. In some peptide contexts, the translation factor eIF5A [81] binds to the ribosome to aid in peptide bond formation. In the next phase of the elongation cycle, the eEF2-GTP binds to the A site of the ribosome, promoting the back-rotation and back-rolling of the ribosome subunits as well as the translocation of the tRNA molecules to the P/P and E/E sites [82]. After that, eEF2-GDP is released from the ribosome, and an eEF1A-GTP-aminoacyl-tRNA ternary complex binds to the ribosome to start the next cycle of elongation [83].

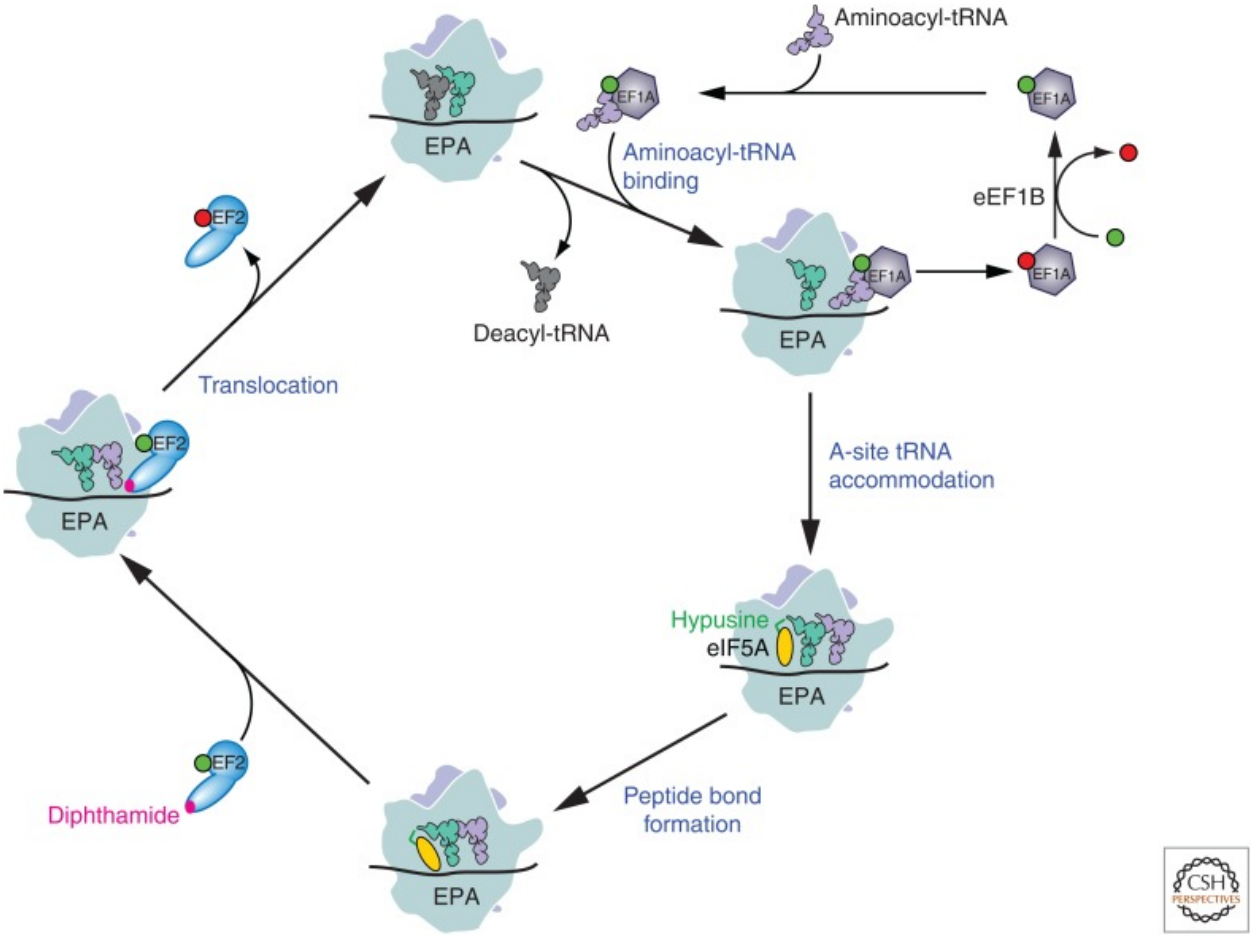

Fig. I2. Model of the eukaryotic translation elongation pathway (Reprinted with permission from Cold Spring Harbor Laboratory Press [72]). Aminoacyl-tRNA is light gray; peptidyl-tRNA is light green; deacylated tRNA is dark gray; GTP is a green ball; GDP is a red ball; EF2 is blue; eIF5A is yellow.

Termination normally occurs when an in frame mRNA stop codon enters the translating ribosome's A site [73]. This process involves at least two eukaryotic release factors (eRFs): eRF1 which regulates high-fidelity stop codon recognition and peptidyl-tRNA hydrolysis, and eRF3, which is a translational GTPase (Fig. I3) [84]. At the stop codon, the eRF1-eRF3-GTP ternary complex binds to the A site of the ribosome. Then eRF3 triggers the hydrolysis of GTP and eRF1 triggers the hydrolysis of the peptidyl-tRNA to release the nascent peptide. This results in a pre-recycling ribosome with eRF1 in the A site, a P-site tRNA, and an E-site tRNA [85].

The recycling stage is initiated by the ABCE1 (Fig. I3) [84], an essential twin-ATPase conserved in both prokaryotes and eukaryotes [86]. ABCE1 binds in the intersubunit space of the ribosome, interacting with both the 40S subunit and eRF1 [87]. ABCE1 triggers ATP hydrolysis and dissociates the post-termination complexes that have dissociated from eRF3 but still have eRF1 in the A site [88].

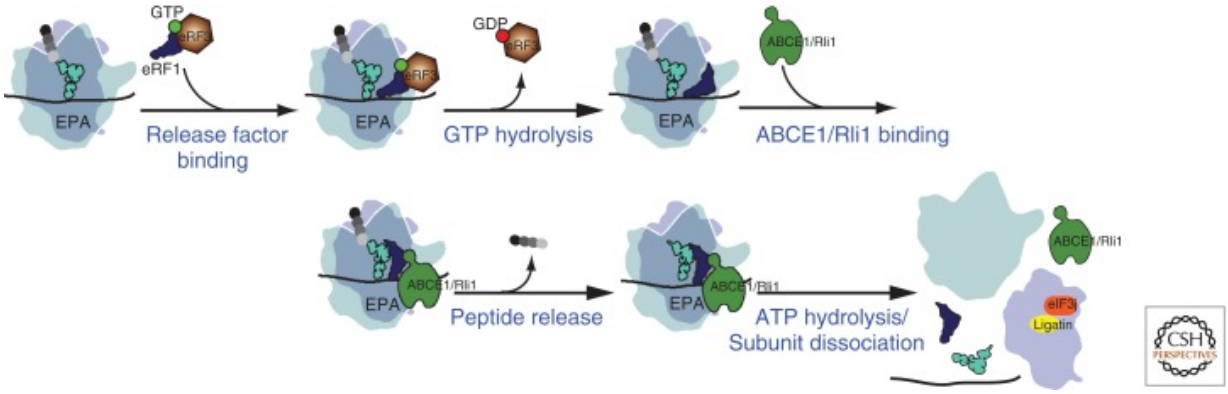

Fig. I3. Model of the eukaryotic translation termination and recycling pathway

(Reprinted with permission from Cold Spring Harbor Laboratory Press [84]).

Aminoacyl-tRNA is dark blue; peptidyl-tRNA is light green; GTP is a green ball; GDP is a red ball; eRF3 is brown; ABCE1(or Rli1 in yeast) is green.

1.5 Inhibitors of eukaryotic translation

Inhibitors of the eukaryotic cap-dependent translation are of great interest because they may contribute to a better understanding of the detailed steps in the translation mechanism and for their potential use in anti-fungal, anti-parasitic, anti-cancer, and anti-inflammatory therapies. A broad array of inhibitors of eukaryotic translation have been discovered and studied [89]. These can be broadly categorized based on the functions they affect.

Some inhibitors affect the aminoacyl-tRNA synthetases. For example, some methionyl adenylate analogues [90] and methionine analogues [91] have been shown to specifically inhibit aminoacylation of Met-tRNA by binding to Met-tRNA synthetase. Reduction of charged tRNA availability inhibits translation.

Some inhibitors affect the activity of translation factors. For example, 4EGI-1 has been shown to bind to the initiation factor and cap-binding protein eIF4E and disrupt its association with the mRNA-binding factor eIF4G, and thus suppress cap-dependent mRNA translation [92]. There are also many inhibitors known to target the initiation factor and RNA helicase eIF4A, such as the hippuristanol [93], rocaglates [94], elisabatin A, and allolaurinterol [95]. Elongation factors eEF1A and eEF2 can also be targets of inhibitors. For example, didemnin A or B [96], aplidine [97], tamandarin [96], and cytotrienin A [98] can block the elongation phase of translation by binding to

eEF1A and preventing its dissociation from the ribosome after GTP hydrolysis. The anti-fungal agent sordarin and its derivatives such as GM193663 and GR135402 can stall the elongation complex in a post-translocational state by binding to eEF2 and making it unable to dissociate from the ribosome [99].

Many important inhibitors of eukaryotic translation directly target the cytosolic ribosomes [100]. Some of them affect the termination phase of translation (such as the anticancer agent girodazole [101]), but the majority of them affect the elongation phase of translation. Some of these compounds bind to the polypeptide exit tunnel (PET) of the LSU. For example, the recently discovered PF06446846, which can reduce the plasma level of proprotein convertase subtilisin/kexin type 9 (PCSK9) and total cholesterol levels in rats, has been shown to inhibit the translation of PCSK9 by binding within the PET and inducing ribosome stalling at near codon 34 due to the altered path of the nascent peptide [102]. Others interfere with the peptidyl transferase center. These include: (1) compounds that bind to the A site, such as anisomycin [103], puromycin [104], and harringtonine [105] that bind to the A site of the LSU; (2) compounds that bind to the P site, such as anthelmycin [106] and blasticidin S [107] that bind to the P site of the LSU; (3) compounds that interfere with both A and P sites, such as sparsomycin and its derivatives [108]. Some compounds inhibit tRNA translocation by binding to the E site. For example, emetine [109] binds to the E site of the SSU, and cycloheximide and lactimidomycin [110] also bind to the E site of the LSU.

1.6 Cycloheximide

Cycloheximide (CHX, $C_{15}H_{23}NO_4$) is the most widely used laboratory inhibitor of eukaryotic protein synthesis [110]. In 1946, It was initially identified by Alma J. Whiffen, a mycologist working at Upjohn, as a product of *Streptomyces griseus* fermentation that she named actidione (diketone produced by an actinomycete); actidione inhibited the growth of fungi but not bacteria [111-113]. In 1963, CHX's function to inhibit eukaryotic protein synthesis was demonstrated using a cell-free translation system from *Saccharomyces pastorianus* [114]. The first induced mutations conferring CHX resistance were isolated and genetically mapped in the model fungus *Neurospora crassa* [115]. Two years later, the direct action of CHX to inhibit translation in a mammalian system was demonstrated using active translation lysates prepared from anucleate rabbit reticulocytes [116]. The early literature on CHX and related molecules has been thoroughly and contemporaneously reviewed [117].

In 1983, Käufer *et al* found that mutations in the *S. cerevisiae* CYH2 gene could cause resistance to CHX, and identified that the corresponding protein was ribosomal protein L29 (uL15 in the new nomenclature) and the mutation was Q37E of L29 [49]. In 1992, Kawai *et al* reported another ribosomal protein, L41 (eL41 in the new nomenclature), to be associated with *Candida maltosa*'s natural resistance to CHX [118]. In 1993, it was demonstrated that *Kluyveromyces lactis*' natural resistance to CHX was also conferred by L41 [119].

In nature, apart from some fungi such as *C. maltosa* and *K. lactis* described above, another major group of organisms that are resistant to CHX are some bacteria, such as the drug-producing *Streptomyces spp*. It had been hypothesized that it was the modification of rRNA, for example, methylation of residue A1067 in 23S ribosomal RNA in *Strept. azureus* that made them resistant to CHX [120]. However, with the development of structural biology techniques, we now know that it is not only the rRNA but also the ribosomal proteins that differ between prokaryotic and eukaryotic cytosolic ribosomes in that region (Fig. I4): A2432 and U2431 in the *E. coli* ribosome are two bacterial-specific nucleotides; eL41 in the CHX binding pocket is a protein that only exists in eukaryotic cytosolic ribosomes, but not in bacterial ribosomes [122].

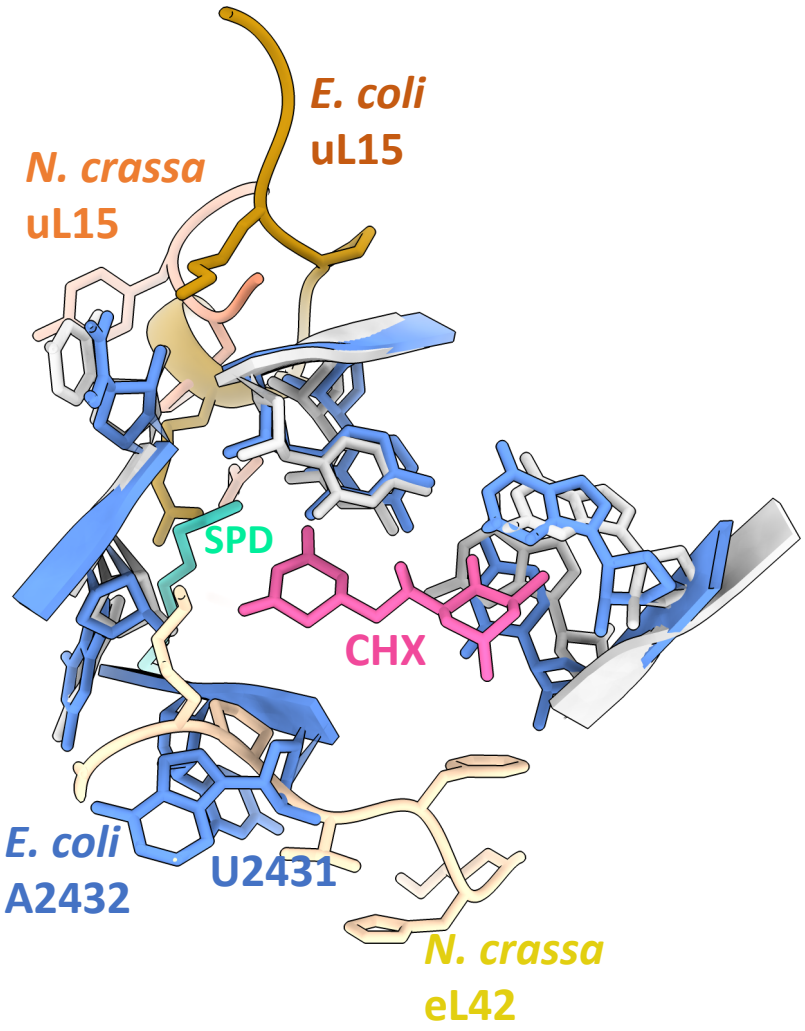

Fig. I4. Differences between *N. crassa* and *E. coli* ribosomes in the CHX binding region. Pink: CHX; cyan: SPD; orange: *N. crassa* uL15; brown: *E. coli* uL15; yellow: *N. crassa* eL42; gray: *N. crassa* rRNA; blue: *E. coli* rRNA (A2432 and U2431 are two bacterial-specific nucleotides). The *N. crassa* structure is described in Chapter II; the *E. coli* structure is obtained from PDB 4YBB.

CHX has been shown to block the elongation phase of eukaryotic translation [110] and has been widely used in experiments. One example is the polysome analysis [123]. Polysomes (polyribosomes) are ribosomes that are grouped together on a single mRNA molecule and are generally considered to be undergoing active translation. Polysome analysis is based on the separation of polysomes from the monosomes and small molecules [124], and can be used to monitor the translation status of the mRNA molecules [123]. CHX is often added to the polysome extraction procedures to "freeze" translation and to prevent the polysomes from dissociating from the mRNA molecules [125]. Another example is *in vitro* translation [16]. It has been widely used to explore the mechanism of translational events, to test the protein synthesis from different programmed mRNAs, and to test the functions of translation inhibitors [126]. CHX is added to the *in vitro* translation system to stop the synthesis of the reporter protein, or sometimes can serve as a good negative control when added at time 0. Ribosome profiling, or Ribo-Seq, is another example of experiment that often uses CHX. It can monitor translation directly by deep sequencing of the ribosome footprints, *i.e.*, the mRNA fragments that are protected by the ribosomes. CHX is added to the system when cell lysates are prepared, to keep ribosomes on the mRNA [127].

1.7 Spermidine

Spermidine (SPD, $C_7H_{19}N_3$) is a polyamine participating in various biological processes [128]. In 1678, it was first discovered by Antonie van Leeuwenhoek, as a crystalline

substance in human semen [129], but was not characterized until 1924 when Rosenheim established its structure and synthesized the compound [130]. In 1967, A. M. Liquori *et al.* established the secondary structure of SPD [131].

Since 1970 when studies of the effects of SPD on eukaryotes were initiated [132], many researchers have been interested in how SPD regulates reproduction [133], growth [134], and development [135]. Though the exact mechanism remains unclear, SPD has been shown to be essential to not only the reproductive processes in males, but also ovarian follicle development and ovulation in females, as well as embryo implantation, placental development, and embryo development [133]. The external supply of SPD has been shown to have longevity-enhancing effects on yeast, nematodes, flies, and mice [136]. There is also epidemiological evidence suggesting that the increased dietary SPD intake is linked to increased life span in humans [137]. By inducing autophagy, SPD has dual effects on cancer: it could prevent tumor initiation but could also promote tumor progression [138], and therefore has been considered a biomarker for cancer diagnosis and a target for cancer therapy.

SPD has been demonstrated to be involved in translation. Cohen *et al.* reported in 1969 that some SPD molecules were associated with rRNA [139] and some were associated with tRNA in *E. coli* [140]. Mandal *et al.* showed that depletion of SPD resulted in an arrest in protein synthesis, loss of polysomes, and suppressed cell growth in mammalian cells [141]. SPD has been shown to enhance translational efficiency and accuracy in

cell-free translation systems [142]. It is a polycation and is thought to function similarly to Mg^{2+} [143]. SPD has also been shown to affect the translation factor eIF5A by serving as the amino-butyl group donor for the post-translational modification of eIF5A [144].

1.8 Previously published structures of ribosomes bound with CHX

The first structure of the ribosome bound with CHX was determined in 2014, using X-ray crystallography [121] (Fig. I5. A). In this study, *S. cerevisiae* vacant 80S ribosomes were purified and then incubated with CHX prior to crystallization. The resulting structure (PDB ID: 4U3U) shows that CHX binds to the E site of the LSU, and the binding pocket consists of some universally conserved nucleotides of the 23S rRNA, ribosomal proteins eL42 and uL15, and a Mg^{2+} ion. Based on the position of the CHX-binding site and previous biochemical data, CHX was proposed to compete with the tRNA CCA-end in binding to the E-site of the LSU.

The first structure of human ribosome containing CHX was determined in 2016, using cryo-EM ([145], EMD-4070, PDB ID: 5LKS) (Fig. I5. B). In this study, ribosomes were purified from HeLa cells and CHX was added subsequently. The structures of ribosomes with or without CHX were compared. Though neither structure has A- or P- site tRNA, the comparison revealed that CHX binds to the E site on the LSU and also results in a disordered L1 region.

Structures of the *S. cerevisiae* ribosome [121] and the human ribosome [145] containing CHX tightly bound at the ribosome E site have given significant insight into its mechanism of action. Based on the position of the CHX-binding site, CHX is proposed to interfere with the translocation of P-site tRNA to the E site. However, both of these CHX-containing structures were obtained using vacant ribosomes lacking tRNA, and therefore did not establish the specific step(s) in the translation cycle at which CHX inhibits elongation. If E-site translocation is blocked as predicted, then this structure is consistent with ribosomes in the pre-translocation (PRE) state with either the nascent peptide on the P-site tRNA and the incoming amino acid on A-site tRNA or in the PRE state with the nascent peptide transferred to A-site tRNA. Both models appear in the literature, with single-molecule FRET studies supporting the latter [110, 146]. Furthermore, the ribosome subunits can have different relative rotational orientations even while containing A/A and P/P tRNA: a classical PRE state can be discriminated from a rotated PRE* state [147]. Thus, there are a variety of states in which CHX could potentially arrest the ribosome even prior to tRNA translocation.

In 2020, more structures of human ribosomes bound with CHX were reported [148]. The authors aimed to isolate translating ribosomes in the presence of CHX and determine the dynamics of uS19 C-terminal tail movement during the elongation cycle. They used the affinity purification process, during which CHX was maintained in buffers at a concentration of 100 μg/mL. The resulting cryo-EM data revealed the presence of ribosomes in three distinct major conformations, including classical-PRE (EMD-10668,

PDB ID: 6Y0G) (Fig. I5. C), hybrid-PRE (EMD-10690, PDB ID: 6Y57), and the POST (EMD-10674, PDB ID: 6Y2L) states. The ribosome in the classical-PRE state (*i.e.* post-decoding pre-translocation state with A/A tRNA and P/P tRNA) contains CHX bound at the E site of the LSU; the uS19 C-terminal tail is well resolved. The ribosome in the hybrid-PRE state (*i.e.* rotated state with A/P tRNA and P/E tRNA) does not contain CHX; the uS19 C-terminal tail is disordered. The ribosome in the POST state (*i.e.* post-translocation state with P/P tRNA) contains CHX bound at the E site of the LSU; the uS19 C-terminal tail is disordered. Because of the large fraction of ribosomes lacking CHX in the hybrid-PRE state, we hypothesized that during the purification process, some CHX molecules dissociated from the ribosomes and resulted in the significant subpopulations of ribosomes lacking CHX.

An *S. cerevisiae* 80S ribosome in complex with eIF5A and decoding A-site and P-site tRNAs (EMD-10537, PDB ID: 6TNU) (Fig. I5. D) also contains CHX [149]. In the peptidyl transferase center, well-resolved extra density was observed, indicating the existence of a nascent peptide attached to the CCA-end of the A-site tRNA. However, in the presence of eIF5A, the L1 stalk is structured, and the E site's structure, therefore, differs from that of the previously published ribosome structures bound with CHX. Furthermore, though the relative position between the LSU and SSU in this ribosome resembled that of the human classical-PRE ribosome, the uS19 C-terminal tail is not resolved in this structure, distinct from that in the human classical-PRE ribosome which has a structured uS19 C-terminal tail (Fig. I6.). These indicate that the ribosome

containing both eIF5A and CHX is not in the same state as ribosomes containing CHX alone.

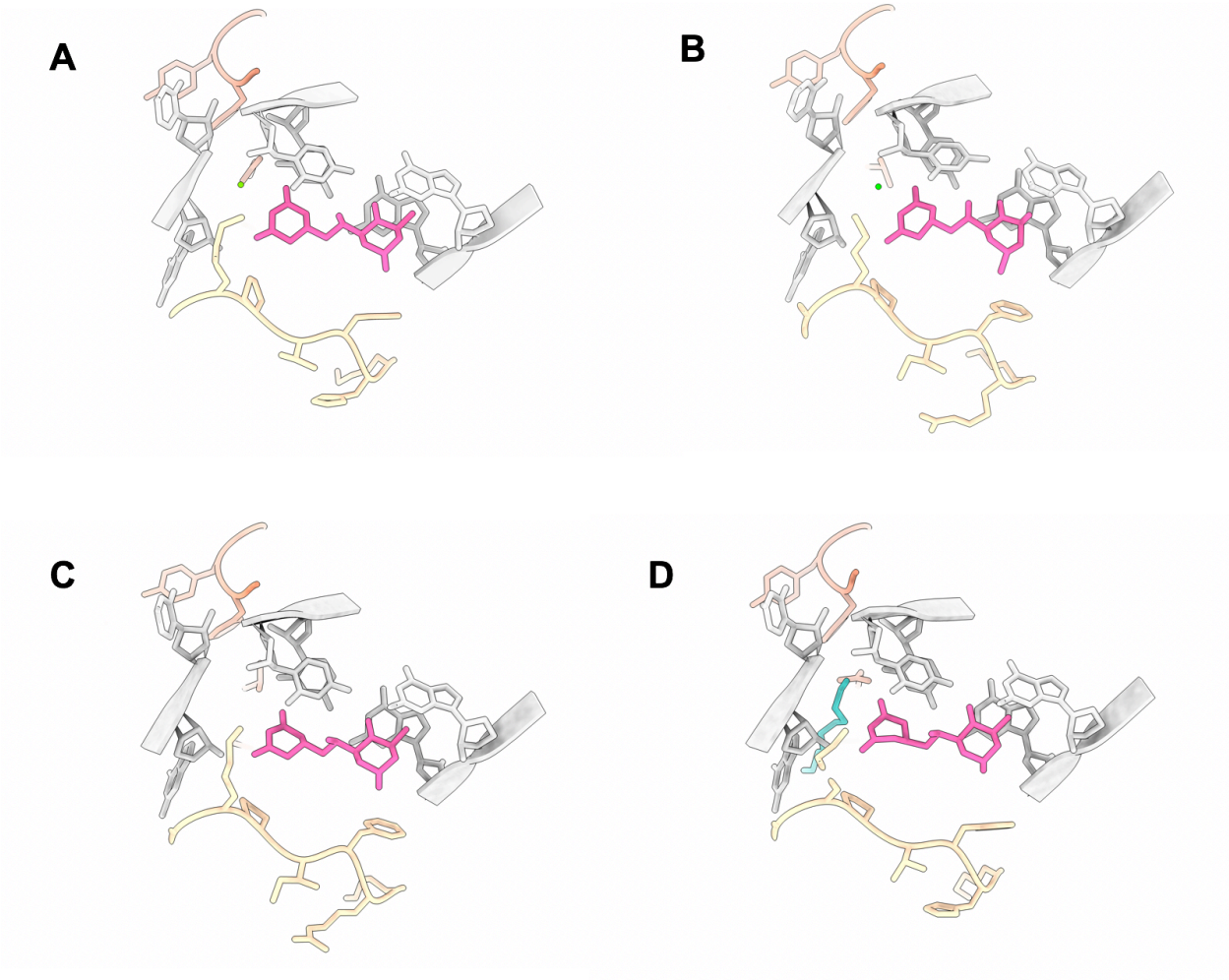

Fig. I5. Models of cycloheximide (CHX) binding pocket in the previously published structures of ribosomes bound with CHX, including (A) *S. cerevisiae* ribosome crystal structure (PDB ID: 4U3U); (B) human vacant ribosome (PDB ID: 5LKS); (C) human ribosome obtained using affinity purification (PDB ID: 6Y0G); (D) *S. cerevisiae* ribosome in complex with eIF5A (PDB ID: 6TNU). CHX is fuchsia; SPD is cyan; rRNA is gray; eL42 and uL15 are yellow and orange, respectively.

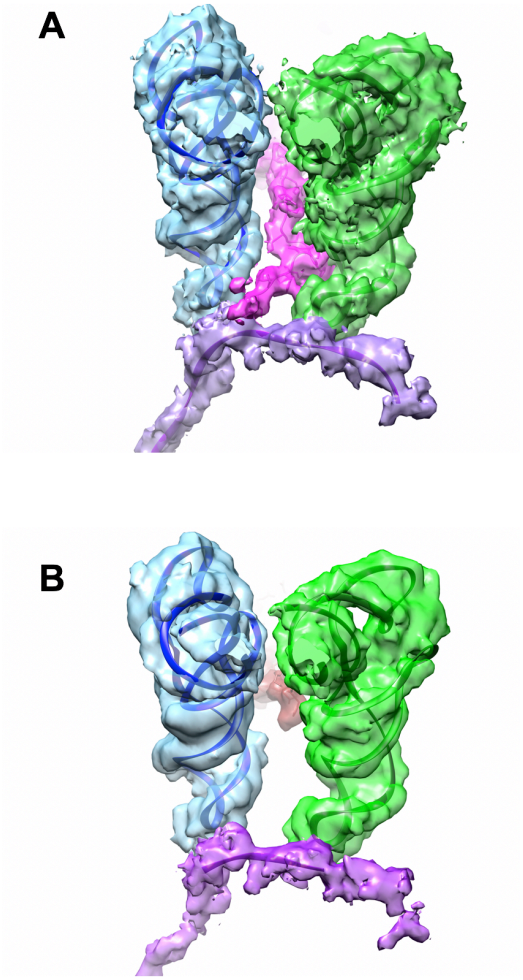

Fig. I6. The uS19 C-terminal tail in the yeast ribosome structure 6TNU is not resolved, distinct from that in the human classical-PRE ribosome which has a structured uS19 C-terminal tail. (A) Human uS19 position (fuchsia) in the classical-PRE ribosome (EMD: 10668, PDB ID: 6Y0G). (B) *S. cerevisiae* uS19 position (red) in the ribosome in complex with eIF5A (EMD: 10537, PDB ID: 6TNU). The density of mRNA is low-pass-filtered to 10 Å for clarity, and the surface 807 is displayed in purple. tRNA densities (green: A-site tRNA, blue: P-site tRNA) were extracted from the cryo-EM map using ChimeraX.

Looking back at the literature reporting the structures of the ribosomes bound with CHX, we proposed that our experimental design should be improved in at least four ways: (1) Instead of using vacant ribosome, we should use actively translating ribosomes that are associated with tRNA, mRNA, and nascent peptide. (2) Instead of adding CHX after the ribosome purification step, we should add CHX before harvesting, in the polysome extraction step, and maintain it throughout all subsequent procedures until the vitrification step for Cryo-EM. (3) Instead of using up to 100 μg/mL of CHX as all previous studies did [121, 145, 148, 149], we should increase the amount of CHX. This is because CHX binding is reversible [150]. Recent measurements of the dissociation constant of CHX from ribosomes yielded values of 1 ± 0.4 μM for *S. cerevisiae* ribosomes and 4 ± 1 μM for human ribosomes [151]. A 1 μM dissociation constant corresponds to a half-life of 0.7 s for a first-order reaction [152]. An insufficient amount of CHX or lack of CHX in any step during the process may cause the dissociation and rebinding of CHX with tRNA translation occurring in between, and may lead to artifacts in the final structure. The solubility of CHX in water is approximately 20 mg/ml, so we chose 2 mg/ml as the final concentration of CHX in all media or buffer throughout the experiment. (4) The purification process should maintain the native condition as much as possible. We should avoid affinity purification if possible, since it may increase the chance of getting partially assembled complexes [148].

1.9 Introduction of the work in this thesis

Here we determined the cryo-electron microscopic (cryo-EM) structure of translating *N. crassa* ribosomes with CHX at 2.7 Å resolution. To accomplish this, we isolated polysomes from actively growing cells to which CHX was added and maintained CHX at a high concentration throughout all subsequent procedures until the vitrification step of cryo-EM sample preparation. We built a model for the *N. crassa* ribosome that differs from *S. cerevisiae* ribosomes and more closely resembles higher eukaryotic ribosomes in that it contains ribosomal protein eL28. Comparisons of structures with CHX bound to ribosomes showed that the CHX-binding position is highly conserved in *N. crassa*, *S. cerevisiae*, and human ribosomes. However, unlike the canonical CHX-bound structures of vacant yeast [121] and human ribosomes [145] which contained an Mg^{2+} ion adjacent to the CHX-binding pocket, the *N. crassa* ribosome contained spermidine (SPD) in place of the Mg^{2+} ion. We sequenced previously identified *N. crassa* mutations that confer CHX-resistance. All amino acid changes in these mutants, including an amino acid change at a previously unidentified position among eukaryotic mutations that confer CHX-resistance, map to conserved residues in the CHX-binding pocket. In addition, P/P and A/A site tRNAs were present in the *N. crassa* structure, and the nascent peptide was resolved on the A-site tRNA. Finally, CHX did not appear to interfere with termination as it does with elongation in an *N. crassa* cell-free translation extract, consistent with CHX interfering with translocation of tRNA to the E site but not peptidyl-transfer events at the A site. The observation that terminating ribosomes are not arrested by CHX could

be significant for analyses of the levels of ribosomes mapping to termination codons when CHX is included in ribosome profiling analyses.

This work provides a structural basis for a mechanistic understanding of CHX action. It also provides a new high-resolution model for a fungal ribosome that differs from the *S. cerevisiae* ribosome.

1.10 References

1. Davis, R.H. and D.D. Perkins, *Neurospora: a model of model microbes.* Nature Reviews Genetics, 2002. 3(5): p. 397-403.
2. Beadle, G.W. and E.L. Tatum, *Genetic Control of Biochemical Reactions in Neurospora.* Proc Natl Acad Sci U S A, 1941. 27(11): p. 499-506.
3. Schmit, J.C. and S. Brody, *Biochemical genetics of Neurospora crassa conidial germination.* Bacteriol Rev, 1976. 40(1): p. 1-41.
4. Mishra, N.C., *Genetics and Molecular Biology of Neurospora crassa**This article is dedicated to the memory of the late Professor E. L. Tatum on the fiftieth anniversary of the formulation of the one gene-one enzyme hypothesis*, in *Advances in Genetics*, J.G. Scandalios and T.R.F. Wright, Editors. 1991, Academic Press. p. 1-62.
5. Strauss, B.S., *Biochemical Genetics and Molecular Biology: The Contributions of George Beadle and Edward Tatum.* Genetics, 2016. 203(1): p. 13-20.

6. Galagan, J.E., et al., *The genome sequence of the filamentous fungus Neurospora crassa.* Nature, 2003. 422(6934): p. 859-868.

7. Baker, C.L., J.J. Loros, and J.C. Dunlap, *The circadian clock of Neurospora crassa.* FEMS Microbiol Rev, 2012. 36(1): p. 95-110.

8. Hammond, T.M., *Sixteen Years of Meiotic Silencing by Unpaired DNA.* Adv Genet, 2017. 97: p. 1-42.

9. Kuwabara, K., et al., *Analysis of localization of cell-cycle regulators in Neurospora crassa.* Fungal Biol, 2020. 124(7): p. 613-618.

10. Herzog, S., M.R. Schumann, and A. Fleißner, *Cell fusion in Neurospora crassa.* Curr Opin Microbiol, 2015. 28: p. 53-9.

11. Wei, J., et al., *The stringency of start codon selection in the filamentous fungus Neurospora crassa.* J Biol Chem, 2013. 288(13): p. 9549-62.

12. Karki, S., et al., *Circadian clock control of eIF2α phosphorylation is necessary for rhythmic translation initiation.* Proc Natl Acad Sci U S A, 2020. 117(20): p. 10935-10945.

13. Honda, S., et al., *Establishment of Neurospora crassa as a model organism for fungal virology.* Nat Commun, 2020. 11(1): p. 5627.

14. Itoh, Y., et al., *Analysis of translating mitoribosome reveals functional characteristics of translation in mitochondria of fungi.* Nat Commun, 2020. 11(1): p. 5187.

15. Wang, Z. and M.S. Sachs, *Arginine-specific regulation mediated by the Neurospora crassa arg-2 upstream open reading frame in a homologous, cell-free in vitro translation system.* J Biol Chem, 1997. 272(1): p. 255-61.

16. Wang, Z. and M.S. Sachs, *Ribosome stalling is responsible for arginine-specific translational attenuation in Neurospora crassa.* Mol Cell Biol, 1997. 17(9): p. 4904-13.

17. Ivanov, I.P., et al., *Translation Initiation from Conserved Non-AUG Codons Provides Additional Layers of Regulation and Coding Capacity.* mBio, 2017. 8(3).

18. Caster, S.Z., et al., *Circadian clock regulation of mRNA translation through eukaryotic elongation factor eEF-2.* Proc Natl Acad Sci U S A, 2016. 113(34): p. 9605-10.

19. Fang, P., C. Wu, and M.S. Sachs, *Neurospora crassa supersuppressor mutants are amber codon-specific.* Fungal Genetics and Biology, 2002. 36(3): p. 167-175.

20. Yu, C.H., et al., *Codon Usage Influences the Local Rate of Translation Elongation to Regulate Co-translational Protein Folding.* Mol Cell, 2015. 59(5): p. 744-54.

21. Wei, J., C. Wu, and M.S. Sachs, *The arginine attenuator peptide interferes with the ribosome peptidyl transferase center.* Mol Cell Biol, 2012. 32(13): p. 2396-406.

22. Heintzen, C. and Y. Liu, *The Neurospora crassa circadian clock.* Adv Genet, 2007. 58: p. 25-66.

23. McCluskey, K., A. Wiest, and M. Plamann, *The Fungal Genetics Stock Center: a repository for 50 years of fungal genetics research.* J Biosci, 2010. 35(1): p. 119-26.

24. Brenner, S., *RNA, ribosomes, and protein synthesis.* Cold Spring Harb Symp Quant Biol, 1961. 26: p. 101-10.

25. Rivera, M.C., B. Maguire, and J.A. Lake, *Purification of 70S ribosomes.* Cold Spring Harb Protoc, 2015. 2015(3): p. 300-2.

26. Wilson, D.N. and J.H. Doudna Cate, *The structure and function of the eukaryotic ribosome.* Cold Spring Harb Perspect Biol, 2012. 4(5).

27. Greber, B.J. and N. Ban, *Structure and Function of the Mitochondrial Ribosome.* Annu Rev Biochem, 2016. 85: p. 103-32.

28. Zoschke, R. and R. Bock, *Chloroplast Translation: Structural and Functional Organization, Operational Control, and Regulation.* Plant Cell, 2018. 30(4): p. 745-770.

29. Tiller, N. and R. Bock, *The translational apparatus of plastids and its role in plant development.* Mol Plant, 2014. 7(7): p. 1105-20.

30. de Vries, H. and R. Koogh-Schuuring, *Physicochemical characteristics of isolated 55-S mitochondrial ribosomes from rat-liver.* Biochem Biophys Res Commun, 1973. 54(1): p. 308-14.

31. O'Brien, T.W., *Properties of human mitochondrial ribosomes.* IUBMB Life, 2003. 55(9): p. 505-13.

32. Watson, Z.L., et al., *Structure of the bacterial ribosome at 2 Å resolution.* Elife, 2020. 9.

33. Graf, M., et al., *Cryo-EM structure of the spinach chloroplast ribosome reveals the location of plastid-specific ribosomal proteins and extensions.* Nucleic Acids Res, 2017. 45(5): p. 2887-2896.

34. Lee, H.C., et al., *qiRNA is a new type of small interfering RNA induced by DNA damage.* Nature, 2009. 459(7244): p. 274-7.

35. Selker, E.U., et al., *Dispersed 5S RNA genes in N. crassa: structure, expression and evolution.* Cell, 1981. 24(3): p. 819-28.

36. Selker, E. and C. Yanofsky, *Nucleotide sequence and conserved features of the 5.8 S rRNA coding region of Neurospora crassa.* Nucleic Acids Res, 1979. 6(7): p. 2561-7.

37. Rodnina, M.V. and W. Wintermeyer, *The ribosome goes Nobel.* Trends Biochem Sci, 2010. 35(1): p. 1-5.

38. Clemons, W.M., Jr., et al., *Structure of a bacterial 30S ribosomal subunit at 5.5 A resolution.* Nature, 1999. 400(6747): p. 833-40.

39. Schmeing, T.M., et al., *A pre-translocational intermediate in protein synthesis observed in crystals of enzymatically active 50S subunits.* Nat Struct Biol, 2002. 9(3): p. 225-30.

40. Yonath, A., *The search and its outcome: high-resolution structures of ribosomal particles from mesophilic, thermophilic, and halophilic bacteria at various functional states.* Annu Rev Biophys Biomol Struct, 2002. 31: p. 257-73.

41. Waudby, C.A., et al., *Protein folding on the ribosome studied using NMR spectroscopy.* Prog Nucl Magn Reson Spectrosc, 2013. 74(100): p. 57-75.

42. Brown, A. and S. Shao, *Ribosomes and cryo-EM: a duet.* Curr Opin Struct Biol, 2018. 52: p. 1-7.

43. Ben-Shem, A., et al., *The structure of the eukaryotic ribosome at 3.0 Å resolution.* Science, 2011. 334(6062): p. 1524-9.

44. Klinge, S., et al., *Crystal structure of the eukaryotic 60S ribosomal subunit in complex with initiation factor 6.* Science, 2011. 334(6058): p. 941-8.

45. Rabl, J., et al., *Crystal structure of the eukaryotic 40S ribosomal subunit in complex with initiation factor 1.* Science, 2011. 331(6018): p. 730-6.

46. Ban, N., et al., *A new system for naming ribosomal proteins.* Curr Opin Struct Biol, 2014. 24: p. 165-9.

47. Kreader, C.A. and J.E. Heckman, *Isolation and characterization of a Neurospora crassa ribosomal protein gene homologous to CYH2 of yeast.* Nucleic Acids Res, 1987. 15(21): p. 9027-42.

48. Ramírez, M., et al., *Genetic instability of heterozygous, hybrid, natural wine yeasts.* Appl Environ Microbiol, 2004. 70(8): p. 4686-91.

49. Käufer, N.F., et al., *Cycloheximide resistance in yeast: the gene and its protein.* Nucleic Acids Res, 1983. 11(10): p. 3123-35.

50. Wu, C., et al., *Arginine changes the conformation of the arginine attenuator peptide relative to the ribosome tunnel.* J Mol Biol, 2012. 416(4): p. 518-33.

51. Chandrasekaran, V., et al., *Mechanism of ribosome stalling during translation of a poly(A) tail.* Nat Struct Mol Biol, 2019. 26(12): p. 1132-1140.

52. Burkhardt, N., et al., *Ribosomal tRNA binding sites: three-site models of translation.* Crit Rev Biochem Mol Biol, 1998. 33(2): p. 95-149.

53. Moore, P.B., *The ribosome returned.* J Biol, 2009. 8(1): p. 8.

54. Shen, P.S., *The 2017 Nobel Prize in Chemistry: cryo-EM comes of age.* Anal Bioanal Chem, 2018. 410(8): p. 2053-2057.

55. Dubochet, J., et al., *Cryo-electron microscopy of vitrified specimens.* Q Rev Biophys, 1988. 21(2): p. 129-228.

56. Frank, J., *Averaging of low exposure electron micrographs of non-periodic objects.* Ultramicroscopy, 1975. 1(2): p. 159-62.

57. Frank, J., et al., *Reconstruction of glutamine synthetase using computer averaging.* Ultramicroscopy, 1978. 3(3): p. 283-90.

58. Henderson, R., et al., *Model for the structure of bacteriorhodopsin based on high-resolution electron cryo-microscopy.* J Mol Biol, 1990. 213(4): p. 899-929.

59. Crewe, A., et al., *Electron Gun Using a Field Emission Source.* Review of Scientific Instruments, 1968. 39: p. 576-583.

60. Fromm, S.A., et al., *Seeing tobacco mosaic virus through direct electron detectors.* J Struct Biol, 2015. 189(2): p. 87-97.

61. Sigworth, F.J., *A maximum-likelihood approach to single-particle image refinement.* J Struct Biol, 1998. 122(3): p. 328-39.

62. Scheres, S.H., *RELION: implementation of a Bayesian approach to cryo-EM structure determination.* J Struct Biol, 2012. 180(3): p. 519-30.

63. Punjani, A., et al., *cryoSPARC: algorithms for rapid unsupervised cryo-EM structure determination.* Nat Methods, 2017. 14(3): p. 290-296.

64. Bell, J.M., et al., *New software tools in EMAN2 inspired by EMDatabank map challenge.* J Struct Biol, 2018. 204(2): p. 283-290.

65. Zivanov, J., et al., *New tools for automated high-resolution cryo-EM structure determination in RELION-3.* Elife, 2018. 7.

66. Wu, M. and G.C. Lander, *Present and Emerging Methodologies in Cryo-EM Single-Particle Analysis.* Biophys J, 2020. 119(7): p. 1281-1289.

67. Quast, C., et al., *The SILVA ribosomal RNA gene database project: improved data processing and web-based tools.* Nucleic Acids Research, 2012. 41(D1): p. D590-D596.

68. Lorenz, R., et al., *ViennaRNA Package 2.0.* Algorithms for Molecular Biology, 2011. 6(1): p. 26.

69. Liebschner, D., et al., *Macromolecular structure determination using X-rays, neutrons and electrons: recent developments in Phenix.* Acta Crystallogr D Struct Biol, 2019. 75(Pt 10): p. 861-877.

70. Das, R. and D. Baker, *Macromolecular modeling with rosetta.* Annu Rev Biochem, 2008. 77: p. 363-82.

71. Merrick, W.C. and G.D. Pavitt, *Protein Synthesis Initiation in Eukaryotic Cells.* Cold Spring Harb Perspect Biol, 2018. 10(12).

72. Dever, T.E., J.D. Dinman, and R. Green, *Translation Elongation and Recoding in Eukaryotes.* Cold Spring Harb Perspect Biol, 2018. 10(8).

73. Hellen, C.U.T., *Translation Termination and Ribosome Recycling in Eukaryotes.* Cold Spring Harb Perspect Biol, 2018. 10(10).

74. Hinnebusch, A.G., *The scanning mechanism of eukaryotic translation initiation.* Annu Rev Biochem, 2014. 83: p. 779-812.

75. Batool, A., S. Aashaq, and K.I. Andrabi, *Eukaryotic initiation factor 4E (eIF4E): A recap of the cap-binding protein.* J Cell Biochem, 2019. 120(9): p. 14201-14212.

76. Tauber, D., et al., *Modulation of RNA Condensation by the DEAD-Box Protein eIF4A.* Cell, 2020. 180(3): p. 411-426.e16.

77. Gulay, S., et al., *Distinct interactions of eIF4A and eIF4E with RNA helicase Ded1 stimulate translation in vivo.* Elife, 2020. 9.

78. Rozovsky, N., A.C. Butterworth, and M.J. Moore, *Interactions between eIF4AI and its accessory factors eIF4B and eIF4H.* Rna, 2008. 14(10): p. 2136-48.

79. Eliseev, B., et al., *Structure of a human cap-dependent 48S translation pre-initiation complex.* Nucleic Acids Res, 2018. 46(5): p. 2678-2689.

80. Nag, N., et al., *eIF1A/eIF5B interaction network and its functions in translation initiation complex assembly and remodeling.* Nucleic Acids Res, 2016. 44(15): p. 7441-56.

81. Schuller, A.P., et al., *eIF5A Functions Globally in Translation Elongation and Termination.* Mol Cell, 2017. 66(2): p. 194-205.e5.

82. Kaul, G., G. Pattan, and T. Rafeequi, *Eukaryotic elongation factor-2 (eEF2): its regulation and peptide chain elongation.* Cell Biochem Funct, 2011. 29(3): p. 227-34.

83. Sasikumar, A.N., W.B. Perez, and T.G. Kinzy, *The many roles of the eukaryotic elongation factor 1 complex.* Wiley Interdiscip Rev RNA, 2012. 3(4): p. 543-55.

84. Dever, T.E. and R. Green, *The elongation, termination, and recycling phases of translation in eukaryotes.* Cold Spring Harb Perspect Biol, 2012. 4(7): p. a013706.

85. Beißel, C., et al., *Translation termination depends on the sequential ribosomal entry of eRF1 and eRF3.* Nucleic Acids Res, 2019. 47(9): p. 4798-4813.

86. Gouridis, G., et al., *ABCE1 Controls Ribosome Recycling by an Asymmetric Dynamic Conformational Equilibrium.* Cell Rep, 2019. 28(3): p. 723-734.e6.

87. Preis, A., et al., *Cryoelectron microscopic structures of eukaryotic translation termination complexes containing eRF1-eRF3 or eRF1-ABCE1.* Cell Rep, 2014. 8(1): p. 59-65.

88. Pisarev, A.V., et al., *The role of ABCE1 in eukaryotic posttermination ribosomal recycling.* Mol Cell, 2010. 37(2): p. 196-210.

89. Dmitriev, S.E., D.O. Vladimirov, and K.A. Lashkevich, *A Quick Guide to Small-Molecule Inhibitors of Eukaryotic Protein Synthesis.* Biochemistry (Mosc), 2020. 85(11): p. 1389-1421.

90. Lee, J., et al., *Methionyl adenylate analogues as inhibitors of methionyl-tRNA synthetase.* Bioorg Med Chem Lett, 1999. 9(10): p. 1365-70.

91. Lee, J., et al., *Methionine analogues as inhibitors of methionyl-tRNA synthetase.* Bioorg Med Chem Lett, 1998. 8(24): p. 3511-4.

92. Takrouri, K., et al., *Structure-activity relationship study of 4EGI-1, small molecule eIF4E/eIF4G protein-protein interaction inhibitors.* Eur J Med Chem, 2014. 77: p. 361-77.

93. Cencic, R. and J. Pelletier, *Hippuristanol - A potent steroid inhibitor of eukaryotic initiation factor 4A.* Translation (Austin), 2016. 4(1): p. e1137381.

94. Chu, J., et al., *Amidino-Rocaglates: A Potent Class of eIF4A Inhibitors.* Cell Chem Biol, 2019. 26(11): p. 1586-1593.e3.

95. Tillotson, J., et al., *ATP-competitive, marine derived natural products that target the DEAD box helicase, eIF4A.* Bioorg Med Chem Lett, 2017. 27(17): p. 4082-4085.

96. Marco, E., et al., *Structural basis for the binding of didemnins to human elongation factor eEF1A and rationale for the potent antitumor activity of these marine natural products.* J Med Chem, 2004. 47(18): p. 4439-52.

97. Losada, A., et al., *Translation Elongation Factor eEF1A2 is a Novel Anticancer Target for the Marine Natural Product Plitidepsin.* Sci Rep, 2016. 6: p. 35100.

98. Lindqvist, L., et al., *Inhibition of translation by cytotrienin A--a member of the ansamycin family.* Rna, 2010. 16(12): p. 2404-13.

99. Capa, L., et al., *Translation elongation factor 2 is part of the target for a new family of antifungals.* Antimicrob Agents Chemother, 1998. 42(10): p. 2694-9.

100. Yusupova, G. and M. Yusupov, *Crystal structure of eukaryotic ribosome and its complexes with inhibitors.* Philos Trans R Soc Lond B Biol Sci, 2017. 372(1716).

101. Colson, G., et al., *Mode of action of the antitumor compound girodazole (RP 49532A, NSC 627434).* Biochem Pharmacol, 1992. 43(8): p. 1717-23.

102. Lintner, N.G., et al., *Selective stalling of human translation through small-molecule engagement of the ribosome nascent chain.* PLoS Biol, 2017. 15(3): p. e2001882.

103. Blaha, G., et al., *Mutations outside the anisomycin-binding site can make ribosomes drug-resistant.* J Mol Biol, 2008. 379(3): p. 505-19.

104. Cary, G.A., et al., *Identification and characterization of a drug-sensitive strain enables puromycin-based translational assays in Saccharomyces cerevisiae.* Yeast, 2014. 31(5): p. 167-78.

105. Fresno, M., A. Jiménez, and D. Vázquez, *Inhibition of translation in eukaryotic systems by harringtonine.* Eur J Biochem, 1977. 72(2): p. 323-30.

106. Rodriguez-Fonseca, C., R. Amils, and R.A. Garrett, *Fine structure of the peptidyl transferase centre on 23 S-like rRNAs deduced from chemical probing of antibiotic-ribosome complexes.* J Mol Biol, 1995. 247(2): p. 224-35.

107. Svidritskiy, E., et al., *Blasticidin S inhibits translation by trapping deformed tRNA on the ribosome.* Proc Natl Acad Sci U S A, 2013. 110(30): p. 12283-8.

108. Barbacid, M., M. Fresno, and D. Vazquez, *Inhibitors of polypeptide elongation on yeast polysomes.* J Antibiot (Tokyo), 1975. 28(6): p. 453-62.

109. Wong, W., et al., *Cryo-EM structure of the Plasmodium falciparum 80S ribosome bound to the anti-protozoan drug emetine.* Elife, 2014. 3.

110. Schneider-Poetsch, T., et al., *Inhibition of eukaryotic translation elongation by cycloheximide and lactimidomycin.* Nat Chem Biol, 2010. 6(3): p. 209-217.

111. Whiffen, A.J., N. Bohonos, and R.L. Emerson, *The Production of an Antifungal Antibiotic by Streptomyces griseus.* J Bacteriol, 1946. 52(5): p. 610-1.

112. Leach, B.E., J.H. Ford, and A.J. Whiffen, *Actidione, an antibiotic from Streptomyces griseus.* J Am Chem Soc, 1947. 69(2): p. 474.

113. Whiffen, A.J., *The Production, Assay, and Antibiotic Activity of Actidione, an Antiobiotic from Streptomyces griseus.* J Bacteriol, 1948. 56(3): p. 283-91.

114. Siegel, M.R. and H.D. Sisler, *INHIBITION OF PROTEIN SYNTHESIS IN VITRO BY CYCLOHEXIMIDE.* Nature, 1963. 200: p. 675-6.

115. Hsu, K.S., *THE GENETIC BASIS OF ACTIDIONE RESISTANCE IN NEUROSPORA.* J Gen Microbiol, 1963. 32: p. 341-7.

116. Colombo, B., L. Felicetti, and C. Baglioni, *INHIBITION OF PROTEIN SYNTHESIS BY CYCLOHEXIMIDE IN RABBIT RETICULOCYTES.* Biochem Biophys Res Commun, 1965. 18: p. 389-95.

117. Sisler, H.D. and M.R. Siegel, *Cycloheximide and Other Glutarimide Antibiotics*, in *Antibiotics: Volume I Mechanism of Action*, D. Gottlieb and P.D. Shaw, Editors. 1967, Springer Berlin Heidelberg: Berlin, Heidelberg. p. 283-307.

118. Kawai, S., et al., *Drastic alteration of cycloheximide sensitivity by substitution of one amino acid in the L41 ribosomal protein of yeasts.* J Bacteriol, 1992. 174(1): p. 254-62.

119. Dehoux, P., J. Davies, and M. Cannon, *Natural cycloheximide resistance in yeast. The role of ribosomal protein L41.* Eur J Biochem, 1993. 213(2): p. 841-8.

120. Cundliffe, E., *Recognition sites for antibiotics within rRNA*, in *The ribosome: structure, function, and evolution*, A.E.D. W. E. Hill, R. A. Garrett, P. B. Moore, D. Schlessinger, and J. R. Warner (ed.), Editor. 1990, American Society for Microbiology: Washington, D.C.

121. Garreau de Loubresse, N., et al., *Structural basis for the inhibition of the eukaryotic ribosome.* Nature, 2014. 513(7519): p. 517-522.

122. Tamm, T., I. Kisly, and J. Remme, *Functional Interactions of Ribosomal Intersubunit Bridges in Saccharomyces cerevisiae.* Genetics, 2019. 213(4): p. 1329-1339.

123. Luo, Z., M. Freitag, and M.S. Sachs, *Translational regulation in response to changes in amino acid availability in Neurospora crassa.* Mol Cell Biol, 1995. 15(10): p. 5235-45.

124. Esposito, A.M., et al., *Eukaryotic polyribosome profile analysis.* J Vis Exp, 2010(40).

125. Wolf, D.A., J. Bähler, and J.A. Wise, *Schizosaccharomyces pombe Polysome Profile Analysis and RNA Purification.* Cold Spring Harb Protoc, 2017. 2017(4): p. pdb.prot091637.

126. Wu, C., et al., *The cell free protein synthesis system from the model filamentous fungus Neurospora crassa.* Methods, 2018. 137: p. 11-19.

127. Michel, A.M. and P.V. Baranov, *Ribosome profiling: a Hi-Def monitor for protein synthesis at the genome-wide scale.* Wiley Interdiscip Rev RNA, 2013. 4(5): p. 473-90.

128. Madeo, F., et al., *Spermidine in health and disease.* Science, 2018. 359(6374).

129. van, A.L., *Observationes de Anthonii Leeuwenhoeck, de natis e semine genital aminalculis.* Phil. Trans., 1678. 12 (1678), pp. 1040-1043.

130. Rosenheim, O., *The Isolation of Spermine Phosphate from Semen and Testis.* Biochem J, 1924. 18(6): p. 1253-1262.1.

131. Liquori, A.M., et al., *Complexes between DNA and polyamines: a molecular model.* Journal of Molecular Biology, 1967. 24(1): p. 113-122.

132. Hölttä, E., R. Sinervirta, and J. Jänne, *Synthesis and accumulation of polyamines in rat liver regenerating after treatment with carbon tetrachloride.* Biochemical and Biophysical Research Communications, 1973. 54(1): p. 350-357.

133. Lefèvre, P.L.C., M.-F. Palin, and B.D. Murphy, *Polyamines on the Reproductive Landscape.* Endocrine Reviews, 2011. 32(5): p. 694-712.

134. Igarashi, K. and K. Kashiwagi, *The functional role of polyamines in eukaryotic cells.* Int J Biochem Cell Biol, 2019. 107: p. 104-115.

135. Tiburcio, A.F., et al., *The roles of polyamines during the lifespan of plants: from development to stress.* Planta, 2014. 240(1): p. 1-18.

136. Eisenberg, T., et al., *Induction of autophagy by spermidine promotes longevity.* Nature Cell Biology, 2009. 11(11): p. 1305-1314.

137. Kiechl, S., et al., *Higher spermidine intake is linked to lower mortality: a prospective population-based study.* Am J Clin Nutr, 2018. 108(2): p. 371-380.

138. Novita Sari, I., et al., *Metabolism and function of polyamines in cancer progression.* Cancer Letters, 2021. 519: p. 91-104.

139. Cohen, S.S., S. Morgan, and E. Streibel, *The polyamine content of the tRNA of E. coli.* Proc Natl Acad Sci U S A, 1969. 64(2): p. 669-76.

140. Cohen, S.S., S. Morgan, and E. Streibel, *THE POLYAMINE CONTENT OF THE tRNA OF E. coli.* Proceedings of the National Academy of Sciences, 1969. 64(2): p. 669-676.

141. Mandal, S., et al., *Depletion of cellular polyamines, spermidine and spermine, causes a total arrest in translation and growth in mammalian cells.* Proc Natl Acad Sci U S A, 2013. 110(6): p. 2169-74.

142. Igarashi, K., et al., *Increase of fidelity of polypeptide synthesis by spermidine in eukaryotic cell-free systems.* Eur J Biochem, 1982. 128(2-3): p. 597-604.

143. Athwal, G.S. and S.C. Huber, *Divalent cations and polyamines bind to loop 8 of 14-3-3 proteins, modulating their interaction with phosphorylated nitrate reductase.* Plant J, 2002. 29(2): p. 119-29.

144. Dever, T.E. and I.P. Ivanov, *Roles of polyamines in translation.* J Biol Chem, 2018. 293(48): p. 18719-18729.

145. Myasnikov, A.G., et al., *Structure-function insights reveal the human ribosome as a cancer target for antibiotics.* Nat Commun, 2016. 7: p. 12856.

146. Budkevich, T., et al., *Structure and dynamics of the mammalian ribosomal pretranslocation complex.* Mol Cell, 2011. 44(2): p. 214-24.

147. Behrmann, E., et al., *Structural snapshots of actively translating human ribosomes.* Cell, 2015. 161(4): p. 845-57.

148. Bhaskar, V., et al., *Dynamics of uS19 C-Terminal Tail during the Translation Elongation Cycle in Human Ribosomes.* Cell Rep, 2020. 31(1): p. 107473.

149. Buschauer, R., et al., *The Ccr4-Not complex monitors the translating ribosome for codon optimality.* Science, 2020. 368(6488).

150. Wettstein, F.O., H. Noll, and S. Penman, *EFFECT OF CYCLOHEXIMIDE ON RIBOSOMAL AGGREGATES ENGAGED IN PROTEIN SYNTHESIS IN VITRO.* Biochim Biophys Acta, 1964. 87: p. 525-8.

151. Pellegrino, S., et al., *Understanding the role of intermolecular interactions between lissoclimides and the eukaryotic ribosome.* Nucleic Acids Res, 2019. 47(6): p. 3223-3232.

152. Pollard, T.D., *A guide to simple and informative binding assays.* Mol Biol Cell, 2010. 21(23): p. 4061-7.

CHAPTER II

Structure of the translating *Neurospora* ribosome arrested by cycloheximide

2.1 Materials and methods

2.1.1 Strains and culture conditions

The *N. crassa* wild-type strain FGSC 2489 (74-OR23-1V A) and CHX-resistant N. crassa strains (Table S3) were obtained from the Fungal Genetics Stock Center (Manhattan, KS) [1] and maintained as described [2, 3]. Homokaryons of all strains were obtained by microconidiation [4]

2.1.2 Preparation, analyses, and purification of *N. crassa* polysomes

N. crassa polysomes were prepared and analyzed as previously described, with minor changes [5]. Suspension of conidia was inoculated onto 50 ml of solid Vogel's sucrose medium in a 250 ml flask. The culture was incubated at room temperature for 14 days, and conidia were harvested through two layers of cheesecloth. The number of conidia was counted and the concentration was calculated. Conidia were inoculated to 500 ml of Vogel's sucrose medium to make the final concentration of 1 x 107 conidia/ml, and the culture was incubated at 32°C with orbital shaking (180 rpm). After about 6 hr when 90% of the conidia show germ tubes, cycloheximide (2 mg/ml) was added to the culture

5 min before harvesting, and the germlings were harvested by vacuum filtration onto Whatman 541 filter paper. The mycelial pad was peeled off the filter paper and weighed. Mycelial pads (0.25 g each) were transferred to 2-ml screw-cap tubes containing ice-cold 0.75 ml of polysome extraction buffer (100 mM KCl, 20 mM HEPES-KOH [pH 7.5], 2 mM magnesium acetate, 15 mM 2-mercaptoethanol, 2 mg/ml cycloheximide) and 0.5 g of zirconia/silica beads (0.5 mm diameter). The tubes were disrupted using a beadbeater at 4°C for 50 sec and centrifuged at 16,100 g at 4°C for 5 min. Supernatants (0.45 ml) were transferred to fresh 2-ml screw-cap tubes, frozen in liquid nitrogen, and stored at -80°C.

For polysome analyses, 400 µl (about 18 A260 units) of homogenate was layered on 12-ml linear sucrose gradients which contain 10%-50% [wt/wt] sucrose, 10 mM HEPES-KOH [pH 7.5], 70 mM ammonium acetate, 4 mM magnesium acetate, and 2 mg/ml cycloheximide. Gradients were centrifuged using a Beckman SW41 rotor at 41,000 rpm at 4°C for 2 hr. BioComp Gradient Station Model 153 and Gilson Fraction Collector FC203B were used to generate the sucrose gradients and to analyze and fractionate the gradients, respectively. Polysome profiles were generated, and 26 fractions were collected from each gradient, flash-frozen in liquid nitrogen, and stored at -80°C.

Fractions corresponding to the polysomes (disomes and greater) from multiple gradients were pooled, washed, and concentrated using Corning® Spin-X® UF 6 mL Centrifugal Concentrators (100,000 MWCO). The washing buffer was the buffer A that has been

used to prepare N. crassa cell-free extract for in vitro translation (30 mM HEPES-KOH pH7.6, 100 mM KOAc pH7.0, 3 mM Mg(OAc)2 pH7.0, 2 mM DTT) supplemented with 2 mg/ml CHX. For each centrifugation, about 15 ml of the washing buffer was used, and the volume was concentrated to about 1ml. The washing/concentrating was repeated six times to remove sucrose. Finally, the ribosomes were concentrated to about A260=10.

2.1.3 Cryo-EM sample preparation

Cryogrids were prepared as previously described [6]. A total of 3 ul of the purified *N. crassa* polysomes was applied onto glow-discharged C-Flat 2/1 holey grids. The grids, equilibrated at 16°C and 100% relative humidity, were plunged into liquid ethane to freeze them using a Vitrobot Mark III (FEI company, The Netherlands).

2.1.4 Cryo-EM single-particle data acquisition

The frozen grids were imaged under a Titan Krios cryo-electron microscope (Thermo Fisher Scientific) operated at 300 kV. The condenser lens aperture was 50 μm, spot size was 7, and the parallel beam had an illuminated area of 1.08 μm in diameter. Data were automatically collected using EPU software on a K2 Summit direct electron camera (Gatan) equipped with a Bioquantum energy filter with an energy slit of 20 eV, in the counting mode. The nominal magnification used was 130,000×, corresponding to a calibrated sampling of 1.06 Å per physical pixel. The recording rate was 5 raw frames

per second and the total exposure time was 5 seconds, yielding 25 frames per stack, and a total dose of 32 e-/Å^2. A total of 1,836 movie stacks were collected.

2.1.5 Cryo-EM image processing

All micrographs were imported into RELION-3.1 [7] for image processing. The motion correction was performed using MotionCor2 [8]. The defocus and astigmatism were determined using CTFFIND4 [9]. All particles were autopicked using the convolutional neural network (CNN)-based script e2boxer.py in EMAN2 [10, 11] and further checked manually to remove bad particles. After 2D classification in RELION-3.1, a total of 206,276 particles were subjected to 3D classification in RELION-3.1. The 3D classification of LSU and SSU was performed in RELION-3.1 to further remove bad particles. Then, a total of 196,154 particles were subjected to Bayesian polishing in RELION-3.1, followed by 3D reconstruction using cryoSPARC [12]. A sharpening B-factor of -65.4 Å2 was applied to the resulting cryo-EM map. The global resolution of the final sharpened map is 2.7 Å, estimated by the "gold-standard" 0.143 criterion of the FSC curve. Local resolution maps were determined in RELION-3.1.

2.1.6 Molecular modeling

The sequences of *N. crassa* 5S. 5.8S, 18S, and 26S rRNA used to build the model were obtained through NCBI (GenBank IDs K02469.1, M10692.1, FJ360521.1, and

FJ360521.1, respectively). Template-based comparative modeling was performed using modeRNA [13]. The *S. cerevisiae* 80S structures (PDB ID codes: 4U3U and 6T4Q) [14, 15] were chosen as the templates. The sequences were aligned using the SILVA ACT website (https://www.arb-silva.de/aligner/) [16]. The structures of the rRNA expansion segments were manually built using Rosetta [17] and Coot [18] with the aid of the secondary structures that were predicted by RNAfold WebServer (http://rna.tbi.univie.ac.at/cgi-bin/RNAWebSuite/RNAfold.cgi) [19]. The rRNA structures were refined using Rosetta and PHENIX [20].

The sequences of *N. crassa* ribosomal proteins were obtained from the UniProt database. For each ribosomal protein, the initial homology model was generated using MODELLER [21] and then refined into the cryo-EM map using Rosetta [17]. The best model was then selected based on both the geometry and the fitting scores.

The tRNA model used for A- and P-site tRNAs was the eukaryotic ICG-anticodon tRNA that decodes Arg codons (PDB ID: 6T4Q) [15]. The mRNA model and nascent peptide model were adapted from the mRNA model and nascent peptide model in a human classical-PRE ribosome structure (PDB ID: 6Y0G) [22].

CHX and SPD modeling was done with the electronic Ligand Builder and Optimisation Workbench (eLBOW) [23]. The models of Mg2+ ions were adapted from the S. cerevisiae ribosome structure (PDB ID: 6T4Q [15]).

The models of all rRNA, ribosomal proteins, tRNA, mRNA, nascent peptide, CHX, SPD, and Mg2+ were then merged into one model, refined using Rosetta and PHENIX, and inspected and adjusted using Coot.

The statistics obtained by using PHENIX and MolProbity [24] of the refined 80S ribosome model are listed in Table S4.

2.1.7 Structural figures preparation

All figures were made using UCSF Chimera [25] and UCSF ChimeraX [26].

2.1.8 Sequencing of *N. crassa cyh-1* and *cyh-2* alleles

Genomic DNA was isolated as described [5]. For each strain, the DNA sequences of both *cyh-1* (NCU00706) and *cyh-2* (NCU03806) genes were determined by PCR amplification of genomic DNA, followed by sequencing of the PCR product. For *cyh-1*, oligo-pair OLS041 (GACCTCACACATCAACGA)/OLS042 (TTCGCAACCTCGCTACCA) were used for amplification and sequencing and an additional oligo, OLS057 (TCATGTCGCGTCGAGCTCTGT), was also used for sequencing. For *cyh-2*, oligo-pairs CYH2F1 (CGAGACCCGTGAAGCGTCT)/CYH2R1 (TTGAGGATGGGGGCCCAC) and CYH2F2

(GACGATGACGGATAGACC)/CYH2R2 (GGCTTCTGGACGAATGTT) were used for both amplification and sequencing. The *cyh-1* sequencing reads were aligned to NCBI Reference Sequence: XM_959447.3, and the *cyh-2* sequencing reads were aligned to GenBank: AL513466.1 (which includes *cyh-2*) to identify the mutations.

2.1.9 Determination of CHX-resistance levels *in vivo*

For testing CHX-resistance, conidia (104 in 50 µl of sterile water) from wild-type and mutant strains were inoculated into 16 x 125 mm tubes containing 3 ml of Vogel's minimal medium/2% sucrose/2% agar supplemented with CHX after autoclaving. Cultures were grown for eight days at room temperature. Tubes were scored for growth and photographed.

2.1.10 Preparation of cell-free translation systems, determination of CHX-resistance levels in vitro, and toeprinting

The procedures for preparation of CFTS, preparation of in vitro synthesized capped and polyadenylated luciferase (LUC) RNA for translation, and for toeprinting without and with CHX, were as previously described [27, 3]. For testing CHX-sensitivity and Hyg-sensitivity, drugs at the indicated concentrations were added at T0.

2.1.11 Data Availability

The Coulomb potential map and atomic coordinates have been deposited in the Electron Microscopy Databank (EMDB code: EMD-24307) and Protein Data Bank (PDB ID code: 7R81).

2.2 Results

2.2.1 Overall *N. crassa* ribosome structure

The original structures of eukaryotic ribosomes containing CHX were obtained using X-ray crystallography or cryo-EM by adding CHX to non-translating vacant ribosomes [14, 28]. Here we obtained structures of actively translating ribosomes inhibited by CHX from the filamentous fungus *N. crassa* using cryo-EM and the workflow outlined in Fig. S1. CHX was added to growing *N. crassa* cells, and clarified extracts were prepared, layered, and fractionated on sucrose gradients. Ribosomes were collected from the polysome-containing region of the gradients (Fig. S1A) and prepared for cryo-EM imaging. CHX reversibly binds to ribosomes [29]; therefore, we sought to maximize CHX association with ribosomes throughout the isolation and imaging procedures. To accomplish this, we added a high concentration of CHX (2 mg/ml) to the growth medium to arrest translation *in vivo* and maintained this concentration of CHX at all subsequent steps to obtain samples on grids for imaging.

The cryo-EM map of the 80S ribosome at an overall resolution of 2.7 Å (Fig. S1C and D) was determined using the approach in Fig. S1B. We modeled *N. crassa* rRNAs and ribosomal proteins and fitted them into the cryo-EM map (Fig. 1, Fig. S1E, Table S1, Table S2). This model of the *N. crassa* 80S ribosome included 93.6% of 26S, 100% of 5S, 100% of 5.8S, and 98.5% of 18S rRNA nucleotides, 42 ribosomal proteins in the large subunit (LSU), and 32 ribosomal proteins in the small subunit (SSU). Heterogeneity of 5S rRNAs has been shown in *N. crassa* [30]; the 5S rRNA model in our structure is based on the major α 5S rRNA sequence. As is seen with other 80S eukaryotic ribosome structures, *N. crassa* CPC-2 [31], the homolog of RACK1/ASC1, a non-ribosomal protein, is stably associated and similarly positioned on the 40S subunit (Fig. 1). The *N. crassa* ribosome structure obtained also contains A-site and P-site tRNAs, CHX, spermidine, and nascent peptide, as discussed below. Additionally, cryo-EM densities for 260 of the 269 Mg2+ ions identified in the *S. cerevisiae* ribosome structure 6T4Q [15] were confirmed in the *N. crassa* data. Finally, in this CHX-stalled conformation, regions of the ribosome corresponding to the P1 stalk and L1 stalk were not resolved, and therefore uL10, uL11 (P1 stalk), and uL1 (L1 stalk) are not in the modeled structure.

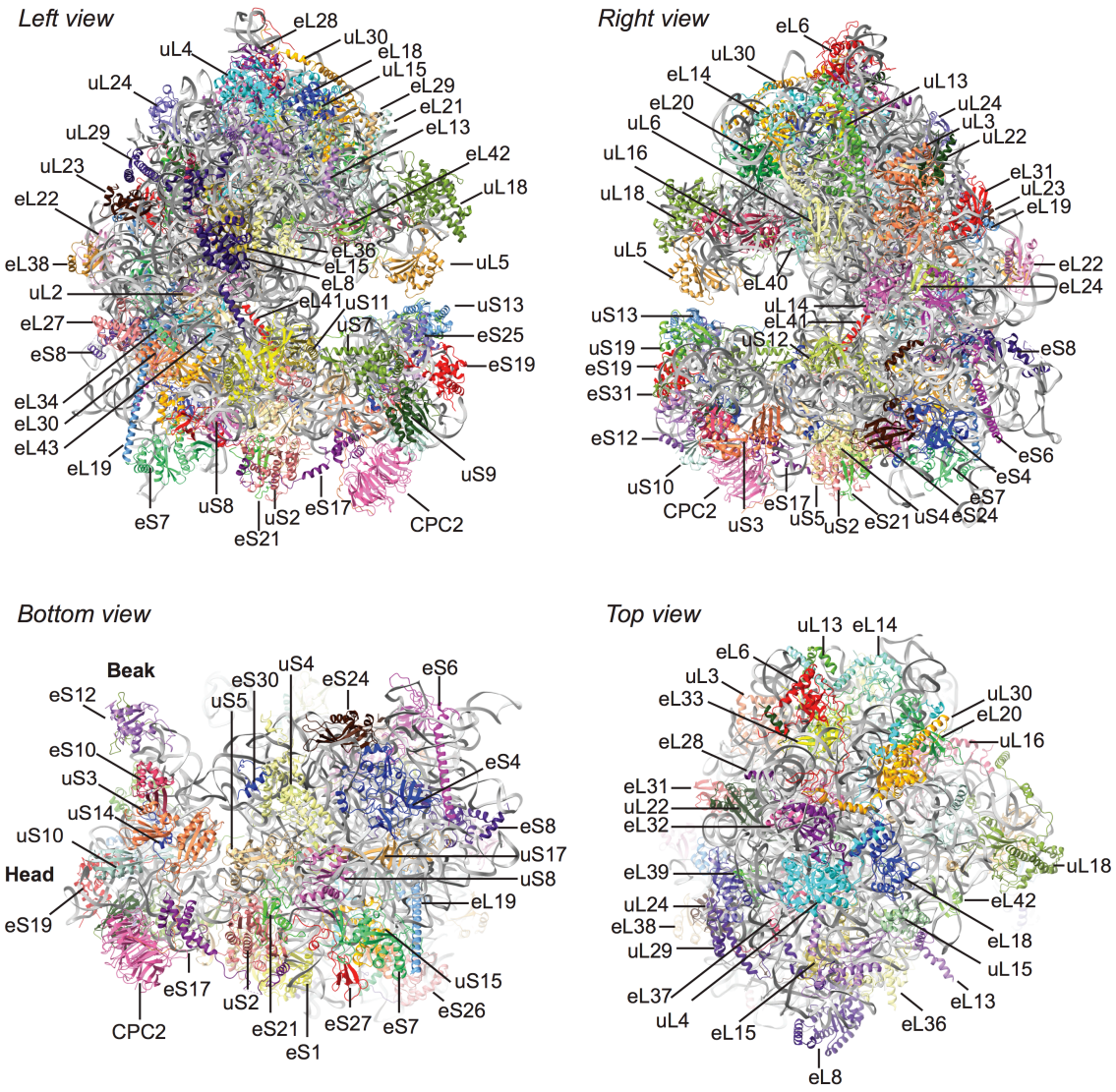

Fig. 1. Positions of *N. crassa* proteins associated with the 80S *N. crassa* ribosome. *N. crassa* proteins were fitted to the *N. crassa* cryo-EM map as described in the text. Left and right views are rotated 180° as are top and bottom views. Proteins are individually colored; rRNAs are all gray. Models for tRNAs, mRNA, CHX, spermidine, Mg^{2+}, and nascent peptide are not shown.

We next compared the overall structure of the *N. crassa* ribosome to *S. cerevisiae* ribosomes (Fig. S2A) and human ribosomes (Fig. S2B). *N. crassa* and *S. cerevisiae* ribosomes are overall similar except for a striking difference at the top of the LSU (Fig. S2A) comprising rRNA expansion segments ES7L, ES15L, and ribosomal protein eL6 [32, 33]. Here, the *N. crassa* ribosome, like the human ribosome, contains ribosomal protein eL28, while the *S. cerevisiae* ribosome does not (Fig. S2A). *N. crassa* eL28 is encoded by NCU06210, which is annotated as a hypothetical protein in NCBI (Gene ID: 3879074). The interaction of *N. crassa* ES7L with eL28 is similar to that in the human ribosome (Fig. S3A and B). We looked at this difference between the fungal ribosomes more closely. Most Saccharomycotina, including *S. cerevisiae* and *Kluyveromyces lactis*, lack an eL28 gene, and there is no such protein in these two yeasts' ribosome structures (Fig. S3C and D). The structured region of the rRNA near *N. crassa* and human eL28 is not structured in purified *S. cerevisiae* and *K. lactis* ribosomes (Fig. S3A-D). However, the rRNAs from these yeasts contain the corresponding sequences. Interestingly, while *S. cerevisiae* ES7 is unstructured in this region in the absence of additional factors (Fig. S3C), when the ribosome is associated with NatA [34], a protein complex that binds at the ribosome exit pore (Fig. S3E), ES7 adapts a different structure which is closer to the *N. crassa* ES7 structure (Fig. S3F and G). An additional difference between the *N. crassa* and *S. cerevisiae* structures is that the *S. cerevisiae* ribosome contains density that corresponds to a structured L1 stalk and eIF5A (the large orange-shaded area in the *S. cerevisiae* ribosome left view, Fig. S2A) while *N. crassa* does not; this is discussed further below. Finally, the most striking differences between the *N. crassa* and human

ribosomes (Fig. S2B) are that human ribosomal rRNAs contain longer expansion segments than fungal rRNAs that can contribute to the structure [32].

2.2.2 Localization of CHX in the *N. crassa* ribosome

We observed well-resolved extra density for CHX near the E site of the LSU (Fig. 2A and B, Fig. S4A). CHX is located in a region demarcated by eL42, conserved 26S rRNA residues, and uL15. Comparison of the position of CHX in the *N. crassa* ribosome with its positions in the *S. cerevisiae* and human ribosomes reveals strong conservation of its orientation in the ribosome and the rRNA and ribosomal proteins surrounding it (Compare Fig. 2B, C, and D).

Importantly, additional density was present close to the *N. crassa* CHX binding site. We identified it as spermidine (SPD) (Fig. 2A, B, and Fig. S5A). SPD was also recently modeled in a similar site in the submitted structure of the *S. cerevisiae* ribosome containing bound CHX and eIF5A [6tnu, ref. 35] (Fig. S5B). In cryo-EM maps of human ribosomes containing CHX, modeled Mg2+ or unmodeled SPD appear to be present (Fig. S5C and D) [28, 22]. In other structures of human and *S. cerevisiae* ribosomes containing E/E-site or P/E-site tRNA [15, 22], unmodeled SPD is also present in a similar position (Fig. S5E and F). Thus, SPD binding to this region of the eukaryotic ribosome near the CHX binding site appears to be a common feature. Its structural and

functional role(s), which remain to be determined, may well be of interest given its close vicinity to such an important functional site of the ribosome.

The comparisons of ribosomes containing CHX and containing E-site tRNA (Fig. S5) support the proposed functional role of CHX to prevent the binding of deacylated tRNA [14, 28]. CHX would clash with tRNA as the tRNA entered the E site upon transition from the P/P into the hybrid P/E position after peptidyl transfer.

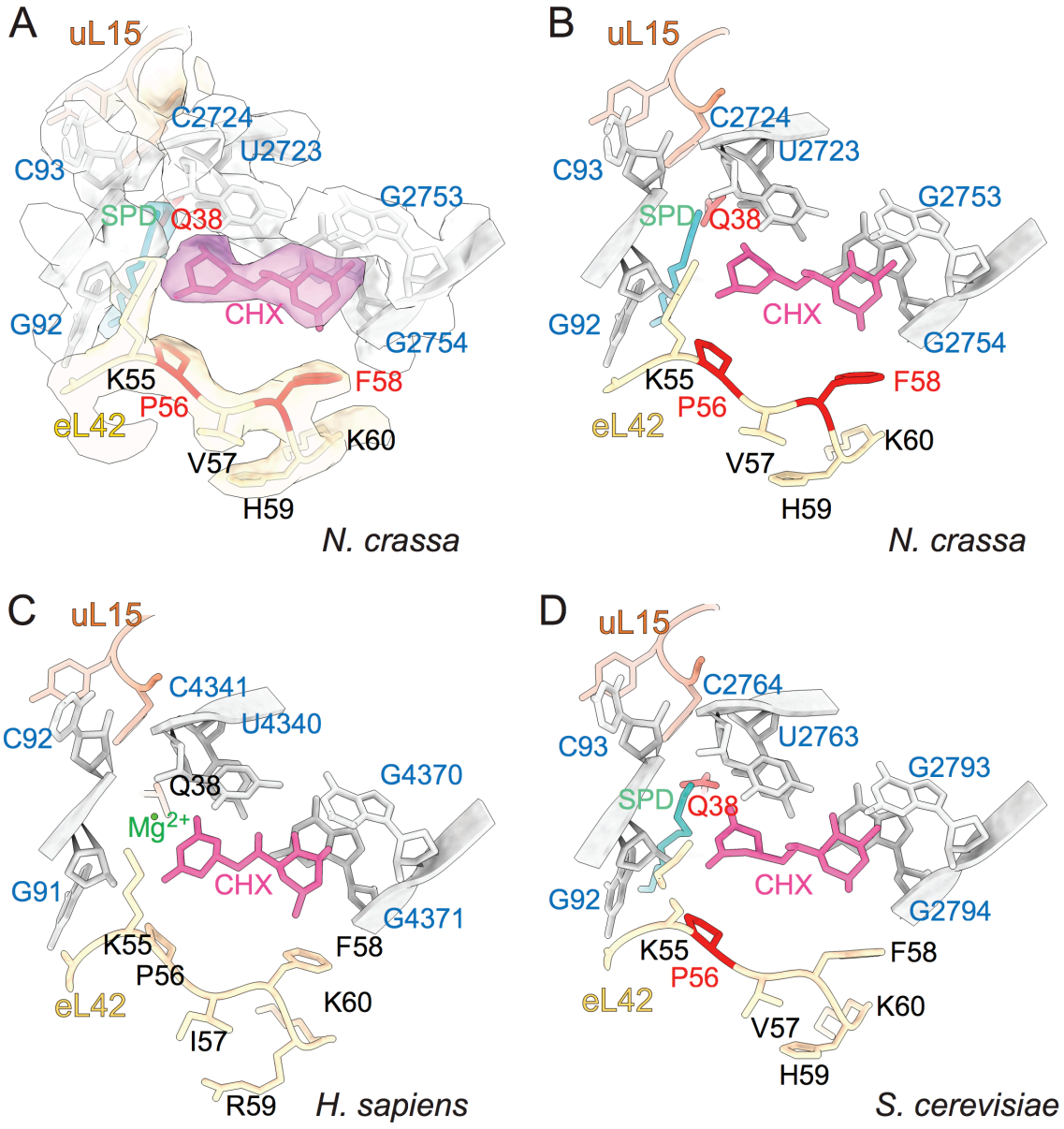

Fig. 2. Cycloheximide (CHX) and spermidine (SPD) are both present in the *N. crassa* ribosome E site in actively translating ribosomes arrested by CHX. *(A)* Densities corresponding to CHX, SPD, and nearby *N. crassa* ribosomal components are indicated as surfaces and models as sticks and ribbons. *(B-D)* comparisons of models of

CHX and spermidine or Mg^{2+} in the *(B)* translating *N. crassa* ribosome; *(C)* translating *S. cerevisiae* ribosome (PDB ID: 6TNU); *(D)* vacant human ribosome (PDB ID: 5LKS). CHX is fuchsia; SPD is cyan; rRNA is gray; eL42 and uL15 are yellow and orange, respectively, with residues at which mutations in the corresponding organism are known to result in CHX-resistance shaded red.

2.2.3 *N. crassa* mutations that cause CHX-resistance map to the CHX binding site

CHX-resistant alleles of two identified genes that confer CHX-resistance were obtained from the Fungal Genetics Stock Center. Three alleles of *cyh-1* (NCU00706) and two alleles of *cyh-2* (NCU03806) were sequenced (Table S3). The *cyh-1* mutations, which affect eL42, were P56L (two independent alleles) and F58L. The two alleles of *cyh-2* are two different mutations of the same residue in uL15: Q38K and Q38L. Like ribosomal mutations in *S. cerevisiae* and other organisms that result in CHX-resistance, these mutations are close to the CHX-binding site; the affected residues are indicated in red in Fig. 2. In addition, one of these residues identified by mutations in *N. crassa* and *S. cerevisiae*, uL15 Q38, and another residue identified in *S. cerevisiae*, H39, are also in close proximity to SPD (Fig. 2). All of the *N. crassa* mutants were more resistant to CHX than the wild type *in vivo* (Fig. S6) and in cell-free translation systems (CFTSs) derived from these strains (Fig. S7A). In contrast, mutant and wild-type CFTSs were similarly sensitive to hygromycin B (Fig. S7B), an aminoglycoside translation inhibitor that binds near the decoding site [36], consistent with CHX and HYG targeting different regions of the ribosome. These data, including the identification of a new mutation at a conserved residue that affects CHX-resistance (F58L) and that maps to the CHX-binding site, highlight the importance of the specific amino residues in this region for modulating the sensitivity of these ribosomes to inhibition by CHX.

2.2.4 The positions of tRNAs, nascent peptide, mRNA, and ribosome components show that CHX-arrested ribosomes are in the classical PRE state

The structure of the CHX binding site is highly conserved in eukaryotic ribosomes. Ribosomes go through many different conformations during the various steps in the elongation cycle [37]. At what step(s) does CHX inhibit elongation? We could answer this question by analyses of the peptidyltransferase center in the *N. crassa* ribosome structure. The CHX-ribosome structure determined here differs from previously published CHX-containing structures obtained from vacant ribosomes to which CHX was added [14, 28] and from subsets of translating ribosomes that contained CHX but were affinity-purified based on some other distinguishing feature [35, 22]. The structure of the *N. crassa* ribosome containing CHX shows A/A- and P/P-site tRNAs (Fig. 3A). We wanted to know whether any subclass(es) of these ribosomes had tRNA in hybrid or other states since mammalian ribosomes purified with CHX were observed to be in three major classes: classical-PRE, hybrid-PRE, and POST [22]. Therefore, we did a 3D classification of these particles into ten subclasses. Every subclass had A/A- and P/P-site tRNA, and none had P/E- or A/P-site hybrid tRNA (Fig. S8). These data indicated that the purification procedure we used maintained ribosomes in a CHX-arrested classical PRE state.

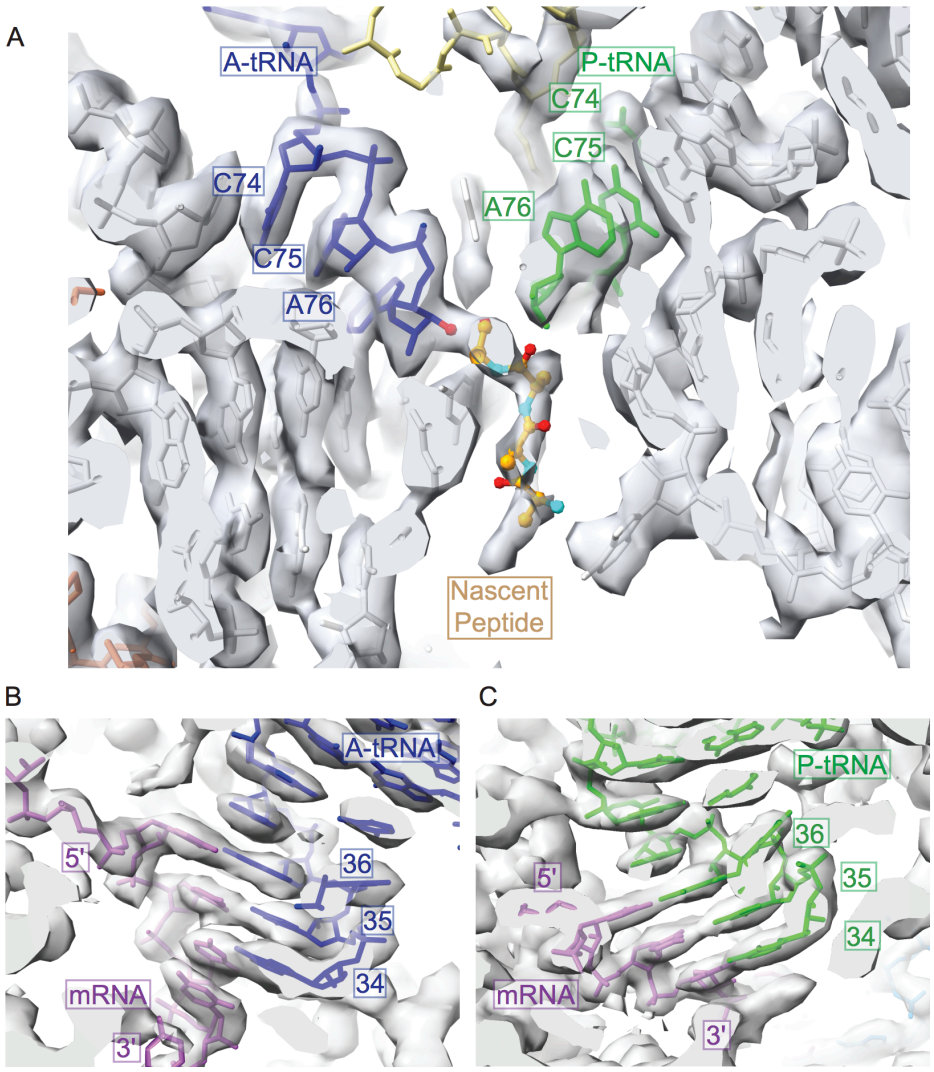

Fig. 3. CHX arrests ribosomes in the PRE state with the nascent peptide attached to the A-site tRNA. *(A)* A- and P-site tRNAs at the peptidyltransferase center, with the nascent peptide attached to the A-site tRNA CCA-end. *(B)* A-site tRNA anticodon interaction with the mRNA A-site codon. *(C)* P-site tRNA anticodon interaction with the mRNA P-site codon. A-site tRNA, blue; P site-tRNA, green; mRNA, purple; nascent peptide, various colors; rRNA, gray; uL16, yellow; uL3, orange.

No specific tRNAs are represented in the peptidyltransferase centers of polysomal ribosomes. Therefore, we adapted the tRNA model for a eukaryotic ICG-anticodon tRNA that decodes Arg codons (PDB ID: 6T4Q) [15] to model the tRNA densities of both A- and P-site tRNAs. Fitting the models to the tRNA densities allowed visualization of both A-site and P-site tRNAs in the peptidyltransferase center (Fig. 3A) and visualization of A-site and P-site mRNA-tRNA codon-anticodon interactions (Fig. 3B and C). Importantly, we observed extra density corresponding to the nascent peptide attached to the 3'-hydroxyl group of the A-site tRNA, but not the P-site tRNA (Fig. 3A). The map's local resolution at the position of this peptide-tRNA bond was approximately 2.6 Å (Fig. S4B). The density corresponding to the nascent peptide was not fully modeled due to the presence of many different nascent peptide species and nascent peptide conformations in polysomes. In contrast to the limited resolution of nascent peptide density, the density corresponding to the ribosome exit tunnel, including the constriction site important for nascent peptide interactions with the ribosome, could be confidently modeled (Fig. S9).

The positions of the A/A- and P/P-site tRNAs and the nascent peptide's attachment to the A-site tRNA indicated that the *N. crassa* ribosome arrested by CHX is in the PRE state. Several conformations of the PRE state in human ribosomes can be discriminated by the relative orientations of the SSU and LSU and the positions of tRNAs [37]. The conformation of the *N. crassa* ribosome with CHX (Fig. 4A), assessed by comparing the

relative SSU-LSU configurations, better resembled the human classical-1 PRE state determined in the absence of CHX (Fig. 4B) than the rotated PRE* state (Fig. 4C).

Additional structural analyses support the assignment of the CHX-stalled *N. crassa* ribosome to the classical PRE state. Recently, the C-terminal tail of human uS19 was shown to change conformation depending on the functional state of the ribosome [22]. This uS19 domain is positioned between the A- and P-site tRNAs near the anticodon-codon interaction with mRNA. Consistent with the *N. crassa* ribosome assignment to the classical PRE state, the position of *N. crassa* uS19 C-terminal tail in the CHX-stalled conformation is highly similar to the human uS19 in the classical PRE conformation (Fig. 4D and E). These regions of *N. crassa* and human uS19 share identical amino acid sequences, while the *S. cerevisiae* uS19 C-terminal tail differs in sequence (Fig. S10A). When comparing uS19 structures in *N. crassa*, human and *S. cerevisiae* ribosomes containing CHX, all three uS19 structures are similar except that the *S. cerevisiae* model lacks this C-terminal tail (Fig. S10B). Thus, the A- and P-site tRNAs, uS19, and CHX are similarly positioned in the *N. crassa* and human structures, based on both models and cryo-EM maps, showing that CHX-bound ribosomes in both species are in the classical PRE state. However, unlike the case for the *N. crassa* ribosome, we do not see density corresponding to the nascent peptide on the A-site tRNA in the corresponding cryo-EM map for the mammalian classical PRE ribosome (EMD-10668) [22], possibly because the peptide is disordered.

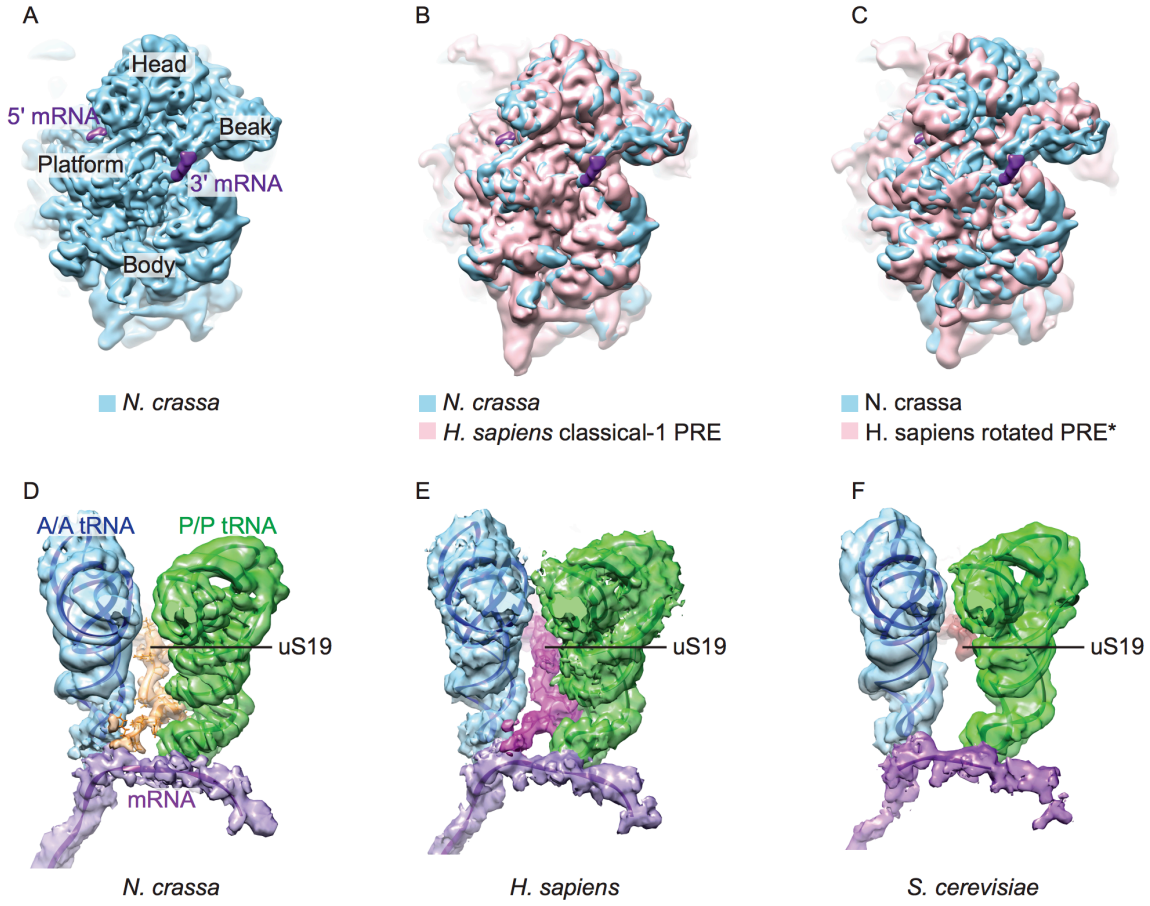

Fig. 4. The *N. crassa* CHX-bound ribosome is in the classical PRE state conformation. (A-C) Bottom view of the 80S ribosomes from *N. crassa* and *H. sapiens* low-pass-filtered to 10 Å for clarity. The 60S subunits are all aligned to the *N. crassa* 60S subunit. (A) The 40S subunit of *N. crassa* ribosome (blue). *N. crassa* mRNA is purple. (B) The 40S subunits of *N. crassa* ribosome (blue) and *H. sapiens* classical-1 PRE state ribosome (pink, EMD-2909) align well. (C) The 40S subunit of *H. sapiens* PRE* state ribosome (pink, EMD-2906) is rotated slightly counterclockwise compared to the 40S subunit of *N. crassa* ribosome (blue). (D-F) *N. crassa* uS19 (tan) and human

uS19 (fuchsia) have similar contacts and conformations in the CHX-bound PRE state ribosome. The view given is similar to that in Bhaskar *et al.* [148] for comparison of the position of the uS19 C-terminal tail. The density of mRNA is low-pass-filtered to 10 Å for clarity, and the surface is displayed in purple. The C-terminal tails of both uS19 proteins interact with mRNA, A-site tRNA (blue), and P-site tRNA (green). (D) *N. crassa* uS19 position (tan) in the ribosome. (E) Human uS19 position (fuchsia) in the ribosome (EMD-10668, PDB ID: 6Y0G). tRNA densities were extracted from the cryo-EM map using ChimeraX. (F) *S. cerevisiae* uS19 position (rose) in the ribosome (EMD-10537, PDB ID: 6TNU).

In conclusion, the structural data indicate that the CHX-arrested translating *N. crassa* ribosome is in the classical-1 PRE state with the nascent peptide transferred to the A-site tRNA.

2.2.5 CHX does not inhibit a translation termination event

CHX does not interfere with A site reactivity during elongation since the nascent peptide is transferred to the A-site tRNA. Therefore, in the presence of CHX, termination should still occur since release factors enter the A site to cause chain termination, and chain termination does not require tRNA translocation [38]. Analyses of the positions of ribosomes in fungal CFTSs by primer-extension inhibition (toeprint) assays demonstrated that adding CHX before adding RNA to the system results in stabilization of ribosomes with the initiation codons of ORFs in the P site and the second ORF codon in the A site [39]. This is consistent with CHX causing elongation-arrest at initiation codons. Toeprinting of CFTS translating RNA in the absence of CHX reveals the positions of ribosomes engaged in initiation, elongation, and termination [27]. Early evidence that CHX does not interfere with termination was obtained using toeprinting to map the positions of ribosomes on mRNA in an *S. cerevisiae* CFTS [27]. Since we had the structure of the *N. crassa* ribosome with CHX, we looked at the effect of CHX on termination kinetically using an *N. crassa* CFTS. We toeprinted ribosomes on a luciferase reporter RNA with an upstream open reading frame (uORF) specifying the arginine-attenuator peptide (AAP), which causes well-established arginine-dependent

transient stalling of ribosomes with a termination codon in the A site [40]. If CHX did not inhibit termination, then ribosomes should be released from stalling through eventual successful termination. However, if CHX inhibited termination, then the transient Arg-dependent termination stall should be stabilized by CHX, as are elongation stalls. The results show that while CHX stabilizes ribosomes engaged in elongation (Fig. 5, indicated by arrowheads and brackets), it does not stabilize terminating ribosomes (Fig. 5, indicated by stars). Specifically, toeprint analyses of CFTS to which CHX had been added for 0, 2.5, or 5 min showed progressively decreased signals of ribosomes stalled at termination codons (Fig. 5, compare lanes 2, 3, and 4, and compare lanes 6, 7, and 8), consistent with termination occurring in its presence. Stalling of ribosomes at the AAP termination codon, which is Arg-dependent, is most obvious when CFTS were analyzed immediately (0 min) after adding CHX (Fig. 5, compare lanes 2 and 6). In striking contrast, after 5 min in CHX, there was little difference in the signal from ribosomes at the AAP termination codon in low or high Arg (Fig. 5, compare lanes 4 and 8). This indicates that ribosomes at the termination codon are not stabilized by CHX. In contrast, toeprints corresponding to ribosomes engaged in elongation within the AAP coding region, including those with the initiation codon in the ribosome P site, remained stable or increased during incubation with CHX, consistent with their expected stabilization by CHX.

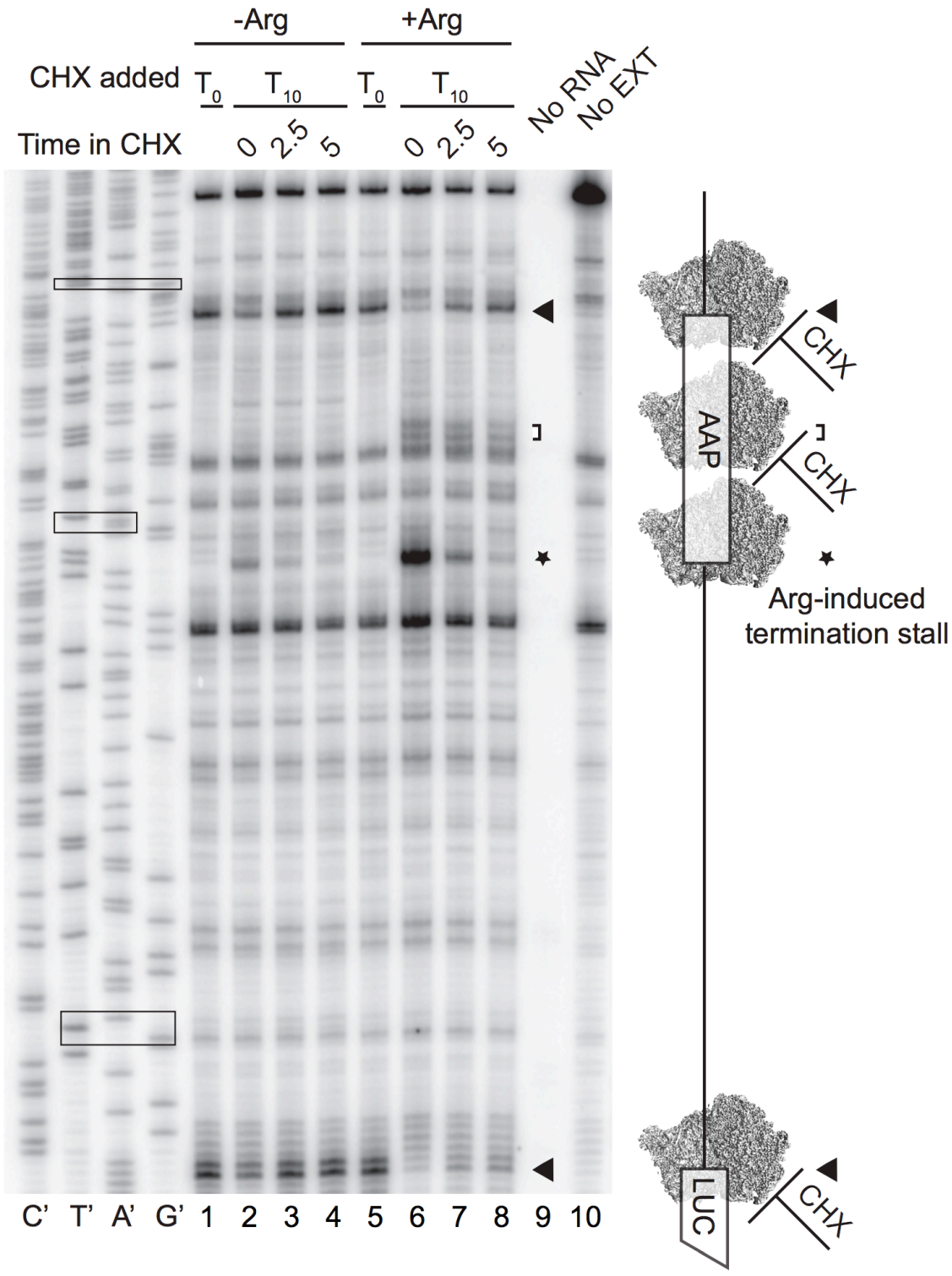
-Arg
+Arg
CHX added
T0
T10
T0
T10
No RNA
No EXT
Time in CHX
0
2.5
5
0
2.5
5
C'
T'
A'
G'
1
2
3
4
5
6
7
8
9
10
CHX
AAP
CHX
Arg-induced
termination stall
LUC
CHX

Fig. 5. Toeprinting shows that terminating ribosomes release from RNA in the presence of CHX, but elongating ribosomes do not. *In vitro* synthesized capped and polyadenylated luciferase (LUC) reporter mRNA containing the wild-type AAP uORF was translated in the *N. crassa* CFTS in the presence of 10 μM (-) Arg or 2 mM (+) Arg (low or high Arg). CHX (final concentration 0.5 μg/μl) was added to the CFTS reactions either before the addition of mRNA (time T_0) or after translation was underway for 10 min (steady-state translation, timeT_{10}). Steady-state reactions to which CHX was added were incubated in the presence of CHX for an additional 0, 2.5, or 5 min as indicated. The sequence of the mRNA can be directly deduced from the sequencing lanes reading from top to bottom. Boxed in the nucleotide sequence are the positions of the uORF start and stop codons, and the LUC start codon. The primer extension (toeprint) products corresponding to elongating ribosomes that have the uORF and LUC initiation codons in the P site are indicated by arrowheads; terminating ribosomes with the uORF termination codon in the A site are indicated with a star; elongating ribosomes stalled within the uORF coding region are marked by a bracket. Control samples of reaction mixtures without extract but with mRNA (−EXT) and reaction mixtures with extract but without mRNA (−RNA) are as indicated.

2.3 Discussion

CHX is commonly used to inhibit eukaryotic translation and is an important reagent for ribosome profiling analyses. Thus, it is crucial to understand its action during translation. Despite extensive biochemical work, however, CHX has only been studied from a structural perspective in the context of vacant 80S ribosomes [14, 28]. Here we focused on its action on translating ribosomes. We purified *N. crassa* ribosomes from polysome fractions isolated from cells in which translation was arrested by CHX and obtained their structure through single-particle cryo-EM. These data provide direct structural evidence that CHX's mechanism of action is to arrest ribosomes in the classical PRE state and do not support alternative models for its mechanism of action.

In *N. crassa* ribosomes containing CHX, the tRNAs are in the A/A and P/P sites, and there is no E-site tRNA. CHX has arrested these ribosomes in the classical PRE state with the nascent peptide attached to the A-site tRNA. The bases for assigning the CHX-arrested structure to the classical PRE state are as follows. First, the respective positions of the SSU and the LSU are most similar to the respective positions of human ribosomes in the classical-1 PRE state. Second, the uS19 C-terminal tail is resolved in the *N. crassa* structure and is in a conformation nearly identical to that of uS19 in human ribosomes in the classical PRE state. The classical PRE state is so far the only ribosome conformation for which this uS19 conformation has been observed [22]. Furthermore, the *N. crassa* ribosome, like the human ribosome in the classical PRE state, does not contain eIF5A

and has an unstructured L1 stalk. Also consistent with arrest in the classical PRE state, the CHX-arrested *N. crassa* ribosome does not contain eEF2, which is associated with ribosomes in the process of translocation [37], or eEF1A, which is associated with POST-state ribosomes [41]. This structural determination of the CHX-arrested state of ribosomes in polysomes as classical PRE with the peptide on the A-site tRNA is consistent with single-molecule biophysical data [42].

The use of high concentrations of CHX throughout the structural analysis procedure used here resulted in a population of ribosome particles that lacked any significant ribosome subpopulations containing tRNA in the P/E site. In contrast, in a study in which structural analyses followed purification of ribosomes with lower concentrations of CHX, which also included affinity purification steps, significant subpopulations of ribosomes lacking CHX and ribosomes with tRNAs in hybrid translocation states are also observed [22]. Recent measurements of the dissociation constant of CHX from ribosomes yielded values of 1 ± 0.4 ⎡M for *S. cerevisiae* ribosomes and 4 ± 1 ⎡M for human ribosomes [43]. A 1 ⎡M dissociation constant corresponds to a half-life of 0.7 s for a first-order reaction [44]. Because CHX binding is not irreversible, when it leaves, there is an increased kinetic chance of moving to the hybrid state occurring before CHX rebinding. The high concentrations of CHX we used could minimize these occurrences. The dissociation of CHX resulting in procession through the hybrid state could cause an additional round of elongation, which could be followed by subsequent CHX rebinding and arrest. Such considerations could be the basis for an alternative way to account for

the proposed differences in CHX and lactimidomycin mechanisms of action that are distinct from mechanistic differences arising because of differences in the structures of these molecules [45].

The structure of CHX binding in translating *N. crassa* ribosomes is similar to the corresponding structures in vacant yeast and human ribosomes[14, 28]. Thus, CHX is not altered by the presence of A/A- and P/P-site tRNA. Molecular analyses of the basis for classical *N. crassa* CHX-resistance mutations (all of the alleles of *cyh-1* and *cyh-2* available from the Fungal Genetics Stock Center) showed that they affected residues at the binding site. Mutations at residues previously identified as important for CHX resistance were directly affected by some alleles: uL15 residue Q38 and eL42 residue P56. A mutation at an additional eL42 residue, F58L, was also discovered.

These data can be integrated into the model initially proposed for CHX action based on structural determination of its location in non-translating (vacant) ribosomes in which CHX acts by clashing with occupancy of the E-site tRNA [14], but the structure of the translating ribosome's peptidyltransferase center was not known. Fig. 6 diagrams this integrated model for CHX action. Normally in elongation (Fig. 6A), aminoacyl tRNA enters the A site (i), and peptidyltransferase activity transfers the peptide to it from the P-site tRNA (ii). Translocation of the tRNAs occurs (iii and iv), and deacylated tRNA leaves the E site (v). When CHX is in the E site (Fig. 6B), aminoacyl tRNA entry into the A site and transfer of the peptide onto the A-site aminoacyl tRNA occur (i and ii),

but translocation cannot happen. Therefore, the ribosome is arrested in the classical PRE state with the peptide on the A-site tRNA. Consistent with this model, our data indicate that CHX does not interfere with termination because termination does not require translocation of tRNA (Fig. 6C and D).

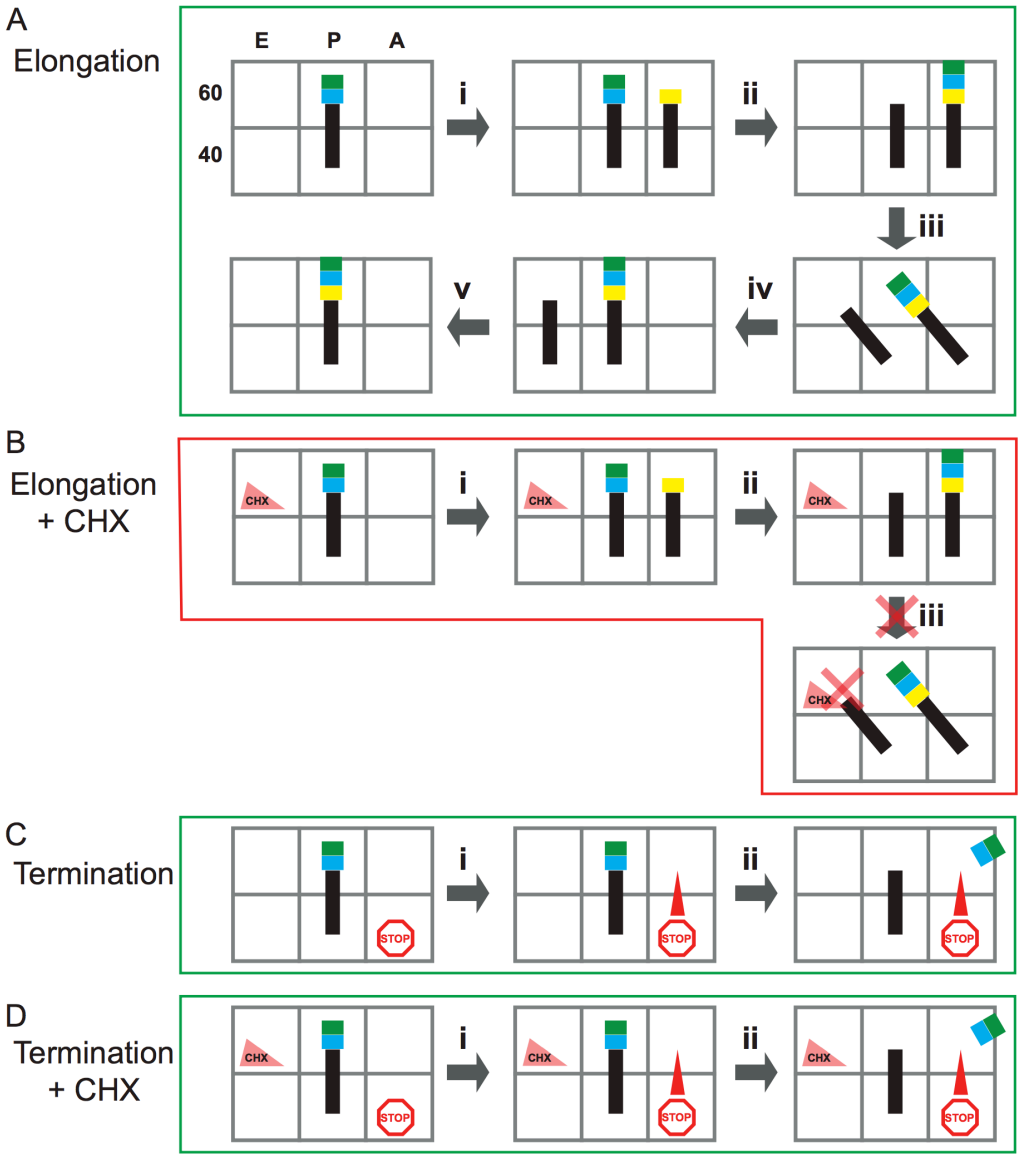

Fig. 6. Model for CHX action. E, P, and A sites of the 60S and 40S subunits are cartooned as open boxes; tRNAs are black lines; amino acids are blue, green, and yellow boxes; CHX is a triangle in the 60S E site. For a single elongation cycle, in the absence of CHX (top row), the aminoacyl-tRNA enters the empty A site (i), followed by nascent peptide transfer to the A site tRNA (ii). Translocation occurs [(iii) and (iv)], and the

deacylated tRNA leaves the E site to complete the cycle (v). When CHX is bound in the E site (bottom row), the aminoacyl-tRNA enters the empty A site (i), and transfer of the nascent peptide to the A site tRNA occurs (ii). However, CHX in the E site prevents translocation of the P site tRNA to the E site, arresting the ribosome in the PRE state with the polypeptide attached to the A site tRNA and deacylated tRNA in the P site.

The loss of ribosomes with a termination codon in their A site from an mRNA in the continued presence of CHX, while ribosomes engaged in elongation on that mRNA are stabilized, has implications for assessing signals from terminating ribosomes in ribo-seq studies employing CHX to maintain ribosomes association with mRNA. The levels of ribosomes observed at termination codons could depend on differential effects of preparation and analysis conditions that do not have similar consequences for levels of ribosomes arrested during elongation because these latter ribosomes are generally stabilized by CHX.

We observed an additional density close to the *N. crassa* CHX binding site and unambiguously identified it as SPD (Fig. 2A, B, and Fig. S5A). SPD is a polycation and is thought to function similarly to Mg2+ [46]. Indeed, this SPD site is occupied by Mg2+ in the structure of the vacant human 80S ribosome bound with CHX (Fig. S5C) and the vacant *S. cerevisiae* ribosome bound with CHX [14, 28]. We sought to determine the generality of this finding of SPD instead of Mg2+. SPD was recently modeled in the submitted structure of the *S. cerevisiae* ribosome containing bound CHX and eIF5A [35], and it is at the corresponding site (Fig. S5B). While not modeled, densities for SPD at the corresponding sites are also present in *S. cerevisiae* ribosome without CHX but with E-site tRNA, and human ribosomes with CHX or with E-site tRNA (Fig. S5F, D and E, respectively). These data, therefore, identify a conserved SPD binding site in eukaryotic ribosomes. It is worth noting that, when we looked at 269 assigned Mg2+ binding sites in the *S. cerevisiae* ribosome in the *N. crassa* ribosome, we saw density

corresponding to 260 of these Mg2+ molecules; in no case did we see density corresponding to SPD in these locations. Thus, while Mg2+ and SPD could potentially function interchangeably, it appears that the SPD binding site near the CHX binding site is different than other Mg2+ binding sites. In a published structure of rabbit 80S ribosome stalled on a poly(A) tail, two SPD molecules were provisionally included in the model (PDB ID: 6SGC) near the CCA 3' end of P-site tRNA [47]. However, we do not see corresponding densities in the *N. crassa* structure, nor do we see density corresponding to SPD in the E site in this rabbit ribosome structure. Finally, some binding sites of SPD have been identified in high-resolution prokaryotic ribosome structures (PDB ID codes: 7NHN (Crowe-McAuliffe *et al.,* unpublished), 4YBB [48], 5IT8 [49]). We compared these structures with the *N. crassa* ribosome structure and did not see densities for those SPD molecules in the corresponding regions of the *N. crassa* ribosome.

As is the case for the CHX-bound *N. crassa* ribosome, *S. cerevisiae* ribosomes that contain both CHX and eIF5A also have the nascent peptide attached to the A/A-site tRNA [35]. However, in the presence of eIF5A, the L1 stalk is structured, and the E site's structure, therefore, differs from that of the *N. crassa* ribosome. Furthermore, the C-terminal tail of uS19 is not resolved in this *S. cerevisiae* structure (Fig. 4F), consistent with the idea that a structured uS19 C-terminal tail as observed in the *N. crassa* and human classical PRE ribosomes is a distinct feature of that translational step. Thus, while there are similarities between the *N. crassa* and *S. cerevisiae* structures, as they

each contain CHX, SPD, and nascent peptide on the A/A tRNA, these ribosomes are not in the same state. Therefore, the *S. cerevisiae* ribosome likely represents an eIF5A-specific state distinct from the classical PRE state seen in the presence of CHX alone.

To our knowledge, this ribosome structure from the Ascomycete *N. crassa* represents the first near-atomic structure of a cytosolic ribosome from a filamentous fungus. The structure of the *N. crassa* mitochondrial ribosome was also recently determined [50]. The structure of the *N. crassa* cytosolic ribosome differs from the Ascomycete yeast *S. cerevisiae* in that it contains eL28 while the yeast ribosome does not. Thus, as with the demonstration of the structure of a human-like translation factor eIF3 in *N. crassa* that is more complex than *S. cerevisiae* eIF3 [51], and the existence of mammalian-like exon junction complex-mediated nonsense mediated mRNA decay in *N. crassa* that *S. cerevisiae* lacks [2, 52], this structure provides insight into important similarities and differences in the eukaryotic translational machinery. The 80S *K. lactis* ribosome structure [53] also lacks eL28; the yeast *K. lactis*, like *S. cerevisiae*, is a Saccharomycetes member. Interestingly, while eL28 is present in some protozoa, it is also missing in the ribosome structure from the protozoan *Trichomonas vaginalis* [33]. How the loss of eL28 figures in these organisms' evolutionary history, and the consequences of its presence versus absence for ribosome function, are questions that remain to be answered.

In summary, we obtained the structure of the translating *N. crassa* ribosome arrested by CHX. This structure provides direct evidence that CHX arrests ribosomes in the classical PRE state with the nascent peptide on the A-site tRNA. The reactivity of the A site in the presence of CHX is also demonstrated by toeprinting analyses which showed that termination, unlike elongation, is not arrested by CHX. These studies also revealed that the *N. crassa* ribosome is structurally different than its budding yeast counterpart in containing eL28 and, in this respect, more closely resembles the ribosomes of mammals. Most non-yeast fungi have eL28, and the *N. crassa* ribosome structure could be paradigmatic for these species, which include important Ascomycete pathogens such as *Aspergillus fumigatus* and Basidiomycete pathogens such as *Cryptococcus neoformans*. This work thus provides a structural basis for understanding CHX action and provides a new model for a fungal ribosome.

2.4 Supplementary figures

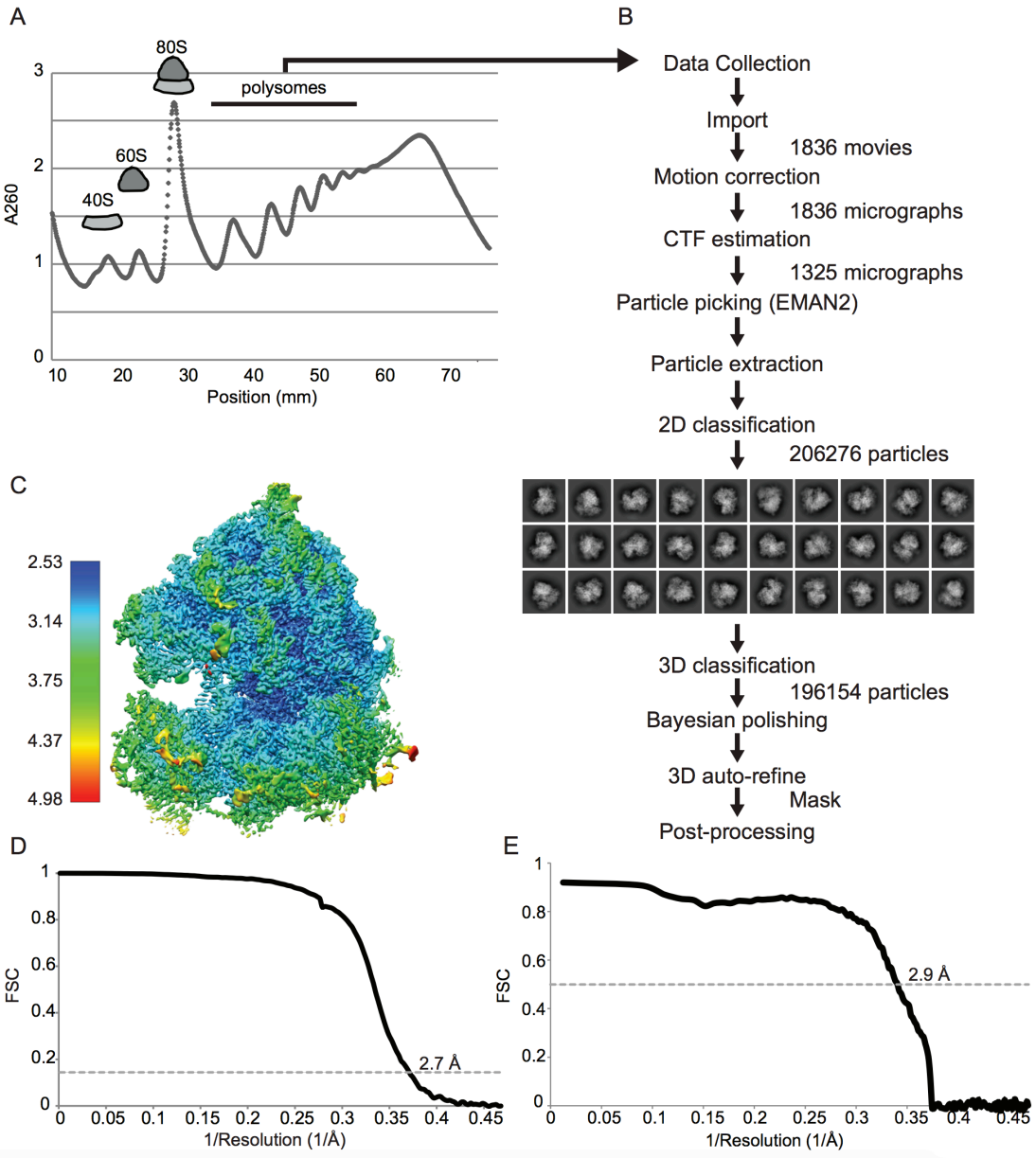

Fig. S1. Workflow for obtaining the cryo-EM map to determine the structure of the translating *N. crassa* ribosome arrested by CHX. (A) Polysome isolation. CHX (2

mg/ml) was added to *N. crassa* cultures 5 min prior to harvesting; harvested cells were broken in 2 mg/ml CHX, and sucrose gradients containing 2 mg/ml CHX were used to obtain polysome fractions for structural analysis. A representative of the multiple sucrose gradients used for isolation is shown with the positions indicated for 40S SSU, 60S LSU, 80S monosome, and the polysome region that was used for imaging. (B) Flowchart for obtaining the cryo-EM map. The top 30 2D class averages are shown; 3D classes are shown in Fig. S8. (C) Local resolution of the map of the *N. crassa* 80S ribosome. (D) Fourier Shell Correlation (FSC) curve calculated from two independently refined half-maps. The overall resolution is 2.7 Å at the "gold-standard" cutoff (FSC = 0.143). (E) FSC curve calculated by comparing the final map and model. The overall resolution is 2.9 Å at FSC = 0.5.

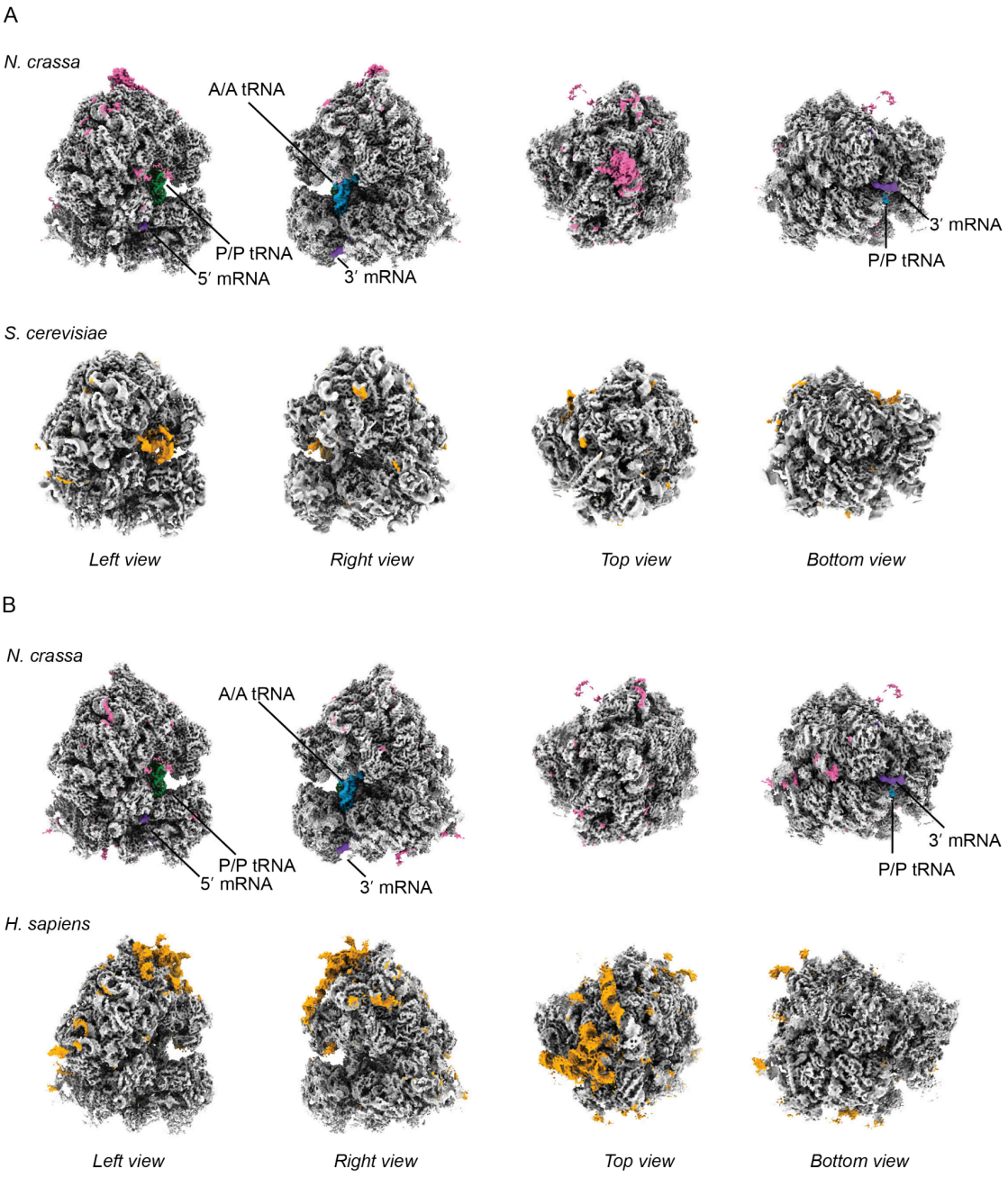

Fig. S2. Comparison of *N. crassa* ribosomes with *S. cerevisiae* and human ribosomes. (A) Comparison with *S. cerevisiae* ribosomes. (First row) *N. crassa* ribosome cryo-EM map. A/A tRNA, P/P tRNA, and mRNA are blue, green, and purple,

respectively. Pink indicates structure that is present in the *N. crassa* cryo-EM map but is absent in the *S. cerevisiae* ribosome model (PDB ID: 6TNU). This extra density is mainly at the top of the *N. crassa* LSU (see left, right, and top views) and corresponds to eL28 and part of $ES7^{L}$. (Second row) *S. cerevisiae* ribosome cryo-EM map (EMD-10537). The map contains A/A tRNA, P/P tRNA, and mRNA, but they are not indicated here. Orange indicates structure that is present in the *S. cerevisiae* cryo-EM map but is absent in the *N. crassa* model. It is mainly in the region where there is resolved structure for the L1 stalk and eIF5A in the *S. cerevisiae* ribosome but not the *N. crassa* ribosome. (B) Comparison with human ribosomes. (First row) *N. crassa* ribosome cryo-EM map. A/A tRNA, P/P tRNA, and mRNA are as in panel A. Pink indicates structure that is present in the *N. crassa* cryo-EM map but is absent in the human ribosome model (PDB ID: 6Y0G). (Second row) Human ribosome cryo-EM map (EMD-10668). It has A/A tRNA, P/P tRNA and mRNA, but they are not indicated here. Orange indicates structure that is absent in the *N. crassa* model: it corresponds mainly to the longer rRNA expansion segments that are lacking in *N. crassa* and fungi generally.

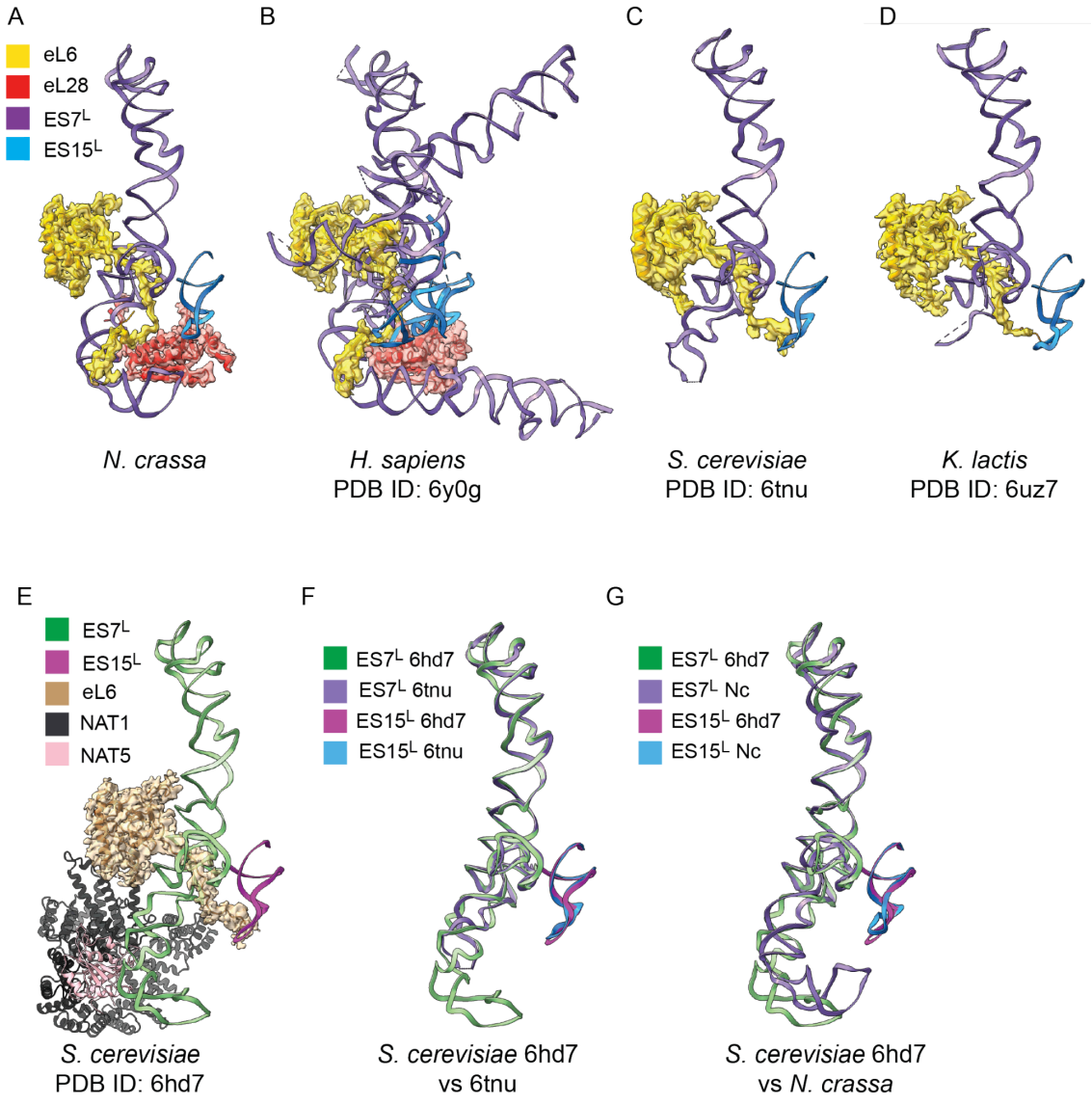

Fig. S3. Comparison of the LSU region containing eL6, ES7^{L} and ES15^{L} from (A) *N. crassa*, (B) human, (C) *S. cerevisiae*, and (D) *K. lactis*. *N. crassa* and human ribosomes contain eL28; *S. cerevisiae* and *K. lactis* ribosomes do not. Yellow: eL6; red: eL28; purple: ES7^{L}; blue: ES15^{L}. (E) Structure of *S. cerevisiae* ribosome region containing ES7^{L} complexed with NatA; green: ES7^{L}; plum: ES15^{L}; brown: eL6; black:

N-terminal acetyltransferase A complex subunit NAT1; pink: N-alpha-acetyltransferase NAT5; (F) comparison of *S. cerevisiae* ES7 and ES15 elements with NatA compared to *S. cerevisiae* without NatA; green and plum: $ES7^{L}$ and $ES15^{L}$ in yeast 6hd7, lavender, and blue: $ES7^{L}$ and $ES15^{L}$ in yeast 6TNU; (G) comparison of *S. cerevisiae* ES7 and ES15 elements with NatA to *N. crassa* ES7 and ES15 elements. Colors: green and plum: $ES7^{L}$ and $ES15^{L}$ in yeast 6hd7; lavender and blue: $ES7^{L}$ and $ES15^{L}$ in *N. crassa*.

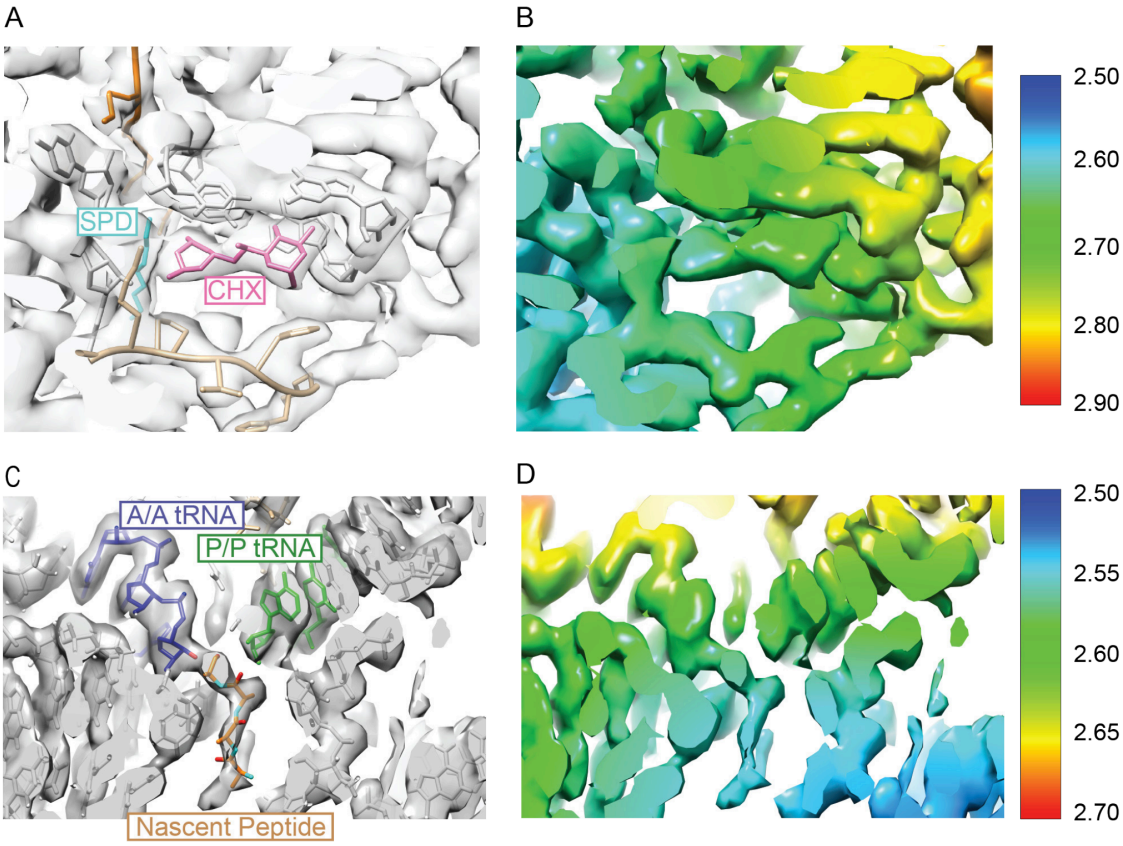

Fig. S4. Local resolution visualization of the CHX-binding region and the peptidyltransferase center of the *N. crassa* ribosome. (A) CHX-binding region; pink: CHX model; cyan: SPD model; (B) local resolution map of the CHX-binding region; (C) peptidyltransferase center; blue: A/A tRNA; green: P/P tRNA; brown: nascent peptide; (D) local resolution map of the peptidyltransferase center.

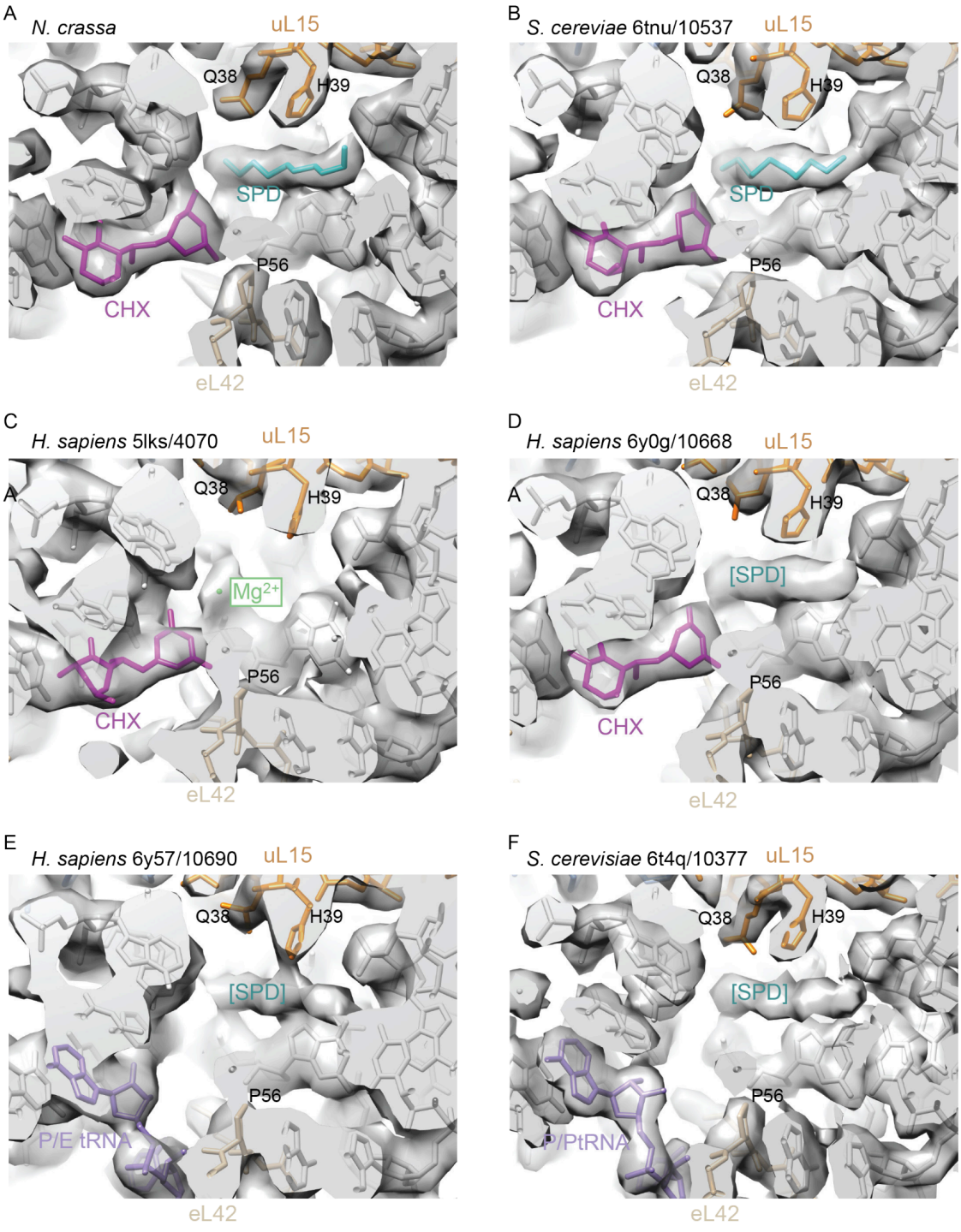

Fig. S5. SPD appears to be similarly positioned in *N. crassa*, *S. cerevisiae*, and human ribosomes independent of the presence of CHX. When SPD is not present,

Mg^{2+} is present. (A) *N. crassa* ribosome with CHX has modeled SPD; (B) *S. cerevisiae* ribosome with eIF5A and CHX has modeled SPD (EMD-10537, PDB ID: 6TNU) [35]; (C) *H. sapiens* ribosome with CHX added subsequently has Mg^{2+} instead of SPD at the corresponding position (EMD-4070, PDB ID: 5LKS)[28]; (D) *H. sapiens* PRE-state ribosome with CHX has unmodeled SPD (EMD-10668, PDB ID: 6Y0G) [22]; (E) *H. sapiens* rotated hybrid-PRE state ribosome with P/E tRNA has unmodeled SPD (EMD-10690, PDB ID: 6Y57) [22]; (F) *S. cerevisiae* ribosome with CGA-CCG stalled E/E tRNA has unmodeled SPD (EMD-10377, PDB ID: 6T4Q) [15]

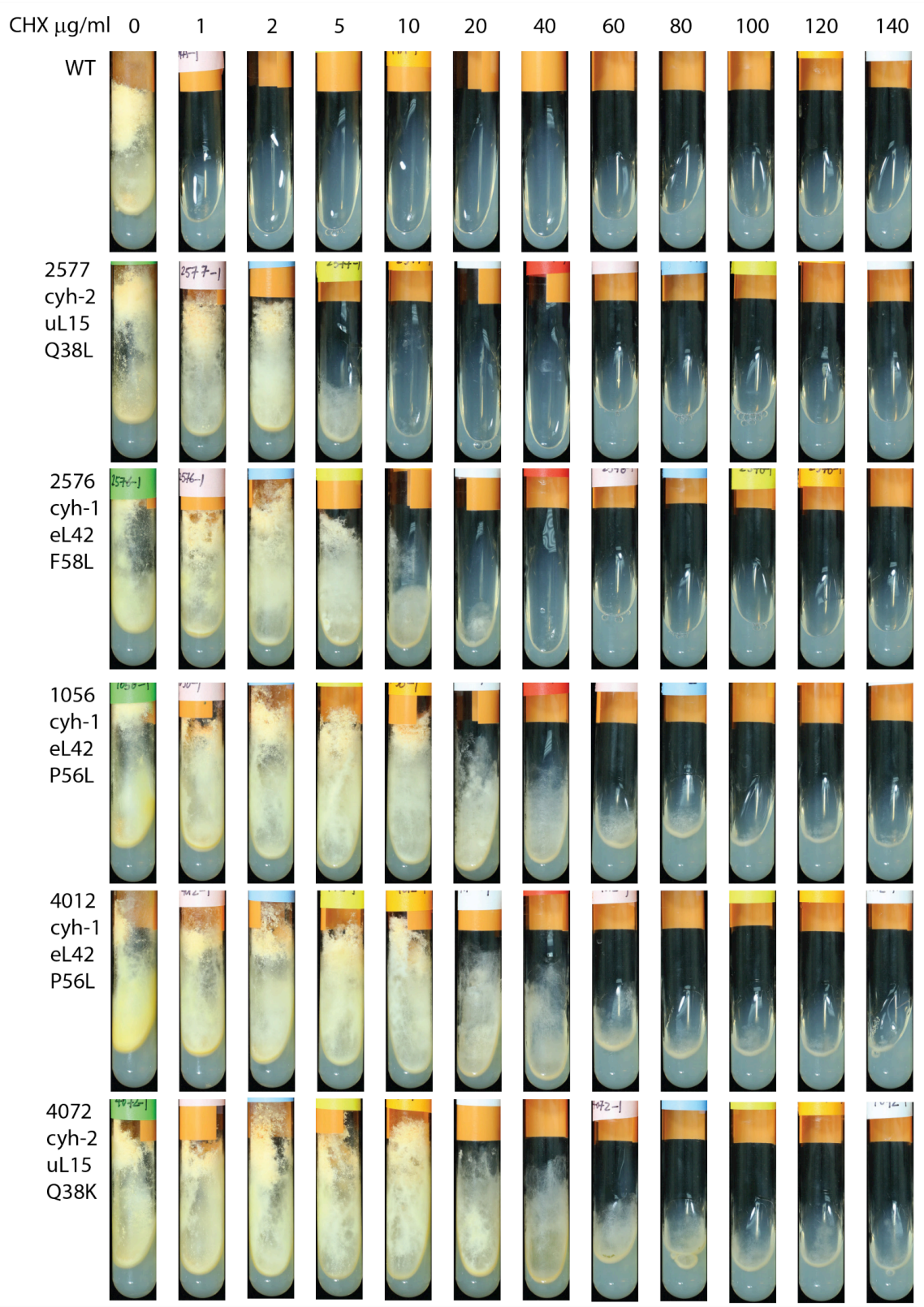
CHX μg/ml
0
1
2
5
10
20
40
60
80
100
120
140
WT
2577
cyh-2
uL15
Q38L
2576
cyh-1
eL42
F58L
1056
cyh-1
eL42
P56L
4012
cyh-1
eL42
P56L
4072
cyh-2
uL15
Q38K

Fig. S6. Growth of *N. crassa* wild-type and CHX-resistant mutants in the presence of CHX. Strains are indicated on the left, with their FGSC strain numbers, the mutated ribosomal protein, and the mutated residue; concentrations of CHX in the medium are indicated at the top. Growth was for eight days at room temperature.

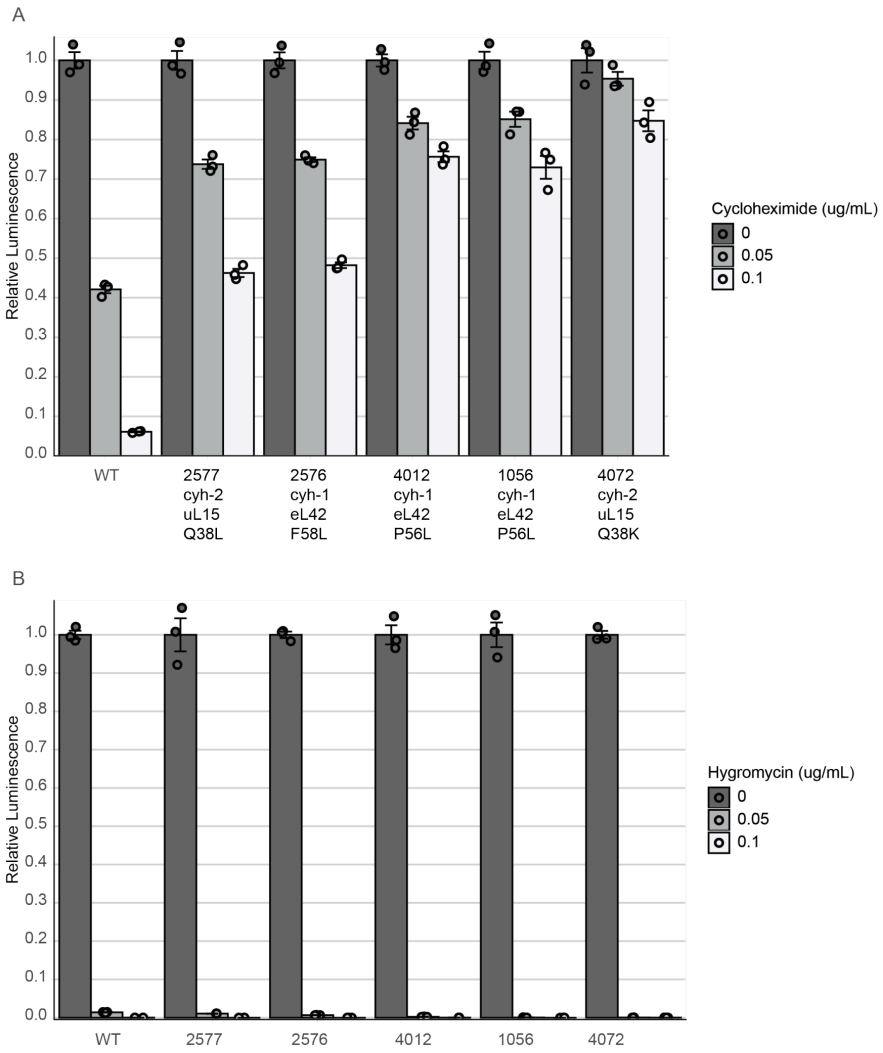

Fig. S7. Resistance of wild-type and mutant *N. crassa* ribosomes to CHX in cell-free translation extracts. Mutant but not wild-type (WT) translation is resistant to CHX, but translation in all strains is sensitive to hygromycin (HYG), an A site inhibitor. The relative luminescence used to measure relative translation is produced from firefly luciferase synthesized by cell-free translation using three translation replicates for each condition. (A) Translation in the presence of 0, 0.05, and 0.1 μg/ml CHX; (B) Translation in the presence of 0, 0.05, and 0.1 μg/ml hygromycin (HYG).

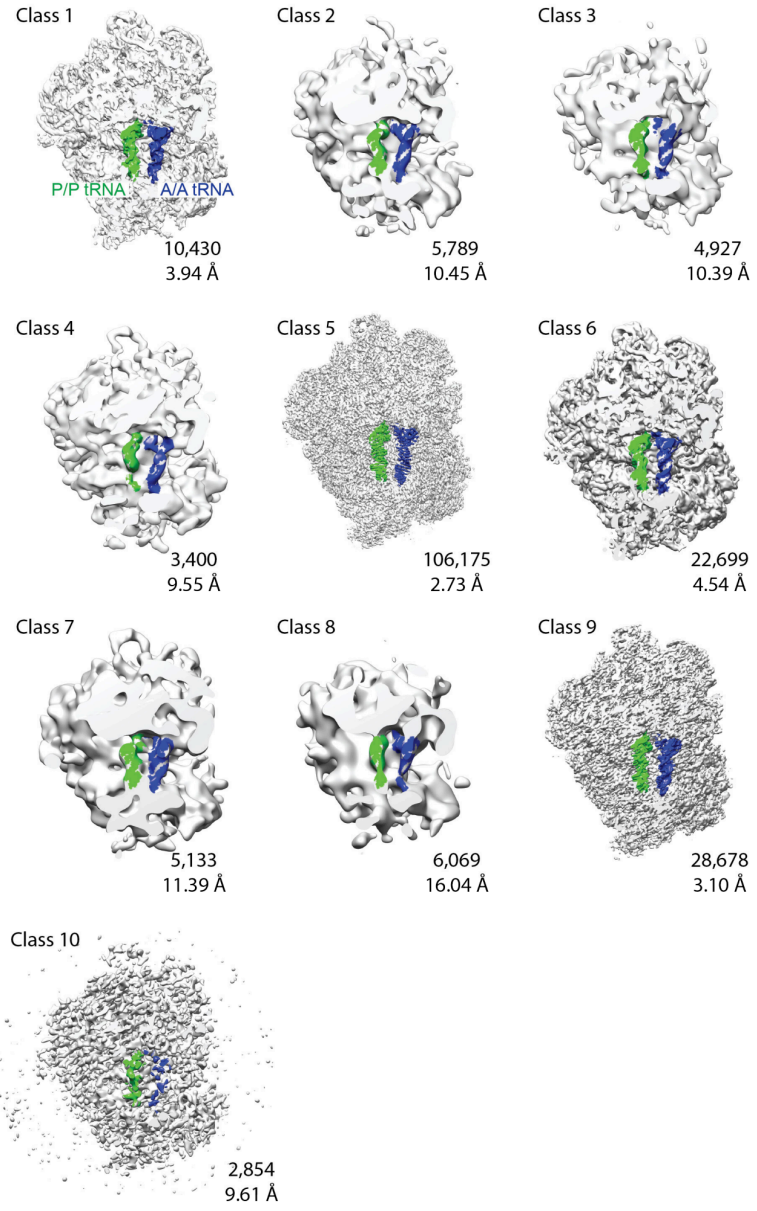

Fig. S8. 3D subclasses all contain A/A and P/P tRNA. The 3D classification of the *N. crassa* ribosomes stalled by CHX was performed in cryoSPARC [63]. Each of the 3D subclasses was further refined to give the maps shown in this figure. The corresponding number of particles and the overall resolution of each subclass are indicated. On each of the maps, the ribosome contains A/A site (blue) and P/P site (green) tRNAs

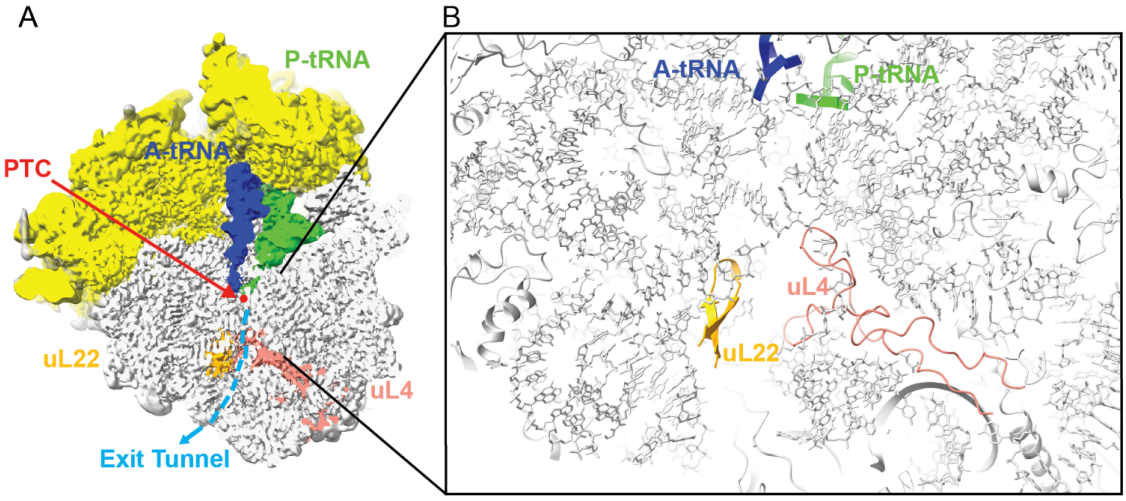

Fig. S9. Exit tunnel of the 60S subunit of the *N. crassa* ribosome. For comparative purposes, this view is similar to that given in [54]. Ribosomal proteins uL4 and uL22, the A- and P-site tRNAs, the path of the exit tunnel, and the PTC are indicated.

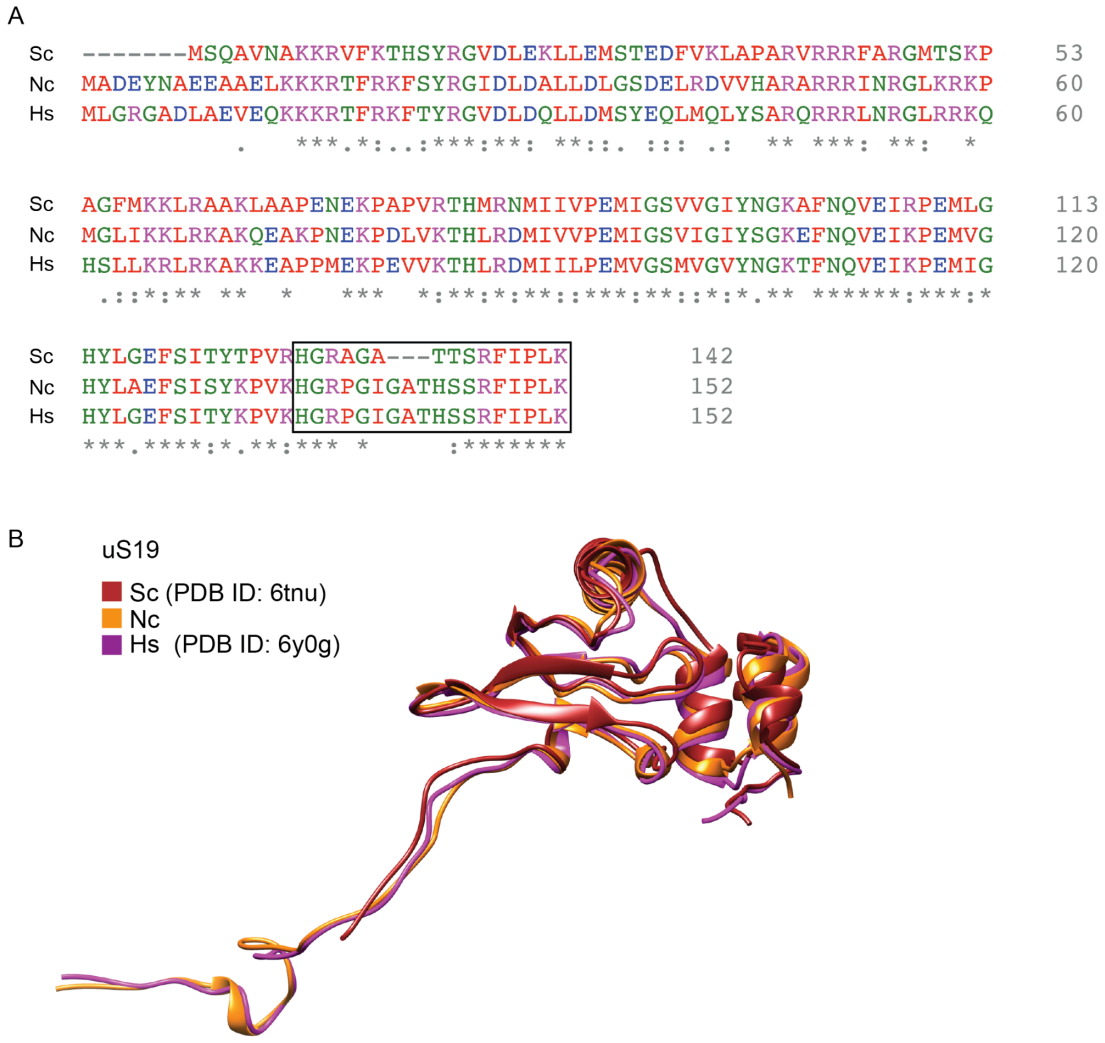

Fig. S10. uS19 alignments. (A) amino acid sequences of uS19 from *S. cerevisiae*, *N. crassa*, and *H. sapiens*, with the sequences of the C-terminal tails boxed; (B) overlay of the uS19 models from *N. crassa* (orange), *H. sapiens* (magenta, PDB ID: 6Y0G), and *S. cerevisiae* (brown, PDB ID: 6TNU). The structures shown in Bhaskar *et al.* [22] indicated that the uS19 C-terminal tail of the human ribosome undergoes dynamic rearrangement depending on the functional state of the translating ribosome. The

sequence of this region in *N. crassa* uS19 is identical to that in *H. sapiens*, and the conformation of the uS19 C-terminal in the *N. crassa* ribosome stalled by CHX is very similar to that in the *H. sapiens* ribosome at the classical-PRE state. The sequence of this region in *S. cerevisiae* is three amino acids shorter, but the arrangement of it shows a larger difference: the last 13 amino acids of the uS19 C-terminal tail are disordered in the *S. cerevisiae* ribosome associated with both CHX and eIF5A.

2.5 Supplementary tables

Table S1. 60S rRNAs and ribosomal proteins

rRNA name	GenBank ID	Full length	Built residues
26S	FJ360521.1	3338	3-995,1021-1548,1552-1933,2057-2405,2468-3338
5S	K02469.1	120	1-120
5.8S	M10692.1	158	1-158

Old name	New name	Uniprot ID	NCU number	Total length	Built residues
L2	uL2	Q7RVQ9	NCU00413	254	2-246
L3	uL3	P59671	NCU06843	392	2-386
L4	uL4	Q1K7B7	NCU03757	361	2-361
L5	uL18	O59953	NCU04331	301	2-301
L6	eL6	Q7SH22	NCU02707	202	2-142,150-202
L7	uL30	Q7SBD5	NCU07829	248	2-248
L8	eL8	Q6MFL6	Gene: B15B10.040	262	27-262
L9	uL6	Q7SGA6	NCU02744	193	1-190
L10	uL16	Q7S7F0	NCU08964	221	2-218
L11	uL5	Q7RVN0	NCU02509	174	10-174
L13	eL13	Q7S709	NCU05554	214	2-214
L14	eL14	Q7SI18	NCU00634	142	2-142
L15	eL15	Q8X034	NCU01776	203	2-203
L16	uL13	V5ILK7	NCU01221	231	33-231
L17	uL22	Q9HE25	NCU03703	186	2-152,170-186
L18	eL18	Q7RXJ4	NCU03988	183	2-183
L19	eL19	Q7S5N9	NCU05804	192	2-192
L20	eL20	V5IQT8	NCU08389	174	2-174
L21	eL21	Q7SDY8	NCU01948	160	2-160
L22	eL22	Q1K6Z3	NCU06661	126	15-115
L23	uL14	Q7SHJ9	NCU02905	139	4-139
L24	eL24	Q7SDU2	NCU03150	156	1-61
L25	uL23	Q7SBS9	NCU06226	156	39-156
L26	uL24	Q1K4V7	NCU03565	136	2-122
L27	eL27	Q1K580	NCU01827	135	1-135
L27A	uL15	P08978	NCU03806	149	2-149
L28	eL28	Q7SBB3	NCU06210	150	2-150
L29	eL29	Q7RZP9	NCU00315	65	2-65
L30	eL30	Q7S7F1	NCU08963	109	14-104
L31	eL31	Q7RW15	NCU08344	122	17-120
L32	eL32	Q7RXY1	NCU00464	131	3-123
L33	eL33	Q7S156	NCU09109	109	2-109
L34	eL34	Q7RVY8	NCU07857	117	2-109
L35	uL29	A7UW39	NCU10498	125	2-39,46-125
L36	eL36	Q7SEP1	NCU03302	104	6-101
L37	eL37	V5IQ48	NCU01966	92	2-89
L38	eL38	Q9C2B9	NCU03635	80	2-74
L39	eL39	Q7S2X9	NCU08990	51	2-51
L40	eL40	V5INI1	NCU05032	52	4-52
hypothetical protein	eL41	U9WGG3	NCU16635	25	1-25
L44	eL42	Q7RVK8	NCU00706	106	2-106
L43	eL43	Q7S1Z1	NCU07562	92	2-86

Table S2. 40S rRNA and ribosomal proteins

rRNA name	GenBank ID	Full length	Built residues
18S	FJ360521.1	1796	1-189, 193-655, 676-690, 694-1795

Old Name	New Name	Uniprot ID	NCU number	Full length	Built residues
S0	uS2	Q01291	NCU03393	290	2-210
S1	eS1	Q871N9	NCU01452	256	22-233
S2	uS5	Q7S503	NCU06047	265	46-257
S3	uS3	Q7RV52	NCU00489	262	8-231
S4	eS4	Q7SE03	NCU02181	261	2-257
S5	uS7	Q7RVI1	NCU09475	213	12-213
S6	eS6	V5INQ2	NCU08502	239	1-222
S7	eS7	O43105	NCU00258	202	7-13, 17-198
S8	eS8	V5IPM8	NCU08500	202	3-122,139-201
S9	uS4	Q7SDY7	NCU01949	190	2-178
S10	eS10	Q873A6	NCU06743	163	1-90
S11	uS17	Q7SFZ2	NCU03102	161	6-21,35-149
S12	eS12	Q7RV74	NCU06432	147	32-147
S13	uS15	Q7SDH0	NCU03038	151	2-151
S14	uS11	NCBI XP_96295 1.1	NCU07830	150	25-150
S15	uS19	Q7SGF1	NCU00971	152	26-152
S16	uS9	Q7SFJ9	NCU08620	142	4-142
S17	eS17	P27770	NCU07014	146	2-94,110-130
S18	uS13	Q7RXX0	NCU00475	156	11-151
S19	eS19	Q7SBD8	NCU07826	149	2-144
S20	uS10	Q7S3G1	NCU06892	117	18-116
S21	eS21	O93798	NCU08627	87	2-87
S22	uS8	Q7RV75	NCU06431	130	2-130
S23	uS12	Q9HE74	NCU01552	145	2-145
S24	eS24	Q1K5V9	NCU07182	136	4-127
S25	eS25	Q7SC06	NCU09476	97	23-93
S26	eS26	P21772	NCU04552	119	2-100
S27	eS27	Q7RVN2	NCU00618	82	2-82
S28	eS28	Q7S6W5	NCU05599	68	6-68
S29	uS14	Q9C2P2	NCU03738	56	2-56
S30	eS30	V5IMG5	NCU06048	63	5-47
S27a	eS31	P14799	NCU04553	154	100-140
CPC2*	CPC2	Q01369	NCU05810	316	3-312

*CPC2 is a stably associated non-ribosomal protein

Table S3. Mutant *N. crassa* strains used

FGSC strain and mating type	Allele	Ribosomal protein	Amino acid change	Codon change
4012 A	cyh-1 KH52(r)	eL42	P56L	CCC56CUC
1056 A	cyh-1 1003(r)	eL42	P56L	CCC56CUC
2576 A	cyh-1 54(r)	eL42	F58L	UUC58CUC
4072 a	cyh-2 KH53(r)	uL15	Q38K	CAG38AAG
2577 A	cyh-2 130(r)	uL15	Q38L	CAG38CUG

Table S4. Statistics for the model of the translating *Neurospora crassa* 80S ribosome

Bond RMSD (Å)	0.003
Angle RMSD (°)	0.699
Molprobity score	1.74
Clashscore, all atoms	7.78, 83rd percentile (N=1784, all resolutions)
Poor rotamers (%)	0.02
Favored rotamer (%)	99.64
Ramachandran outliers (%)	0.08
Ramachandran favored (%)	95.52
Correct sugar puckers (%)	99.72
Good backbone conformation (%)	86.51

2.6 References

1. McCluskey, K., A. Wiest, and M. Plamann, *The Fungal Genetics Stock Center: a repository for 50 years of fungal genetics research.* J Biosci, 2010. **35**(1): p. 119-26.
2. Zhang, Y. and M.S. Sachs, *Control of mRNA Stability in Fungi by NMD, EJC and CBC Factors Through 3'UTR Introns.* Genetics, 2015. **200**(4): p. 1133-48.
3. Wu, C., et al., *The cell free protein synthesis system from the model filamentous fungus Neurospora crassa.* Methods, 2018. **137**: p. 11-19.
4. Ebbole, D.S., M. S. , *A rapid and simple method for isolation of Neurospora crassa homokaryons using microconidia.* Fungal Genetics Reports, 1990. **Vol. 37(1)**.
5. Luo, Z., M. Freitag, and M.S. Sachs, *Translational regulation in response to changes in amino acid availability in Neurospora crassa.* Mol Cell Biol, 1995. **15**(10): p. 5235-45.
6. Yang, K., et al., *Structural insights into species-specific features of the ribosome from the human pathogen Mycobacterium tuberculosis.* Nucleic Acids Res, 2017. **45**(18): p. 10884-10894.
7. Zivanov, J., et al., *New tools for automated high-resolution cryo-EM structure determination in RELION-3.* Elife, 2018. **7**.
8. Zheng, S.Q., et al., *MotionCor2: anisotropic correction of beam-induced motion for improved cryo-electron microscopy.* Nat Methods, 2017. **14**(4): p. 331-332.

9. Rohou, A. and N. Grigorieff, *CTFFIND4: Fast and accurate defocus estimation from electron micrographs.* J Struct Biol, 2015. **192**(2): p. 216-21.

10. Tang, G., et al., *EMAN2: an extensible image processing suite for electron microscopy.* J Struct Biol, 2007. **157**(1): p. 38-46.

11. Bell, J.M., et al., *New software tools in EMAN2 inspired by EMDatabank map challenge.* J Struct Biol, 2018. **204**(2): p. 283-290.

12. Punjani, A., et al., *cryoSPARC: algorithms for rapid unsupervised cryo-EM structure determination.* Nat Methods, 2017. **14**(3): p. 290-296.

13. Rother, M., et al., *ModeRNA: a tool for comparative modeling of RNA 3D structure.* Nucleic Acids Res, 2011. **39**(10): p. 4007-22.

14. Garreau de Loubresse, N., et al., *Structural basis for the inhibition of the eukaryotic ribosome.* Nature, 2014. **513**(7519): p. 517-522.

15. Tesina, P., et al., *Molecular mechanism of translational stalling by inhibitory codon combinations and poly(A) tracts.* Embo j, 2020. **39**(3): p. e103365.

16. Pruesse, E., J. Peplies, and F.O. Glöckner, *SINA: accurate high-throughput multiple sequence alignment of ribosomal RNA genes.* Bioinformatics, 2012. **28**(14): p. 1823-9.

17. DiMaio, F., et al., *Atomic-accuracy models from 4.5-Å cryo-electron microscopy data with density-guided iterative local refinement.* Nat Methods, 2015. **12**(4): p. 361-365.

18. Emsley, P. and K. Cowtan, *Coot: model-building tools for molecular graphics.* Acta Crystallogr D Biol Crystallogr, 2004. **60**(Pt 12 Pt 1): p. 2126-32.

19. Gruber, A.R., et al., *The Vienna RNA websuite.* Nucleic Acids Res, 2008. **36**(Web Server issue): p. W70-4.

20. Adams, P.D., et al., *PHENIX: a comprehensive Python-based system for macromolecular structure solution.* Acta Crystallogr D Biol Crystallogr, 2010. **66**(Pt 2): p. 213-21.

21. Eswar, N., et al., *Comparative protein structure modeling using MODELLER.* Curr Protoc Protein Sci, 2007. **Chapter 2**: p. Unit 2.9.

22. Bhaskar, V., et al., *Dynamics of uS19 C-Terminal Tail during the Translation Elongation Cycle in Human Ribosomes.* Cell Rep, 2020. **31**(1): p. 107473.

23. Moriarty, N.W., R.W. Grosse-Kunstleve, and P.D. Adams, *electronic Ligand Builder and Optimization Workbench (eLBOW): a tool for ligand coordinate and restraint generation.* Acta Crystallogr D Biol Crystallogr, 2009. **65**(Pt 10): p. 1074-80.

24. Williams, C.J., et al., *MolProbity: More and better reference data for improved all-atom structure validation.* Protein Sci, 2018. **27**(1): p. 293-315.

25. Pettersen, E.F., et al., *UCSF Chimera--a visualization system for exploratory research and analysis.* J Comput Chem, 2004. **25**(13): p. 1605-12.

26. Goddard, T.D., et al., *UCSF ChimeraX: Meeting modern challenges in visualization and analysis.* Protein Sci, 2018. **27**(1): p. 14-25.

27. Wu, C., et al., *The use of fungal in vitro systems for studying translational regulation.* Methods Enzymol, 2007. **429**: p. 203-25.

28. Myasnikov, A.G., et al., *Structure-function insights reveal the human ribosome as a cancer target for antibiotics.* Nat Commun, 2016. **7**: p. 12856.

29. Wettstein, F.O., H. Noll, and S. Penman, *EFFECT OF CYCLOHEXIMIDE ON RIBOSOMAL AGGREGATES ENGAGED IN PROTEIN SYNTHESIS IN VITRO.* Biochim Biophys Acta, 1964. **87**: p. 525-8.

30. Selker, E.U., J.N. Stevens, and R.L. Metzenberg, *Heterogeneity of 5S RNA in fungal ribosomes.* Science, 1985. **227**(4692): p. 1340-3.

31. Müller, F., et al., *The cpc-2 gene of Neurospora crassa encodes a protein entirely composed of WD-repeat segments that is involved in general amino acid control and female fertility.* Mol Gen Genet, 1995. **248**(2): p. 162-73.

32. Armache, J.P., et al., *Cryo-EM structure and rRNA model of a translating eukaryotic 80S ribosome at 5.5-A resolution.* Proc Natl Acad Sci U S A, 2010. **107**(46): p. 19748-53.

33. Li, Z., et al., *Cryo-EM structures of the 80S ribosomes from human parasites Trichomonas vaginalis and Toxoplasma gondii.* Cell Res, 2017. **27**(10): p. 1275-1288.

34. Knorr, A.G., et al., *Ribosome-NatA architecture reveals that rRNA expansion segments coordinate N-terminal acetylation.* Nat Struct Mol Biol, 2019. **26**(1): p. 35-39.

35. Buschauer, R., et al., *The Ccr4-Not complex monitors the translating ribosome for codon optimality.* Science, 2020. **368**(6488).

36. Borovinskaya, M.A., et al., *Structural basis for hygromycin B inhibition of protein biosynthesis.* Rna, 2008. **14**(8): p. 1590-9.

37. Behrmann, E., et al., *Structural snapshots of actively translating human ribosomes.* Cell, 2015. **161**(4): p. 845-57.

38. Hellen, C.U.T., *Translation Termination and Ribosome Recycling in Eukaryotes.* Cold Spring Harb Perspect Biol, 2018. **10**(10).

39. Gaba, A., et al., *Physical evidence for distinct mechanisms of translational control by upstream open reading frames.* Embo j, 2001. **20**(22): p. 6453-63.

40. Dever, T.E., I.P. Ivanov, and M.S. Sachs, *Conserved Upstream Open Reading Frame Nascent Peptides That Control Translation.* Annu Rev Genet, 2020. **54**: p. 237-264.

41. Flis, J., et al., *tRNA Translocation by the Eukaryotic 80S Ribosome and the Impact of GTP Hydrolysis.* Cell Rep, 2018. **25**(10): p. 2676-2688.e7.

42. Budkevich, T., et al., *Structure and dynamics of the mammalian ribosomal pretranslocation complex.* Mol Cell, 2011. **44**(2): p. 214-24.

43. Pellegrino, S., et al., *Understanding the role of intermolecular interactions between lissoclimides and the eukaryotic ribosome.* Nucleic Acids Res, 2019. **47**(6): p. 3223-3232.

44. Pollard, T.D., *A guide to simple and informative binding assays.* Mol Biol Cell, 2010. **21**(23): p. 4061-7.

45. Schneider-Poetsch, T., et al., *Inhibition of eukaryotic translation elongation by cycloheximide and lactimidomycin.* Nat Chem Biol, 2010. **6**(3): p. 209-217.

46. Athwal, G.S. and S.C. Huber, *Divalent cations and polyamines bind to loop 8 of 14-3-3 proteins, modulating their interaction with phosphorylated nitrate reductase.* Plant J, 2002. **29**(2): p. 119-29.

47. Chandrasekaran, V., et al., *Mechanism of ribosome stalling during translation of a poly(A) tail.* Nat Struct Mol Biol, 2019. **26**(12): p. 1132-1140.

48. Noeske, J., et al., *High-resolution structure of the Escherichia coli ribosome.* Nat Struct Mol Biol, 2015. **22**(4): p. 336-41.

49. Cocozaki, A.I., et al., *Resistance mutations generate divergent antibiotic susceptibility profiles against translation inhibitors.* Proc Natl Acad Sci U S A, 2016. **113**(29): p. 8188-93.

50. Itoh, Y., et al., *Analysis of translating mitoribosome reveals functional characteristics of translation in mitochondria of fungi.* Nat Commun, 2020. **11**(1): p. 5187.

51. Smith, M.D., et al., *Human-like eukaryotic translation initiation factor 3 from Neurospora crassa.* PLoS One, 2013. **8**(11): p. e78715.

52. Kurilla, A., et al., *Expression of the translation termination factor eRF1 is autoregulated by translational readthrough and 3'UTR intron-mediated NMD in Neurospora crassa.* FEBS Lett, 2020. **594**(21): p. 3504-3517.

53. Huang, B.Y. and I.S. Fernández, *Long-range interdomain communications in eIF5B regulate GTP hydrolysis and translation initiation.* Proc Natl Acad Sci U S A, 2020. **117**(3): p. 1429-1437.

54. Takamatsu, S., et al., *Reverse genetics-based biochemical studies of the ribosomal exit tunnel constriction region in eukaryotic ribosome stalling: spatial allocation of the regulatory nascent peptide at the constriction.* Nucleic Acids Res, 2020. **48**(4): p. 1985-1999.

CHAPTER III

SUMMARY AND CONCLUSION

3.1 Summary and conclusion

Cycloheximide (CHX) is the most widely used laboratory inhibitor of eukaryotic protein synthesis [1] and is an important reagent for ribosome profiling analyses [2]. To understand its mechanism of action, we purified *N. crassa* ribosomes from polysomes arrested by CHX and determined the structure of these ribosomes inhibited by CHX at 2.7 Å resolution using cryo-EM. In this structure, CHX binds near the E site in the LSU. Comparisons of the structures clearly show that the LSU's CHX binding pocket is highly conserved in *N. crassa*, *S. cerevisiae*, and human ribosomes. Interestingly, a SPD molecule was found to bind near the CHX binding site in the *N. crassa* ribosome. This structure provides direct evidence that CHX arrests ribosome in the classical PRE state with the nascent peptide on the A-site tRNA. This structure also shows that *N. crassa* ribosome has eL28, structurally different from budding yeast but more similar to the ribosomes of mammals.

We sequenced the previously isolated mutations that conferred CHX resistance to *N. crassa*, and found that all of the amino acid changes in these mutants mapped to highly conserved residues in two ribosomal proteins in the CHX binding pocket: eL42 P56L (in two independent mutants), eL42 F58L, uL15 Q38L, and uL15 Q38K. Both the growth

tests with different concentrations of CHX and the *in vitro* tests using cell-free translation systems (CFTSs) showed similar relative resistances to CHX: wild type < eL42 F58L <uL15 Q38L <eL42 P56L < uL15 Q38K.

Yeasts in the genus *Candida* are major human fungal pathogens, and antifungal drug-resistance is becoming problematic for treating *Candida* infections [3]. The two species most responsible for candidiasis, *C. albicans* and *C. parasiticus*, are naturally CHX-resistant, and their resistance is a hallmark clinical, microbiological test for their presence in patient samples [4]. A significant factor that confers CHX resistance in these fungi is that their ribosomal protein eL42 has Gln56 instead of the generally conserved Pro56. This is one of the residues that we have shown to be in the CHX binding pocket and the mutation of which (P56L) can cause resistance to CHX in *N. crassa.* In *S. cerevisiae*, eL42 genes containing the P56Q mutation confer high-level CHX resistance to the organism [5, 6]; analyses of substitutions of P56 with each of the other 19 amino acids shows P56Q confers the highest level of resistance [7].

Because ribosomes containing structural E-site differences are known to be more resistant to CHX, such ribosomes could also be differentially sensitive to other inhibitors that bind to the similar region but have different interactions with ribosomes. It might be interesting to study the structural and functional characteristics of the binding of other E site translation inhibitors to the CHX-resistant ribosomes, so as to discover antifungal

molecules that interfere with the activity of the *Candida* ribosomes but not the activity of animal ribosomes.

For example, a new class of small molecule E site interactors in the lissoclimide family has emerged with the potential to provide fundamental insight and practical application for E site inhibition of ribosome activity [19]. Studies have shown that lissoclimides share some structural similarity with CHX and lactimidomycin, which is another imide-containing translation inhibitor that acts at the E site, but have additional interactions with the ribosome [8, 9]. While there are models proposed to explain CHX resistance, no structures have been described that establish definitively how inhibitory imides interact with CHX-resistant ribosomes. Thus, it is important to understand functional differences in imide action and determine the differences in how CHX-resistant ribosomes bind to imides. To accomplish this, biochemical approaches such as toeprinting in CFTSs should be applied to determine specific mechanisms of lissoclimide function compared to CHX and lactimidomycin. Structures of CHX-resistant ribosomes bound with lissoclimides should be obtained and compared. In addition, the compounds' cytotoxicity against fungi and mammalian cells should be evaluated. These studies should significantly advance fundamental and practical understanding of E site drug action, and could fill a critical need to develop novel antifungal drugs directed against the *Candida* pathogens.

The translating ribosomes are not homogenous machines. In eukaryotic cells, rDNAs that encode rRNAs are present in tandem repeats and have large copy numbers [10]. In

N. crassa, it has been shown that 90% of the rDNAs isolated from mycelia were similar but not identical to the other 10% of the rDNAs [11]. The variation among the repeats, the different expression levels, and the processes of subsequent rRNA modification and assembly with ribosomal proteins all increase the chances that rRNA heterogeneity on translating ribosomes can arise [12]. In various organisms, alternative rRNA molecules have been reported (reviewed in [13]). *N. crassa* has been shown to have at least seven types of 5S rRNA [14]. In addition, ribosomes can contain different ribosomal proteins. For example, quantitative mass spectrometry data have revealed the existence of heterogeneous populations among actively translating ribosomes from mouse embryonic stem cells: some ribosomes lack at least one of the ribosomal proteins uL10 (RPL10A), uL11 (RPL11), eL38 (RPL38), eL40 (RPL40), eS7 (RPS7), and eS25 (RPS25) [15]. Several different types of posttranslational modifications such as methylation, phosphorylation, and ubiquitylation of the ribosomal proteins have been shown to affect the translation [16] and thus can contribute to the ribosome heterogeneity as well. Apart from the rRNA and ribosomal proteins, other proteins, such as the various translation factors, associated with ribosomes, can also differ.

N. crassa has long been used as a model organism to study circadian rhythms [17] and recently has been established as a model organism for studying translational control in circadian rhythm [18, 20]. Karki *et al.* have shown that the inhibitory phosphorylation of the translation initiation factor eIF2α is clock controlled in *N. crassa* and that this control is necessary for the rhythmic translation initiation [18]. Quantitative mass spectrometry

data have also indicated that some ribosomal proteins are clock controlled in *N. crassa* (Lamb, *et al.*, data not published). Therefore, it will be interesting to investigate the structures of ribosomes over a circadian time course. Once the polysome samples from the circadian time course are prepared and imaged using cryo-EM, and the cryo-EM data is processed to get the Coulomb potential maps, the current *N. crassa* ribosome model (PDB ID: 7R81) should be fitted into each of the new maps and refined using PHENIX. Then each of the resulting models should be compared with the corresponding Coulomb potential map to identify any lack or addition of ribosomal components or translation factors. The models should also be overlaid for comparison. It is expected that the structures of some rRNA or ribosomal protein regions would be different over the circadian time course.

Combining analyzing the models/maps at the specific residue and comparing other known sequences of that rRNA or ribosomal protein, one could possibly identify whether the difference is due to: (1) an alternative variant (*i.e.* when it is noticed that the number of residues changes, or when the map at some residues and the current model obviously do not fit but significantly resemble another nucleic acid or amino acid), (2) modification of the rRNA or ribosomal protein (*i.e.* when an extra density of map beyond the model is observed at the residue), or (3) same composition but different conformations which are related to different interactions between the ribosomal components and/or other associated components such as mRNA, tRNA, nascent peptide, or translation factors. The investigation of *N. crassa* ribosomes over a circadian time

course would fill the gap in understanding the fundamental mechanism of how clock regulates ribosome structure/function to affect translation.

The *N. crassa* ribosome, unlike the *S. cerevisae* ribosome which does not have eL28, contains ribosomal protein eL28, like the human ribosome. Recent studies have shown that human eL28 may play a role in cancer development. The expression level of eL28 has been shown to affect the proliferation of colorectal cancer cells, and the higher tumor expression level of eL28 is associated with reduced survival in metastatic colorectal cancer patients [21]. In hepatocellular carcinoma cell model that is resistant to sorafenib, which is one of the main treatment options, the gene encoding eL28 has been shown to induce sorafenib resistance [22]. However, the exact mechanism of how eL28 affects cancer development remains unclear.

It might be possible that eL28, as part of the ribosome, regulates translation and therefore is associated with tumor cell proliferation and invasion. It might also be possible that eL28 could regulate cell apoptosis, like some other ribosomal proteins such as uS19 (S15) [23], uL13 (L13A) [24] and uL23 (L23) [25]. It might also be possible that eL28 has some ribosome-independent roles.

In *N. crassa*, eL28 is not an essential gene. It will be of interest to solve the structure of the ribosome isolated from the eL28-knockout (KO) strain FGSC #15780 [26], and compare it with that from a wild-type strain, especially the conformations of eL6, $ES7^{L}$,

and ES15^{L,} which have been shown to interact with eL28 in the wild-type *N. crassa* ribosome. It will also be interesting to compare the phenotypes (for example, growth in minimal medium, growth under stress, and cell cycle analysis), transcriptome, and translatome of the wild-type and eL28-KO strains.

Comparison of the LSU region containing eL6, ES7^{L} and ES15^{L} from *N. crassa*, human, *S. cerevisiae*, and *K. lactis* (Fig. S3) shows that ES7^{L} and ES15^{L} in human ribosome are significantly longer than those in the three fungal ribosomes. This distinct difference reveals that ES7^{L} and ES15^{L} could be potential antibiotic targets. It will be interesting to screen for small molecules that bind to either of ES7^{L} and ES15^{L} in fungi more tightly compared to those in the human ribosome. It has been shown that F-neo, an RNA binding fluorescent probe, binds more tightly to ES7^{L} in *C. albicans* while binds weakly to ES7^{L} in human [27]. *C. albicans* does not have eL28. The interaction of the ES7^{L}-binding drugs with the ES7^{L} may be different in other pathogenic fungi that have eL28, such as *A. fumigatus* and *C. neoformans*, therefore making *N. crassa* an ideal system for antibiotic screening and characterization.

3.2 References

1. Schneider-Poetsch, T., et al., *Inhibition of eukaryotic translation elongation by cycloheximide and lactimidomycin.* Nat Chem Biol, 2010. **6**(3): p. 209-217.

2. Yang, Q., et al., *eRF1 mediates codon usage effects on mRNA translation efficiency through premature termination at rare codons.* Nucleic Acids Res, 2019. **47**(17): p. 9243-9258.

3. Pristov, K.E. and M.A. Ghannoum, *Resistance of Candida to azoles and echinocandins worldwide.* Clin Microbiol Infect, 2019. **25**(7): p. 792-798.

4. Pincus, D.H., S. Orenga, and S. Chatellier, *Yeast identification--past, present, and future methods.* Med Mycol, 2007. **45**(2): p. 97-121.

5. Del Pozo, L., et al., *Two different genes from Schwanniomyces occidentalis determine ribosomal resistance to cycloheximide.* Eur J Biochem, 1993. **213**(2): p. 849-57.

6. Kawai, S., et al., *Drastic alteration of cycloheximide sensitivity by substitution of one amino acid in the L41 ribosomal protein of yeasts.* J Bacteriol, 1992. **174**(1): p. 254-62.

7. Bae, J.H., B.H. Sung, and J.H. Sohn, *Site saturation mutagenesis of ribosomal protein L42 at 56th residue and application as a consecutive selection marker for cycloheximide resistance in yeast.* FEMS Microbiol Lett, 2018. **365**(8).

8. Könst, Z.A., et al., *Synthesis facilitates an understanding of the structural basis for translation inhibition by the lissoclimides.* Nat Chem, 2017. **9**(11): p. 1140-1149.

9. Pellegrino, S., et al., *Understanding the role of intermolecular interactions between lissoclimides and the eukaryotic ribosome.* Nucleic Acids Res, 2019. **47**(6): p. 3223-3232.

10. Kobayashi, T., *Ribosomal RNA gene repeats, their stability and cellular senescence.* Proceedings of the Japan Academy. Series B, Physical and biological sciences, 2014. **90**(4): p. 119-129.

11. Dutta, S.K., N.P. Williams, and D.K. Mukhopadhyay, *Ribosomal RNA genes of Neurospora crassa: multiple copies and specificities.* Mol Gen Genet, 1983. **189**(2): p. 207-10.

12. Genuth, N.R. and M. Barna, *The Discovery of Ribosome Heterogeneity and Its Implications for Gene Regulation and Organismal Life.* Molecular cell, 2018. **71**(3): p. 364-374.

13. Li, D. and J. Wang, *Ribosome heterogeneity in stem cells and development.* The Journal of cell biology, 2020. **219**(6): p. e202001108.

14. Selker, E.U., J.N. Stevens, and R.L. Metzenberg, *Heterogeneity of 5S RNA in fungal ribosomes.* Science, 1985. **227**(4692): p. 1340-3.

15. Shi, Z., et al., *Heterogeneous Ribosomes Preferentially Translate Distinct Subpools of mRNAs Genome-wide.* Mol Cell, 2017. **67**(1): p. 71-83.e7.

16. Xue, S. and M. Barna, *Specialized ribosomes: a new frontier in gene regulation and organismal biology.* Nature reviews. Molecular cell biology, 2012. **13**(6): p. 355-369.

17. Baker, C.L., J.J. Loros, and J.C. Dunlap, *The circadian clock of Neurospora crassa.* FEMS Microbiol Rev, 2012. **36**(1): p. 95-110.

18. Karki, S., et al., *Circadian clock control of eIF2α phosphorylation is necessary for rhythmic translation initiation.* Proc Natl Acad Sci U S A, 2020. **117**(20): p. 10935-10945.

19. Robert, F., et al., *Chlorolissoclimides: new inhibitors of eukaryotic protein synthesis*. Rna, 2006. **12**(5): p. 717-25.

20. Caster, S.Z., et al., *Circadian clock regulation of mRNA translation through eukaryotic elongation factor eEF-2*. Proc Natl Acad Sci U S A, 2016. **113**(34): p. 9605-9610

21. Labriet, A., et al., *Germline variability and tumor expression level of ribosomal protein gene RPL28 are associated with survival of metastatic colorectal cancer patients*. Scientific Reports, 2019. **9**(1): p. 13008.

22. Shi, Y., et al., *The Ribosomal Protein L28 Gene Induces Sorafenib Resistance in Hepatocellular Carcinoma*. Frontiers in Oncology, 2021. **11**(2534).

23. Zhang, C., et al., *Knockdown of ribosomal protein S15A induces human glioblastoma cell apoptosis*. World Journal of Surgical Oncology, 2016. **14**(1): p. 129.

24. Chen, F.W. and Y.A. Ioannou, *Ribosomal proteins in cell proliferation and apoptosis*. International reviews of immunology, 1999. **18**(5-6): p. 429-448.

25. Liu, Y., C. Deisenroth, and Y. Zhang, *RP-MDM2-p53 Pathway: Linking Ribosomal Biogenesis and Tumor Surveillance*. Trends Cancer, 2016. **2**(4): p. 191-204.

26. Colot, H.V., et al., *A high-throughput gene knockout procedure for Neurospora reveals functions for multiple transcription factors*. Proceedings of the National Academy of Sciences, 2006. **103**(27): p. 10352-10357.

27. Gómez Ramos, L.M., et al., *Eukaryotic Ribosomal Expansion Segments as Antimicrobial Targets*. Biochemistry, 2017. **56**(40): p. 5288-5299.